**University of Aveiro**
**2015**
Department of Materials and Ceramic Engineering

**Sara Raquel Marques Sequeira**

# Desenvolvimento de compósitos de zircónia para implantes ortopédicos

Development of zirconia composites for orthopedic implants

**University of Aveiro** Department of Materials and
**2015** Ceramic Engineering

**Sara Raquel Marques Sequeira**

# Desenvolvimento de compósitos de zircónia para implantes ortopédicos

Development of zirconia composites for orthopedic implants

Dissertação apresentada à Universidade de Aveiro para cumprimento dos requisitos necessários à obtenção do grau de Mestre em Materiais e Dispositivos Biomédicos, realizada sob a orientação científica da Doutora Maria Margarida Tavares Lopes de Almeida, Professora Auxiliar do Departamento de Engenharia de Materiais e Cerâmica da Universidade de Aveiro, da Doutora Maria Helena Raposo Fernandes, Professora Catedrática da Faculdade de Medicina Dentária da Universidade do Porto, e do Doutor Nuno Neves, supervisor da empresa Innovnano.

**o jurí**

presidente

Prof. Doutor José Maria da Fonte Ferreira
Professor associado com agregação no Departamento de Engenharia de Materiais e Cerâmica

Prof.ª Doutora Florinda Mendes da Costa
Professora associada no Departamento de Física

Prof.ª Doutora Maria Margarida Tavares Lopes de Almeida
Professora auxiliar no Departamento de Engenharia de Materiais e Cerâmica

**agradecimentos** Na realização de uma tese de mestrado, apesar de ser um trabalho individual, existem contributos de natureza diversa que não podem, nem devem, deixar de ser realçados. Expresso, de seguida, os meus sinceros agradecimentos:

À empresa INNOVNANO, pela oportunidade para a realização deste projecto e pela disponibilização e apoio em todo o equipamento e material necessário.

Á Prof.ª Dra. Margarida Almeida pela forma como activamente me orientou e acompanhou neste trabalho. Agradeço pela competência científica que me transmitiu, toda a disponibilidade e generosidade ao longo destes meses, assim como pelo estímulo, críticas, correcções e sugestões relevantes feitas durante todo este percurso.

Ao Dr. Nuno Neves, pela presença constante durante todos estes meses, pelo conhecimento científico, motivação e valiosas contribuições dadas para este trabalho.

Á Prof.ª Dra. Maria Helena Fernandes por toda a disponibilidade, orientação, e conhecimentos transmitidos principalmente a nível do comportamento celular. Agradeço também todo o apoio prestado com os ensaios celulares.

À Dra. Rosário Soares, do Laboratório Central de Análises, por toda a disponibilidade e apoio prestado na análise dos resultados de difracção de raios-X.

À Engª. Filipa Neves, pelo impulso inicial no trabalho experimental, e pelo apoio e amizade ao longo destes meses.

Aos técnicos do DEMaC pela disponibilidade prestada na caracterização das amostras.

Aos meus colegas de mestrado, que me acompanharam nos bons e maus momentos deste percurso e pelos quais nutro uma grande amizade. Um enorme obrigado.

Ao João, ouvinte atento, por todo o incentivo, apoio e paciência.

Por fim, agradeço aos meus pais, irmã e avós, por me concederem mais uma realização pessoal, e por todo o apoio, compreensão, paciência e carinho demonstrado ao longo da minha vida.

**keywords** Zirconia, Alumina, Y-TZP, Zirconia Toughened Alumina, Alumina Toughened Zirconia, Femoral Heads, Hip Arthroplasty.

**abstract**

Zirconia and alumina are well known bioceramics, used in the field of orthopedics. These materials have been used as hip and knee bearings thanks to their reduced wear rate and excellent biocompatibility. However, these ceramics presented some limitations: the brittleness of alumina and the aging sensitivity of zirconia. The aim became to develop long-lasting hip implants, with less inflammatory response and better designs. Zirconia alumina composites were then studied. In this study, three different grades of alumina toughened zirconia composites (ATZ) from 80 wt% to 90 wt% of zirconia, and three grades of zirconia toughened alumina (ZTA) from 80 wt% to 90 wt% of alumina were developed. Two different types of stabilized zirconia were used: 3 mol% yttria stabilized zirconia (3YSZ) was applied on the ATZ samples, and a 2 mol% yttria stabilized zirconia (2YSZ) on the ZTA samples. The ATZ with the best set of properties (80Z20A) was also tested with the 2YSZ, in order to produce a composite with improved mechanical properties and similar aging resistance to the ATZ with 3YSZ.

Two selected additives, lanthanum oxide and tantalum pentoxide were added to the best ATZ and ZTA composite (80:20 composition) with the aim of enhance the aging resistance and mechanical properties of the produced materials.

After a wet milling stage, the composite powders were achieved by spray-drying, from stabilized suspensions with a controlled nanometric particle distribution. The obtained composite powders were characterized through several techniques, such as scanning electron microscopy, X-ray diffraction, X-ray fluorescence, true density and specific surface area. Two stages of pressing, uniaxial pressing and cold isostatic pressing, were performed in order to improve the density of the green pieces. High density ceramics (with a relative density between 97% and 99%) were achieved with a low sintering temperature (1400ºC). The grain size of the sintered pieces was determined by SEM, and X-ray diffraction was performed in order to verify the present crystallographic phases. A disperse microstructure was obtained for all composites, with a nanometric grain size (under 500 nm). This set of producing stages, lead to the obtention of composites with enhanced mechanical properties. The Vickers Hardness, fracture toughness and flexural strength of the sintered samples were evaluated. Higher values of fracture toughness and flexural strength were achieved for the ATZ samples (up to 5 $MPa.m^{1/2}$ and 1394 MPa respectively), while ZTA samples presented higher values of hardness (up to 1846 HV). As expected, the ATZ with 2YSZ presented enhanced mechanical properties, with

an outstanding fracture toughness of 7.94 MPa.$m^{1/2}$, and 1498 MPa of flexural strength. The addition of the two dopants to both ZTA and ATZ composites induced changes in their properties. The addition of $Ta_2O_5$ successfully improved the mechanical properties of both composites. In comparison with the undoped ATZ and ZTA composites, improvements of the hardness, fracture toughness and flexural strength were verified. The addition of $La_2O_3$ did not lead to an enhancement of the mechanical properties; however, it did not led to a deleterious effect either, and these properties were maintained. Accelerated aging tests were made on all produced composites, accordingly to ISO13356 (2008). The amount of monoclinic zirconia, which is an indicator of degradation on these composites, was quantified by X-ray diffraction analysis for 5,12,24,48 and 96 hours of aging tests. It was determined that, the undoped ZTA samples did not present monoclinic zirconia after 96 hours on an aggressive environment. Regarding the ATZ composites, even though the monoclinic zirconia content increased proportionally to the zirconia content present in the composite, it was found that the extent of degradation was minimal, since it was relegated to the material surface. This fact allowed the maintaining of the mechanical properties of the material throughout all the duration of the aging tests. As expected, the less stable composite, the ATZ with 2YSZ, presented the highest content of monoclinic zirconia. Nonetheless, the mechanical properties tested on the aged composite confirmed that the degradation did not expand to the material bulk. The addition of both dopants, successfully improved the aging resistance of the ATZ composite, presenting a lower amount of monoclinic zirconia after 96 hours of aging tests in comparison with the undoped ones. However, the addition of $Ta_2O_5$ destabilized the 2YSZ present on the ZTA composites, and 10% of monoclinic zirconia was detected after 96 hours of aging tests. Still, the mechanical properties were maintained on all the doped composites, which again confirmed the presence of degradation only at the material surface.

The biocompatibility of these composites was also tested. MG63 cells were seeded on the sintered samples and MTT and alkaline phosphatase activity (ALP) assays were performed. The cell viability/proliferation increased significantly from day 1 to day 4 for all the produced composites. The ZTA composites, with more anchorage sites, presented higher cell adhesion and proliferation in comparison with the ATZ composites. The addition of $La_2O_3$ and $Ta_2O_5$ did not induced significant changes on the cell viability of the ATZ composites. However, the addition of $Ta_2O_5$ on the ZTA composite led to a poor performance, due to its verified hydrophobicity.

The present study shows that optimal compositions of these composites can be achieved, with improved mechanical properties, hydrothermal degradation resistance and satisfactory biocompatibility.

**palavras-chave** Zirconia, Alumina, Y-TZP, *Zirconia Toughened Alumina*, *Alumina Toughened Zirconia*, Cabeças Femorais, Artroplastia da Anca.

**resumo**

Zircónia e alumina são biocerâmicos bastante conhecidos, e são usados principalmente em aplicações ortopédicas. Estes materiais têm sido aplicados em implantes de anca e joelho graças à reduzida taxa de desgaste e à excelente biocompatibilidade que apresentam. No entanto, estes cerâmicos apresentam também algumas limitações: a fragilidade da alumina ao impacto e a sensibilidade da zircónia ao envelhecimento. Devido a estas limitações, o objectivo passou por desenvolver implantes mais resistentes e com uma resposta inflamatória menos intensa. Surgiram, então, estudos de compósitos de zircónia e alumina. Neste estudo, foram desenvolvidas três diferentes composições de Alumina reforçada com Zircónia (ZTA) com 80 wt% a 90 wt% de alumina, e três composições de Zircónia reforçada com Alumina (ATZ) com 80 wt% a 90 wt% de zircónia. Foram usados dois tipos diferentes de zircónia estabilizada: zircónia estabilizada com 3 mol% de yttria (3YSZ) que foi usada nos compósitos ATZ, e zircónia estabilizada com 2 mol% de yttria (2YSZ) aplicada nos compósitos ZTA. A composição ATZ com o melhor conjunto de propriedades foi também testada com a zircónia 2YSZ, de forma a produzir um compósito com melhores propriedades mecânicas e uma resistência à degradação semelhante à apresentada pelo compósito ATZ, com a zircónia 3YSZ.

Foram seleccionados dois aditivos, óxido de lântanio e pentóxido de tântalo, que foram depois adicionados aos compósitos ATZ e ZTA com o melhor conjunto de propriedades (composição 80:20), com o objectivo de melhorar a resistência ao envelhecimento e as propriedades mecânicas dos materiais produzidos.

Após uma etapa de moagem, os pós compósitos foram obtidos por atomização, a partir de suspensões estabilizadas, com uma distribuição de tamanho de partícula nanométrica controlada. Estes pós foram caracterizados através de várias técnicas tais como microscopia electrónica de varrimento, difracção de raios-X, fluorescência de raios-X, densidade real, e área superficial específica. De forma a aumentar a densidade dos corpos em verde, foram efectuadas duas diferentes prensagens, prensagem uniaxial e prensagem isostática a frio (CIP). Foram obtidos cerâmicos com uma elevada densidade (com densidade relativa entre 97% e 99%) a uma baixa temperatura de sinterização (1400ºC). O tamanho de grão das amostras sinterizadas foi observado por SEM e, de forma a verificar as fases cristalográficas presentes, foi realizada difracção de raios-X. Em todos os compósitos foi obtida uma microestrutura dispersa, com um tamanho de grão nanométrico (abaixo dos 500 nm). Este conjunto de etapas de produção aplicado levou à obtenção de

compósitos com propriedades mecânicas melhoradas. Foram estudadas a dureza de Vickers, a tenacidade à fratura e resistência à flexão das amostras sinterizadas. Os compósitos ATZ atingiram os melhores valores de tenacidade à fractura e resistência à flexão (acima de 5 $MPa.m^{1/2}$ e 1394 MPa respetivamente), enquanto os compósitos ZTA apresentaram os melhores valores de dureza (acima de 1846 HV). Como era esperado, o compósito ATZ com zircónia 2YSZ apresentou melhores propriedades mecânicas, tendo sido obtidos 7.94 $MPa.m^{1/2}$ de tenacidade à fratura e 1498 MPa para a resistência à flexão. A aplicação dos dopantes nos compósitos ZTA e ATZ induziram alterações nas suas propriedades. A adição de $Ta_2O_5$ melhorou, com sucesso, as propriedades mecânicas dos dois tipos de compósitos. Foi verificado um aumento dos valores de dureza, tenacidade à fratura e resistência à flexão em relação às amostras sem dopantes. A adição de $La_2O_3$ não levou a melhorias nas propriedades mecânicas mas, no entanto, também não teve um efeito prejudicial, o que levou à sua preservação. Foram realizados testes de envelhecimento de acordo com a norma ISO13356 (2008) em todos os compósitos produzidos. A quantidade de zircónia monoclínica, indicador de degradação, foi determinada por difracção de raios-X após 5,12,24,48 e 96 horas de testes de envelhecimento. Foi determinado que os compósitos ZTA não dopados, não apresentaram zircónia monoclínica após 96 horas em ambiente agressivo. Para os compósitos ATZ, apesar de a quantidade de zircónia monoclínica aumentar proporcionalmente ao conteúdo de zircónia presente no compósito, foi verificado que a extensão da degradação foi mínima, e relegada apenas para a superfície do material. Esta evidência permitiu que as propriedades mecânicas se mantivessem durante todo o período dos testes de degradação. Como era esperado, o compósito com a zircónia menos estável, o ATZ com a zircónia 2YSZ, apresentou o conteúdo mais elevado de zircónia monoclínica. No entanto, o facto de as propriedades mecânicas se manterem ao longo dos testes de degradação, confirmou que a degradação, mais uma vez, não se expandiu para o interior do material. A adição dos dois dopantes levou a melhorias na resistência à degradação dos compósitos ATZ, que apresentaram um conteúdo de zircónica monoclínica menor em comparação com as amostras não dopadas, após 96 horas de testes de degradação. No entanto, a adição de $Ta_2O_5$ teve um efeito desestabilizador na zircónia 2YSZ presente no compósito ZTA, sendo que foi detectada 10% de zircónia monoclínica após as 96 horas de testes de degradação. De novo, foi confirmado que esta degradação esteve presente apenas à superfície do material, visto que as propriedades mecânicas se mantiveram após estes testes. Foi também testada a biocompatibilidade destes compósitos. Células MG63 foram cultivadas nas amostras sinterizadas e foram realizados ensaios MTT

e ensaios de atividade da fosfatase alcalina. Para todos os compósitos produzidos foi verificado que a viabilidade/proliferação celular aumentou significativamente desde o dia 1 para o dia 4. Os compósitos ZTA, que possuíam um maior número de locais de adesão, apresentaram uma maior adesão e proliferação celular, em comparação com os compósitos ATZ. A adição de $La_2O_3$ e $Ta_2O_5$ não induziu diferenças significativas na viabilidade celular dos compósitos ATZ. No entanto, no compósito ZTA, a adição de $Ta_2O_5$ levou a um pior desempenho devido à sua verificada hidrofobicidade.
O presente estudo mostra que podem ser obtidas composições óptimas destes compósitos, com excelentes propriedades mecânicas, resistência à degradação e biocompatibilidade satisfatória.

# Table of Contents

# List of Figures

# List of Tables

## Abbreviations

**ATZ – Alumina Toughened Zirconia**

**ZTA – Zirconia Toughened Alumina**

**YSZ** – Yttria Stabilized Zirconia

**Y-TZP** – Yttria Tetragonal Zirconia Polycristal

**Y-STZ** – Yttria Stabilized Tetragonal Zirconia

**SZ** – Stabilized Zirconia

**3YSZ** – 3mol% Yttria Stabilized Zirconia

**2YSZ** – 2mol% Yttria Stabilized Zirconia

**XRD** – X-ray Diffraction

**SEM** – Scanning Electron Microscopy

**HIP** – Hot Isostatic Pressing

**CIP** – Cold Isostatic Pressing

**UP** – Uniaxial Pressing

**MAJ** – Mehl-Avrami-Johnson (law)

**HUVEC** – Human Umbilical Vein Endothelial Cells

# Chapter 1

## Introduction and Objectives

# 1. Introduction

Biomedical implants have been widely studied and new devices were designed to restore a body function that was deteriorated by a trauma or degenerative disease. Ceramic implants soon caught the attention of various authors because of their biocompatibility and chemical stability.

Zirconia and Alumina are well known bioinert, inorganic oxides. Their good mechanical properties brought new insights to the world of biomaterials, especially, in the development of new restorative devices. These materials have also been used as hip and knee bearings, which are load-bearing applications. Some properties like reduced wear rate (in comparison to metal alloy structural implants) and excellent long term biocompatibility, turn these materials into excellent candidates to be used in orthopedic applications [1], [2].

Alumina was the first oxide to be used in these applications, back in 1970, in the first ceramic total hip replacement bearing. Pierre Boutin was the first to describe the low rates of friction of these all ceramic bearings, and the first implant was developed and implanted in collaboration with Daniel Blanquaert from Ceraver *Inc* [3]. Alumina-alumina bearings presented other various beneficial properties such as biological safety (on both bulk and wear debris), stiffness, corrosion resistance and long term stability, that lead to a reduced rate of aseptic loosening and osteolysis. Osteolysis due to metallic wear debris was a concerning problem on metal couplings, that subsequently lead to a major bone loss and consequent loosening of the implant [4]. Due to these beneficial effects, alumina quickly became the most widely used ceramic in total hip arthroplasty.

However, early clinical evaluation showed a high fracture rate on these ceramic devices, due to slow crack growth that, eventually, led to failure [2]. Some efforts were made to produce fully densified alumina, like using high purity raw powders with a narrow grain size distribution and applying different sintering methods, such as hot isostatic pressing (HIP) [5]. Nevertheless, these devices still presented brittleness, and became unreliable.

The objectives changed, and it was important to increase the strength, flexibility and therefore the reliability of these implants. So, to overcome this brittleness and the consequent potential failure presented by alumina implants, zirconia femoral heads were

introduced twenty years later. The first paper concerning the use of zirconia ball heads for total hip replacement was published in 1988 [6], and the approval of the *Food and Drug Administration* arrived in 1989.

This oxide exhibits good chemical stability, toughness, mechanical strength and a Young's Modulus value similar to stainless steel alloys, which created an increasing interest in using it as a biomaterial [6]. In addition, its properties are superior to those presented by alumina, being possible to design smaller hip implants (like the 22.22 mm diameter femoral heads) and knee joints, which was not possible with alumina, due to a lack of adequate reliability [7].

Zirconia presents a mechanism of phase transformation toughening, which highly increases its fracture toughness and strength (showing a high crack propagation resistance) [2], [6], [8]. This mechanism consists in a stress induced phase transformation, in which metastable tetragonal zirconia is converted into the monoclinic phase at the crack tip [9]–[12]. Due to this transformability, tetragonal zirconia can be very unstable and transform into the monoclinic phase, leading to the degradation of the implant. In order to retain the tetragonal phase, some suitable stabilizers were added to this oxide. The commonly used stabilizer is yttrium oxide ($Y_2O_3$) and the frequently used biomedical grade zirconia contains, typically, 3 mol% yttria [6], [7].

However, these zirconia devices undergo Low-Temperature Degradation. This effect mostly causes loss of strength and micro-cracking in the presence of water, that occurs from room temperature up to 400ºC [7], [13], which causes big concerns related to the human body temperature and sterilization of these devices.

In fact, from 1999 to 2001, St.Gobain Desmarquest, a major manufacturer of these devices, requested a worldwide recall of selected batches, because of their degradability that consequently lead to high fracture rates *in vivo* [8], [14], [15] (Figure1.1).

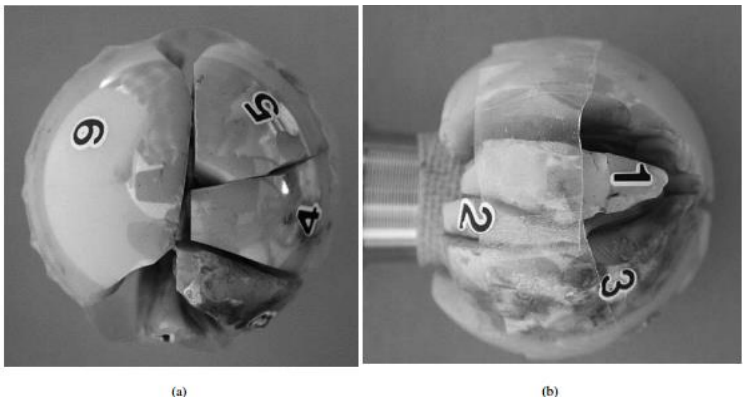


**Figure 1.1 – Reconstitution of the fractured zirconia ball head (stabilized with 3% mole fraction of yttria) (a) Top view (b) Lateral view, from** [16]**.**

The fracture on these implants was originated by the tetragonal to monoclinic transition detected on the surface, microcracking, nucleation and growth that occurred on the low density parts of the material core. These low density parts are created by the presence of the monoclinic phase (which presents a lower value of density) that, under exposure to physiological wet environment and cycling loading are more susceptible to aging [16], [17].

Thus, although zirconia implants presented optimum biological safety, and enhanced strength, there were still problems to be solved: its low hardness, the risk of degradation, and the critical manufacturing process.

A demand for a new material had risen, with the combined properties of alumina and zirconia. This new material should present both zirconia and alumina biocompatibility, the strength of zirconia, the long time *in vivo* stability of alumina and a flexible design to allow the production of bigger ball head necks and diameter, and thinner ceramic inserts. These new designs would help to pursue the demand for total hip replacement bearings for more young and active patients. Therefore, pursuing the overcoming of these limitations, new zirconia-alumina composites started to be widely investigated.

Basically, these composites show less sensibility to aging than zirconia, and higher fracture toughness than alumina. On the other hand, in comparison with the alumina-alumina bearings, the strength of the implant increased thanks to an increase in density and reduction of alumina grain size (since the presence of zirconia controls its grain growth) [10], [12]. The combination of alumina with an intrinsically tough ceramic such as zirconia, gave rise to a new age of new ceramic implants.

There are two different composites according to the two possible compositions: if the composite has a richer side of alumina, a Zirconia-Toughened Alumina (ZTA) composite is presented. On the contrary, if the composite contains a richer side of zirconia, we are in the presence of an Alumina-Toughened Zirconia (ATZ) composite [1]. With both composites higher values of strength, hardness and toughness, than those of the mono-phase oxides can, in fact, be achieved [2], [9], [18].

Since it was approved by *Food and Drugs Administration*, on June 2003, ZTA composites were widely used in total hip arthroplasty. Nowadays, various compositions are created, and the addition of other stabilizers and dopants, like $CeO_2$ or MgO, have been widely studied [7]. Still, the ability to tailor the microstructure of these composites is essential to accomplish the requirements of biomedical materials, and to produce devices with higher success rates, that can be applied to a younger population, with higher life expectancy.

## 1.1 Objectives

The main goal of this study was to develop and characterize various grades of zirconia alumina composites (zirconia toughened alumina (ZTA) and alumina toughened zirconia (ATZ)) for orthopedics implants, using both 2 mol% Yttria Stabilized Zirconia (YSZ), and 3 mol% Yttria Stabilized Zirconia, provided by INNOVNANO.

The various compositions were defined on the basis of the results presented by several authors [2], [10]–[12], [19]–[21].

The ZTA composites were produced by varying the Zirconia amount. Three different composites were defined:

- 10 wt% of $ZrO_2$ and 90 wt% of $Al_2O_3$;
- 15 wt% of $ZrO_2$ and 85 wt% of $Al_2O_3$;
- 20 wt% of $ZrO_2$ and 80 wt% of $Al_2O_3$.

Also, three ATZ composites were made. In this case, the amount of alumina differs on each composite:

- 10 wt% of $Al_2O_3$ and 90 wt% of $ZrO_2$;
- 15 wt% of $Al_2O_3$ and 85 wt% of $ZrO_2$;
- 20 wt% of $Al_2O_3$ and 80 wt% of $ZrO_2$.

For the ZTA composites (which have the higher amount of alumina), the 2 mol% yttria stabilized zirconia was used, in order to take advantage of the stabilizing effect presented by the alumina matrix. Regarding the ATZ composites, the 3 mol% Yttria Stabilized Zirconia was used. In this case, where the composite presents a zirconia matrix, destabilization of zirconia is more likely to occur, so this zirconia with a higher amount of stabilizer was used.

Some characteristics of produced composites were analyzed on the basis of the ISO standard 13356 (2008): Implants for surgery – ceramic materials based on yttria-stabilized tetragonal zirconia (Y-TZP) [22]. Mechanical tests for hardness, fracture toughness and flexural strength were performed. Aging tests were made on the composites, in order to evaluate their resistance to hydrothermal degradation. Biocompatibility tests were also executed.

A research study was accomplished and two additives, tantalum pentoxide ($Ta_2O_5$) and lanthanum oxide ($La_2O_3$) were tested alongside with the ZTA and ATZ composition with better mechanical properties and aging resistance. The dopants were selected in order to provide enhancements on the mechanical properties and Low Temperature

Degradation Resistance. Aging, mechanical and biocompatibility tests were performed in order to fully characterize these composites.

The ATZ composite with the better set of results was also tested using in its composition the less stable zirconia (2 mol% Yttria Stabilized Zirconia) in order to compare the two stabilized zirconias (2 mol% Yttria Stabilized Zirconia and 3 mol% Yttria Stabilized Zirconia) regarding their mechanical properties and aging resistance and therefore inquire on the role of the yttria amount on the properties of these composites.

## 1.2 Document Structure

This document consists of five chapters. The first chapter addresses the interest and objectives of this project. In the second chapter, the literature review about zirconia-alumina composites including their requirements to be used as a suitable material for orthopedic implants is presented to build up a better understanding in this area. The third chapter presents the experimental procedure describing all the characterizations techniques and tests executed during this project. In the fourth chapter, the experimental results achieved will be presented and analyzed. Finally, in the fifth and last chapter, the main conclusions alongside with the plan of future developments and recommendations are presented.

# Chapter 2

## Literature Review

# 2. Literature Review

## 2.1 Properties of zirconia composites

Zirconia can be found in nature as a free oxide with the mineral Baddeleyite. This oxide has an approximate density of 5.7 g/cm$^3$, and three crystallographic forms: tetragonal, monoclinic and cubic. The monoclinic phase is stable from room temperature up to 1170 ºC, and it is the most stable form. The tetragonal form is stable at temperatures of 1170ºC to 2370ºC, and the cubic form is stable at temperatures higher than 2370ºC [23].

In this material, perceptible changes in volume occur during phase transformation. The stress induced phase transformation from tetragonal to monoclinic zirconia at room temperature (on cooling), ahead of a propagating crack, results in a 3-5% volume expansion and approximately 7% shear strain [2], [9], [23] (these values may vary depending on grain size and concentration of stabilizer, which will be explained further in this document). Upon heating, a 5% decrease in volume occurs (Figure 2.1).

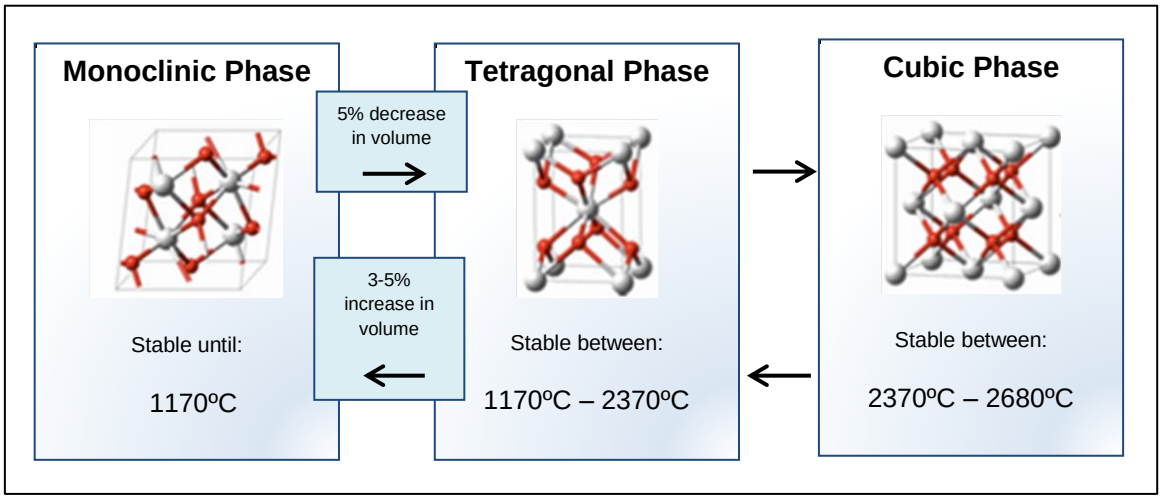


**Figure 2.1 - Temperature Phase Transformation of zirconia, adapted from** [23]**.**

This tetragonal to monoclinic transformation brought new insights for new applications because this transformation is, in fact, a mechanism of transformation toughening of the material, and it is the key issue for the use of zirconia in biomedical applications.

This transformation is martensitic and occurs during sintering and for both heating and cooling [7]. The shear strain and the large increase of volume, previously mentioned,

create internal stresses on cooling. These created stresses are so large that pure zirconia sintered above 1170ºC disintegrates by cracking upon cooling [7]. This mechanism increases the work of fracture and, consequently, the toughening of the composite. However, it is also important to stabilize the tetragonal phase, which has higher density (around 6 g/cm$^3$) than monoclinic zirconia and presents better mechanical properties than alumina, as shown on Table 2.1. The Young's Modulus is similar to stainless steel alloys and the value of strength is one of the highest among ceramic biomaterials. However, alumina still presents a higher value of hardness, which makes this oxide a proper material to be used in zirconia composites.

**Table 2.1 - Properties of tetragonal zirconia and alumina** [6]**.**

| Property | Tetragonal Zirconia | Alumina |
|---|---|---|
| Strength | 900-1200 MPa | >500 MPa |
| Hardness | 1200 HV | 2200 HV |
| Young's Modulus | 210 GPa | 380 GPa |

This zirconia phase transformation toughening is initiated in the presence of large tensile stresses around a crack and, as previously mentioned, the volume expansion of the tetragonal grains can stop the crack propagation, like a zipper mechanism. However, on the proximity of that crack, the grains will be destabilized, forming a transformation zone in the material [7] (Figure 2.2). This means that, when volume expansion occurs, stresses are created on the surroundings of the tetragonal grains, leading them to transform too, all over the material. This phenomenon can cause loss of strength, low temperature degradation and consequent deterioration of the material. For this reason, it is crucial to control this mechanism, in order to obtain the improved crack resistance without losing the properties provided by the tetragonal phase.

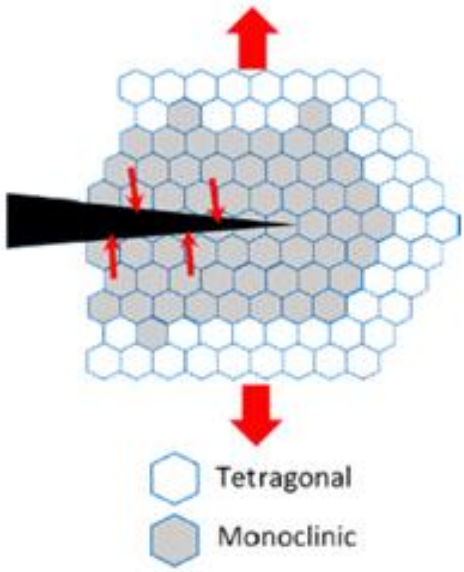


**Figure 2.2 - Transformation zone formed by a crack that induced tetragonal to monoclinic transformation. From** [1]**.**

In terms of the thermodynamics of this transformation, a simple analysis of the conditions for the transformation is expressed in terms of different energy contributions to the overall energy of transformation. The change of total free energy ($\Delta G_{t\text{-}m}$) per units of volume required for the tetragonal-monoclinic transformation in a constrained matrix can be expressed by the following equation [7], [24]:

$$\Delta G_{t-m} = \Delta G_c + \Delta U_{SE} + \Delta U_S \qquad \text{(Equation 1)}$$

$\Delta G_c$ is the difference in chemical free energy associated with the tetragonal to monoclinic transformation. This value is dependent on the temperature and composition (including the amount of oxygen vacancies), and it is negative for temperatures below the equilibrium temperature. The variable $\Delta U_{SE}$ is related to the change in elastic strain energy associated with the transformation of particles, and it is dependent on the modulus of the surrounding matrix, the size and shape of the particles and the presence of stresses (internal, or external). The last term, $\Delta U_S$ is the change of surface free energy. It expresses the changes in energy associated with the formation of new interfaces upon transformation, like microcracks, and it is usually a positive value. Basically, when the overall value $\Delta G_{t\text{-}m}$ is positive, the particles remain on the tetragonal phase. On opposite, when this value is negative, they are metastable and will probably transform into monoclinic [7], [13], [17], [25].

In zirconia alumina composites, this transformation toughening is also present, but it will be constrained. In a ZTA composite, the cracks will preferentially cross the zirconia

particles in the alumina matrix (because of their smaller Young's Modulus), and the stress induced phase transformation will stop the advancing crack, creating a toughening mechanism. Also, when volume expansion occurs, a microcrack network will be created around the transformed particle, and the fracture energy will be dissipated, improving toughness [6]. Nonetheless, the zirconia concentration in the alumina matrix must be carefully controlled so that the stresses created upon phase transformation do not compromise the strength of the biomaterial [6].

Moreover, in a composite, thanks to the encapsulation of the particles, the matrix will slow down the phase transformation, and prevent the entrance of radicals that penetrate the lattice and lead to a premature transformation [9]. This effect is related to the increase of the elastic self-energy $\Delta U_{SE}$ (Equation 1) due to the presence of the alumina (which is a stiffer material) that will affect the matrix modulus. So, for this reason, it can be stated that ZTA composites are more stable. Nevertheless, it has been proposed that, in these composites, the content of zirconia must be controlled, and should be below a percolation limit (which was defined as 16% in an alumina matrix), in order to avoid the deleterious formation of zirconia agglomerates [1], [9], [26]. Zirconia agglomerates are adverse, causing instability in the composite. In these agglomerates, the tetragonal zirconia is more easily converted into the monoclinic phase, which can cause degradation of the mechanical properties.

The processing of these composites is mainly done by wet mixing and subsequent sintering. The temperature and pressure applied during sintering may induce phase transformation and therefore, these parameters must be controlled in order to obtain a composite with the desired properties.

Hence, with a tight control of the composition, grain size, and processing conditions, it is possible to achieve a composite with the high hardness presented by alumina, and the fracture toughness and strength offered by zirconia.

## 2.2 Low Temperature Degradation

The main concern regarding zirconia biomaterials is their sensitivity to Low Temperature Degradation.

Low Temperature Degradation is a kinetic phenomenon that causes aging of the material and occurs in the presence of moisture [7], [17]. Basically, this mechanism is defined as a slow transformation of the tetragonal phase into monoclinic, from room temperature to 400ºC, by nucleation and growth process. It begins at the surface of the

material by a stress corrosion type mechanism that can be extended to the inner parts of the material [7], [8].

An attractive explanation for this phenomenon, reported by Fabris *et al* [27], is that the moisture species penetrate into the tetragonal lattice and destabilize it by annihilating the oxygen ion vacancies, which means that the value of the elastic self-energy of the transformation ($\Delta U_{SE}$) (energy barrier for $t \rightarrow m$ transformation) will decrease [7], and thus, the rate of transformation will increase [28]. As it would be expected, loss of strength and microcracking will occur since monoclinic zirconia presents lower density and thus lower hardness and resistance to crack formation. This will also create porosity on the surface of the material and therefore, a path for the water or biological fluids to penetrate down into the material. In the following figure, a scheme of this phenomenon is presented.

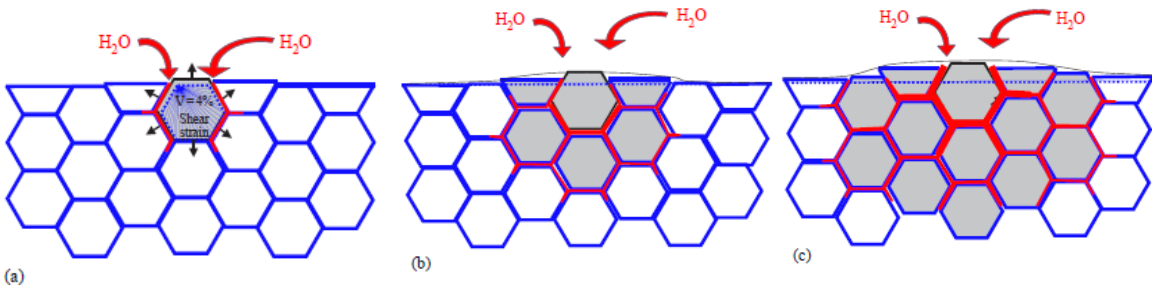


**Figure 2.3 - Illustration of the aging process occurring in a cross section of a zirconia ceramic, from** [8]**. (a) Nucleation, (b) Growth, (c) Penetration of water to bulk from microcracks (red path).**

Initially, the diffusion of water species into the lattice via oxygen vacancies will result in a change of lattice parameters that will lead to instability and consequent transformation, caused by stress accumulation and decrease of the difference in chemical free energy between tetragonal and monoclinic phases ($\Delta G_c$). The nucleation occurs in the most unstable grains subjected to the highest tensile stresses. This will lead to microcracking and will create stresses in the other grains, which will continuously increase the number of monoclinic nuclei. In consequence, the growth of this transformed zone will lead to extensive microcracking and surface roughening, as a result of the volume expansion upon transformation [17]. Further transformation proceeds in the presence of water diffusion and stresses, and the fluids will consequently enter the lattice and extend the monoclinic transformation through the bulk [7], [8], [17], [29].

This is basically an alternative to the resistance to crack propagation, caused by the stress induced transformation for the tetragonal to monoclinic transformation. When the transformation is initiated by a propagating crack, an improved toughening is achieved, but on the other hand, when the $t \rightarrow m$ transformation is caused chemically (like diffusion

of water derived species from surface) a surface roughening occurs, starting various detrimental effects like microcracking, grain pull-out, loss of strength, and wear debris (Figure 2.4). The initial transformation of specific grains can be triggered out by various factors like their non-equilibrium state caused by their size (large grains are more unstable), low stabilizer content, a specific orientation on the surface, or the presence of residual stresses (aging sensitivity is directly linked to the type (compressive or tensile) and amount of residual stresses) [8], [30].

These effects can obviously cause the fracture of the material. This was the reason given by *Food and Drugs Administration* for the removal of various batches of zirconia implants.

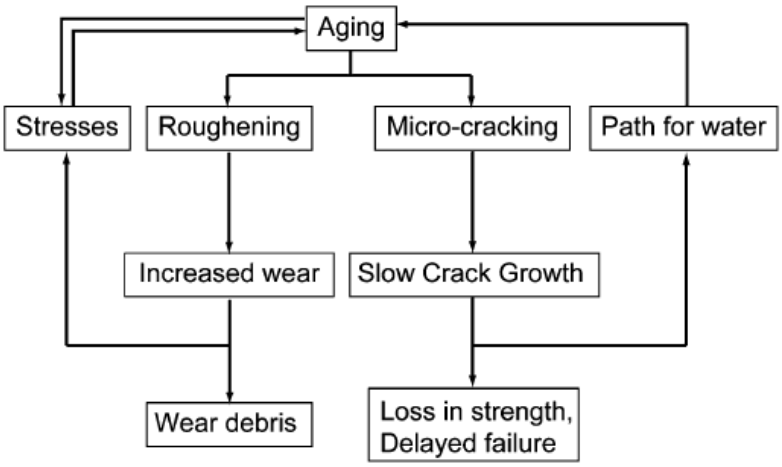


**Figure 2.4 - Consequences of aging on zirconia devices, from** [7]**.**

The sterilization procedure (at 134ºC and 2 bar) consequently led to the surface roughening of the material, leading to grain removal induced by wear, that creates craters on the surface of the material [7], [8], [29], and, consequently to their catastrophic degradation (Figure 2.5).

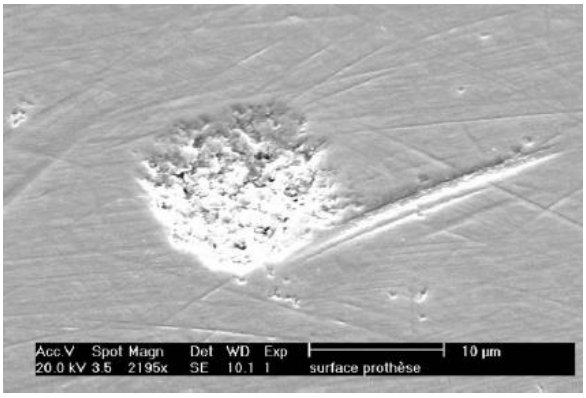


**Figure 2.5 - SEM image of retrieved zirconia ball head for total hip replacement after 4.5 years *in vitro*. A large crater on the surface induced by aging associeated to wear, is presented** [8]**.**

In order to prevent this degradation in zirconia orthopedic devices, it was created an International Standard that specifies the characteristics and test methods for every ceramic implant based on Yttria Stabilized Tetragonal Zirconia (Y-STZ). The second edition of the ISO 13356 [22] was published in 2008, specifies the material properties such as bulk density, chemical composition, microstructure, mechanical properties, and the aging tests.

Every Y-STZ ceramic for implant must be submitted to an accelerated aging test. The zirconia samples must be placed in an autoclave and exposed to steam at (134 ± 2) ºC under a pressure of 0.2 MPa, for 5 hours. These conditions correspond to roughly 15 to 20 years *in vivo* [17], [31] . After this test, the monoclinic fraction must be determined by X-Ray diffraction, and should be equal or below 25%. The residual biaxial and bending strength of the aged composites should not decrease more than 20% after this test.

In the presence of Zirconia Alumina composites, the kinetics of this mechanism is slowed down because the zirconia phase is not microstructurally continuous, implying that there won't be a pathway for the diffusion of species into the composite.

Regarding ZTA composites, which have an alumina matrix, the transformation of the zirconia grains will be obstructed [7], [26]. On the other hand, for ATZ composites, it has been reported that the addition of alumina to zirconia (as little as 0.25%), combined with a finer grain size, effectively slows this deleterious transformation [25], [32], [33]. Higher amounts of alumina also prevent the degradation, although the protection mechanism is different. With the addition of up to 20 wt% of alumina the transformation is delayed because the contact area between zirconia grains is reduced [34], [35].

Therefore, the encapsulation that limits this transformability similarly indicates that these composites are less susceptible to stress induced corrosion in water and body fluids [36]. Pezzoti *el al* [37], confirmed that, after a long exposure to hydrothermal degradation (more than 50 hours), the thickness of phase formed on the surface of pure zirconia was twice the thickness presented by ZTA ceramics (with 80 vol% of alumina, 17 vol% of zirconia and 3 vol% of strontium aluminate), as it can be verified in Figure 2.6. In another study, it has also been reported that the addition of 20 wt% of alumina to zirconia also prevented the aging degradation in comparison with a 3 mol% Yttria Stabilized Zirconia (YSZ), and also increased the strength of these ceramics during long-term aging [35].

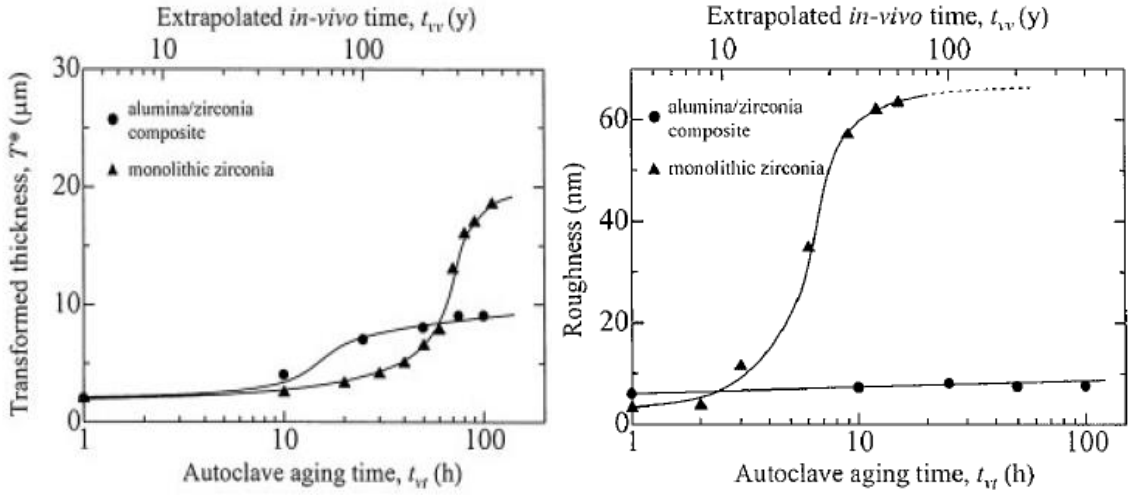


**Figure 2.6 - Experimental results obtained by Pezzotti *et al* [37], on surface femoral heads upon aging tests at 134ºC for monolithic zirconia and ZTA composites. Left: Transformed Thickness (μm); Right: Roughness (nm).**

As it would be expected, the roughness revealed by pure zirconia was much higher than the roughness presented by ZTA composites. Even though the hydrothermal transformation occurred sooner (between 10 and 50 hours of aging) the authors reported that it was limited and it did not affect the surface roughness, since it was maintained on a low value throughout the duration of the aging test. The surface roughness in a zirconia ceramic is a clear sign of a deleterious tetragonal to monoclinic transformation.

Nevertheless, the percolation limit of 16 vol% of zirconia in these composites, mentioned in the previous section of this document, should be considered [1], [9], [26]. Pecharromán *et al,*[26] concluded that 16% volume of zirconia is, in fact, the percolation limit in which a higher content of zirconia will not retard the mechanism of aging (Figure 2.7).

It was reported that both ATZ and ZTA composites show better aging resistance than Yttria Stabilized Zirconia (YSZ) alone [38], [39]. However, ATZ composites still exhibit a certain degree of aging [29], [39]. This is due to the fact that ATZ composites are composed by a higher amount of zirconia, that could be more easily destabilized than the ZTA ones, which have an alumina matrix.

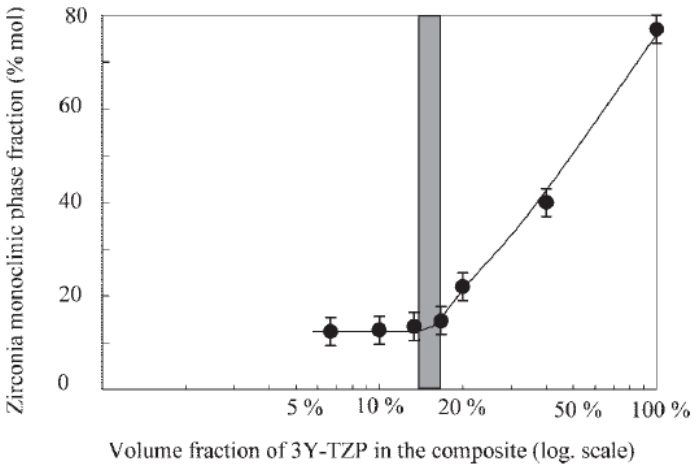


**Figure 2.7 - Monoclinic fraction versus zirconia content in ZTA composites. Zirconia stabilized with 3% of yttria was submitted to a steam treatment (40h at 140ºC)** [26]**.**

The surface finish of the bioceramic can benefit the resistance to aging, or decrease it. In aging environment, the grains are transformed as a function of their disequilibrium state, so, all the grains remain in a similar stress state [40]. However, when a scratch is created in the material surface (by machining or polishing), a homogeneous stress state is created on the surrounding area of the scratch [30]. This area will be susceptible to transformation that will lead to aging. Deville *et al* [30], concluded that rough polishing can produce a compressive surface stress layer that is beneficial for the aging resistance. A 6 µm surface finish produces compressive stresses that will be presented on the surface. On the contrary, a smooth finish from 1 µm to 3 µm will produce tensile stresses. Elastic/Plastic zones will be created and, consequently, preferred regions for nucleation will be formed. These regions can change the stability of zirconia during aging treatments. Tensile stresses are more favorable for transformation than compressive stresses [30].

The sintering temperature can also affect the resistance to aging [25], [34], [41]. It has been reported by Kawai *et al* [34] that with increasing sintering temperature, the fraction of monoclinic zirconia increases in Y-TZPs. For a sintering temperature of 1400ºC, the monoclinic content was around 80%, with penetrated depth of 17.6 µm. In the same study, an ATZ (with 79.7 wt% of Y-SZ and 20.3 wt% of alumina) was sintered at 1450ºC and it only presented a monoclinic content of 60%. For lower sintering temperatures, 1350ºC or 1400ºC, the transformation was suppressed. It is suggested that, the excessive grain growth promoted by the sintering temperature and increasing time, can reduce the protection against degradation [33], [42]. This statement is in agreement with Equation 1, since smaller grains present higher values of $\Delta U_s$, and therefore, higher stability. Zhang *et al* [42] reported the same tendency for a composite with only 0.25 wt%

of alumina. When sintered at 1450ºC (or higher) for 4 hours, the average grain size had risen to 0.25 μm, the degradation of Y-TZPs considerably increased.

## 2.3 Stabilized Zirconia

Zirconia ceramics strongly depend on the selection of the starting powders, composition and size distribution. These parameters can affect the mechanical properties and aging resistance of these ceramics.

The main priority was always to develop a stabilized tetragonal zirconia ceramic with good mechanical properties, specifically, high fracture toughness and strength. The introduction of a stabilizer was studied in order to enhance the stability of the tetragonal phase, and therefore, improve the stability of the bioceramic [43]. Garvie *et al* [44] published in 1975 the first study regarding stabilization of zirconia tetragonal phase. In this study a magnesia partially stabilized zirconia was tested. After this publication, various stabilizers for zirconia were tested during early stages of development.

Essentially, a zirconia stabilizer will stabilize the oxygen ions around $Zr^{4+}$ cations, thus stabilizing the tetragonal (or even the cubic phases) and preventing an undesirable transformation of tetragonal zirconia during cooling at low temperatures. Combinations of zirconia-magnesia ($ZrO_2$-MgO), zirconia-calcia ($ZrO_2$-CaO), zirconia-ceria ($ZrO_2$-$CeO_2$) and zirconia-yttria ($ZrO_2$-$Y_2O_3$) were the most studied combinations used to retain tetragonal zirconia. Some of these stabilizers contain undersized and oversized trivalent cations (which is the yttria case ($Y^{3+}$)) and oversized tetravalent ions (like ceria ($Ce^{4+}$)).

Yttria is the most used stabilizer for zirconia, and this stabilized zirconia is named Yttria-Stabilized Tetragonal Zirconia Polycristal material (Y-TZP) [45]. This stabilizer for zirconia ($Zr^{4+}$) forms oxygen vacancies according to the following equation written in Kroger-Vink notation [45], [46]:

$$Y_2O_3 \xrightarrow{ZrO_2} 2Y'_{Zr} + V_{\ddot{O}} + 3O_O \qquad \text{(Equation 2)}$$

where $Y'_{Zr}$ represents the negatively charged yttrium ion that will substitute the zirconium ion, and $V_{\ddot{O}}$ represents the oxygen vacancy with double positive charge and $3O_o$ is the lattice oxygen [45], [46]. The addition of cations like $Mg^{2+}$, $Ca^{2+}$ or $Y^{3+}$, which have lower valence than the zirconium ion ($Zr^{4+}$), induces the creation of oxygen vacancies (indicated in the Equation 2 as $V_{\ddot{O}}$), in order to compensate the charge difference. For example, the

substitution of $Zr^{4+}$ ion by the $Y^{3+}$ will create a negative charge in the lattice, and for keeping the charge neutrality, an oxygen vacancy is created for each mol of yttria incorporated in the lattice [47]. Two yttria ions are necessary to electrically balance just one oxygen vacancy. Oxygen vacancies are effective in stabilizing both tetragonal and cubic zirconia since they promote the relaxation of the oxygen sublattice [48].

Comparing to MgO-Stabilized Zirconia (SZ), Y-TZPs present a significant advantage, since sintering can be carried out at lower temperatures (in the range of 1400ºC-1500ºC compared to 1800ºC to MgO-SZs) [47]. Besides, the reinforcement by phase transformation is less pronounced in MgO-SZs than in Y-TSZs, and this stabilized zirconia presents a residual porosity and a coarser grain size. All these factors have discouraged the use of magnesia stabilized zirconia in biomedical applications, since the porosity created and bigger grain sizes can lead to a premature degradation, and consequent failure of the implant [23].

A systematic study concluded that the stabilization of tetragonal zirconia with oversized trivalent cations (like $Y^{3+}$) is twice more efficient than stabilization with undersized trivalent cations, since they are most efficient in relieving the oxygen overcrowding around $Zr^{4+}$ ions [7], [49], [50]. Besides, Yttria Stabilized Zirconia (YSZ) presents the best characteristics such as a fine grain microstructure (with a diameter ranging from 0.2 to 2 µm) [6], [47]. Also, with the increase of yttria, the wear rate of ZTA composites (with 17 vol% of Y-TZP) decreases due to its resistance against crack extension and grain pullout. It is also reported that optimal results such as less detrimental transformation and increasing of wear resistance, can be achieved by using a lower grain size zirconia [51].

In order to achieve equivalent mechanical properties, Ceria Stabilized Zirconia requires a three times larger grain size comparing to Y-TZPs [47]. To achieve a $K_{IC}$ of 12 $MPa.m^{1/2}$, a Ce-TZP with a grain size of 8 µm would be needed, while for a Y-TZP a grain size of 2 µm would be sufficient [52]. Table 2.2 presents the typical mechanical properties presented by yttria and ceria stabilized tetragonal zirconia (Y-TZP and Ce-TZP). As it can be verified, a higher amount of ceria is necessary to achieve similar mechanical properties, at a cost of a coarser grain size too.

The exact content of yttria plays an important role in the transformability of zirconia. The yttria content will increase the value of $\Delta U_{SE,}$ previously mentioned (Equation 1). For a content around 3 mol%, this oxide decreases the driving force of the tetragonal-monoclinic transformation at room temperature, and retains the metastable tetragonal grains in dense bodies [17].

**Table 2.2 - Typical mechanical properties presented by Y-TZPs and Ce-TZPs** [47]**.**

| | **Y-TZP** | **Ce-TZP** |
|---|---|---|
| Stabilizer (mol%) | 2-3 | 12-15 |
| Hardness (GPa) | 10-12 | 7-10 |
| Fracture toughness, $K_{IC}$ (RT, MPam$^{1/2}$) | 6-15 | 6-30 |
| Young's Modulus (GPa) | 140-200 | 140-200 |
| Bend strength (MPa) | 800-1300 | 500-800 |

The toughness of this yttria stabilized zirconia is also strongly influenced by the grain size. In order to control the volume expansion presented when tetragonal to monoclinic transformation occurs, it is important to limit the zirconia grain size [47]. The zirconia grain size must range between two critical values: the lower value, $D_c'$, bellow which the transformation is hindered (the tetragonal phase is stabilized, due to its small size), and the highest value, $D_c$, above which spontaneous, catastrophic, transformation occurs. These critical sizes will be affected by the content of stabilizers present in zirconia. An un-stabilized zirconia requires smaller and a most refined grain size range [1] (Figure 2.8). For a 3 mol% YSZ, the critical grain size is approximately 1 μm, and for a content of 2 mol% YSZ, the critical grain size decreases to approximately 0.2 μm [6].

Thus, the amount of zirconia stabilizer is a crucial detail to attain when selecting a zirconia grain size. As previously mentioned, finer, and smaller grain sizes are optimal to achieve better mechanical properties and aging resistance. However, this grain size should be able to trigger and maintain the toughening mechanism presented by tetragonal zirconia.

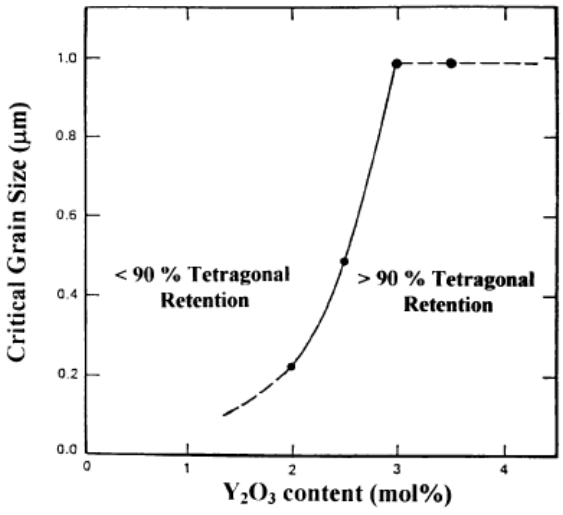


**Figure 2.8 - Critical Grain Size *versus* yttria content in tetragonal zirconia** [6]**.**

Unfortunately, the content of yttria can initiate low temperature degradation. Despite the good mechanical properties presented by Y-TZP in comparison with those presented by Ce-TZP, various authors reported that, due to its trivalent character, this stabilized zirconia shows a higher diffusion rate of species from water, comparing with other zirconia ceramics, like $CeO_2$-doped $ZrO_2$ .Due to the yttria doping, the water species can locate the oxygen vacancy sites present on the surface of the material [38], [53]. The consequent penetration of water radicals leads to a lattice contraction, with the resulting formation of tensile stresses that compromise the stabilization of the tetragonal phase grains [9], [17].

It has been reported that the optimum concentration of yttria, for zirconia-alumina composites (which no adverse effect would be produced) is 2 mol% [9], [11]. Magnani *et al* [11] reported that, for this concentration of yttria, in composites with 50% of zirconia and 50% alumina, it is possible to obtain the best results for fracture toughness, and, for contents higher than 3 mol% of yttria, the fraction of transformable tetragonal phase starts to decrease, as it can be verified in the $ZrO_2$-$Y_2O_3$ phase diagram (Figure 2.9). Therefore, with the decrease of tetragonal phase, the toughness of the composite will also decrease, since there is a decline in the transformability of zirconia.

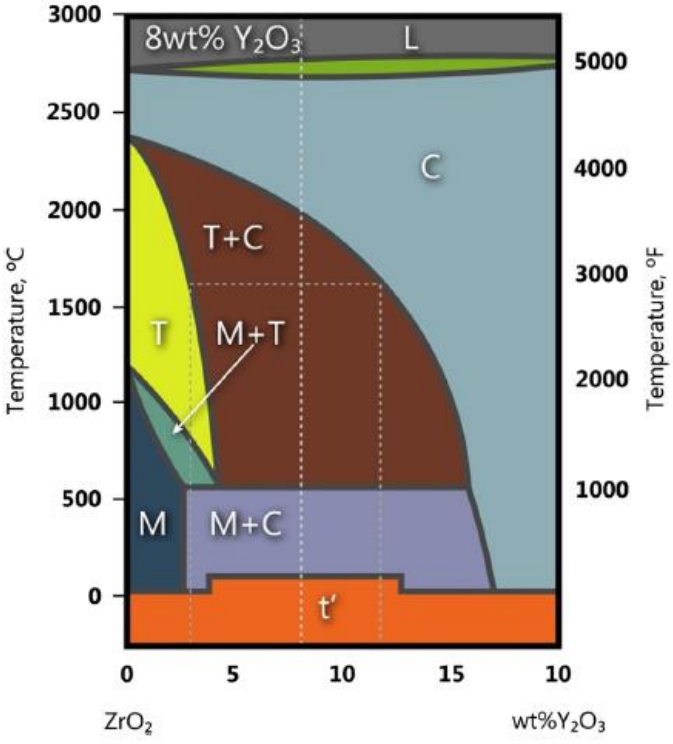


**Figure 2.9 - $ZrO_2$-$Y_2O_3$ phase diagram, where T=tetragonal, M=monoclinic, C=cubic and L=Liquid phase from** [9], [54]**.**

In the presence of an alumina matrix (ZTA), the tetragonal phase of zirconia becomes more stabilized since that, there is no need of a superior amount of yttrium oxide

to stabilize the zirconia. However, the grain size and microstructure must be controlled in order to still achieve good mechanical properties and aging resistance.

On the contrary, when the composite contains a higher amount of zirconia, an ATZ, (which have a zirconia matrix) there are more chances to occur the transformation to monoclinic zirconia. Even though alumina also plays a role in the stability of the zirconia matrix it can be assumed that a higher quantity of yttria is needed, in order to stabilize this higher amount of zirconia.

## 2.4 Additives

Various additives have been tested in order to enhance the mechanical properties and/or provide additional stability against Low Temperature Degradation to stabilized zirconia and zirconia alumina composites. Some examples of these additives are presented, alongside with the reported effects on the characteristics of these ceramics.

### 2.4.1 Strontium Aluminate

Strontium aluminate is used as platelet-like crystals that can block or deflect crack growth [9]. It is reported that these crystals increase the toughness of the composite and diffuse crack energy [9], [55]. With only 3% of the total volume (and a maximum length of 3 μm), these crystals can be formed in the shape of rods that possess higher crack propagation [56]. With the addition of these structures to ZTA composites, the composite becomes more reliable, with enhanced fracture toughness [1], [9] (Figure 2.10). Kuntz [56], [57] stated that, if the average distance between tetragonal zirconia grains is approximately 0,2 μm, (which is similar to the grain size), the reinforcement is activated immediately as soon as any microcrack is initiated.

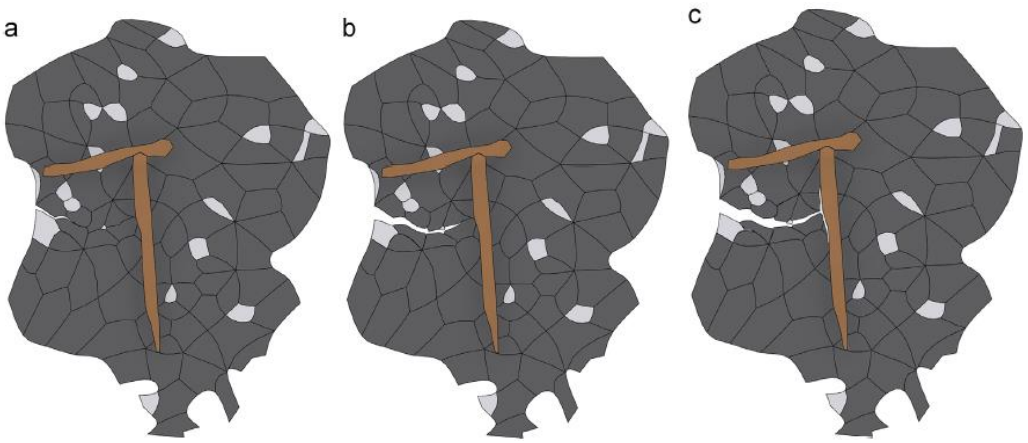


**Figure 2.10 - Strontium Aluminate rods as a reinforcement agent for zirconia alumina composites, from** [9], [58]**.**

In another study by Oungkulsolmongkol *et al* [59] the same results were achieved, since the fracture toughness of a ZTA composite showed an increase. Several compositions were tested and the best results for fracture toughness were achieved for a ZTA with 40 vol% of zirconia and 2 vol% of strontia (Figure 2.11). However, it was reported that, although the fracture toughness has, in fact, an increase, the formation of the hexaluminate could result in a porous microstructure that decreases the hardness of the composite. So, the author reported that the optimum content of strontium hexaluminate must be around 2 vol% relatively to the amount of alumina [59].

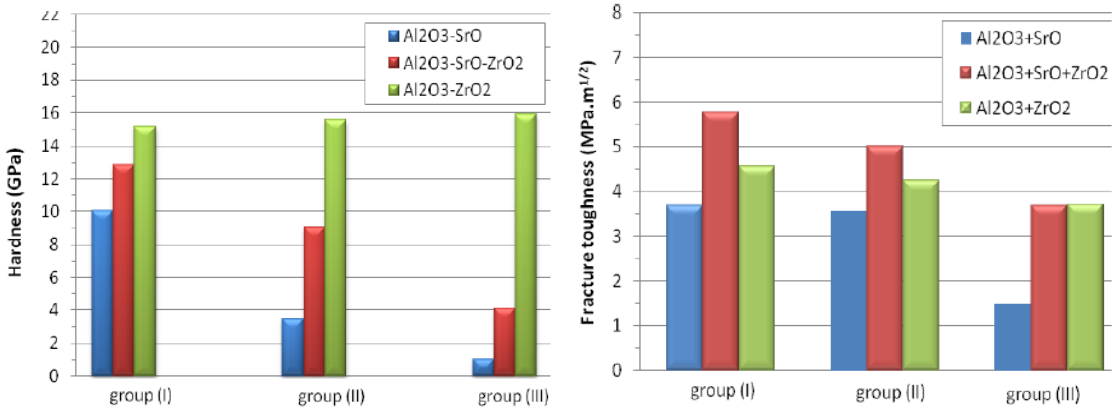


**Figure 2.11 - Hardness and Fracture Toughness - a comparison between various compositions. Group I: Alumina with 40vol% of zirconia; Alumina with 2vol% of strontia. Group II: Alumina with 30vol% of zirconia; Alumina with 5vol% of strontia. Group III: Alumina with 20vol% of zirconia; Alumina with 15vol% of strontia** [59]**.**

This dopant is also used in some commercial brands of zirconia alumina composites in order to enhance its fracture toughness [56], [58].

### 2.4.2 Chromia

The use of chromia is linked to an increase of hardness and wear resistance of the zirconia alumina composites [55]. With this oxide, the tetragonal phase content on the surface shows a slower decrease with the increasing time, which means that, the aging effect will be contained [60]–[62]. Azhar *et al* [62] reported that, with the addition of chromia, the monoclinic zirconia decreases, as evaluated by XRD (Figure 2.12). Stefanic *et al* [61], knowing that the oxygen-deficient surface sites initiate the tetragonal to monoclinic transformation, concluded that $Cr_2O_3$ will cover those sites, resulting in an increased stability of the tetragonal fraction. Also, G.Pezzotti *et al* [60] verified that, in the presence of this dopant, the oxygen vacancies are less concentrated in the matrix.

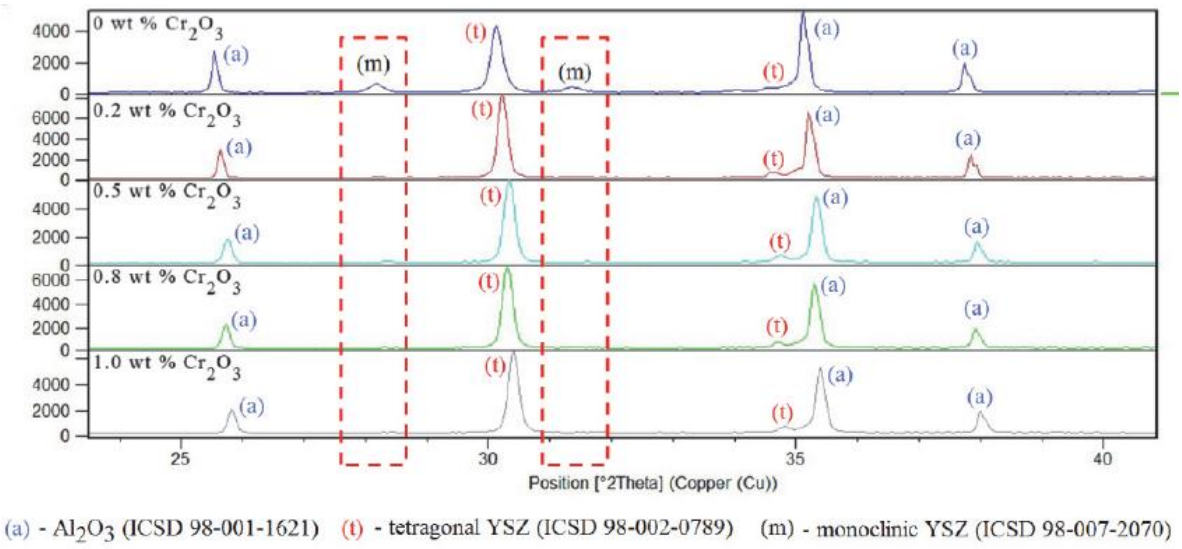


**Figure 2.12 - Comparison of XRD results of various composites with different amounts of chromia** [62]**.**

Basically, this oxide increases the protective effect of the composite, which becomes more resistant to hydrothermal degradation. The hydrothermal attack will be reduced in yttria stabilized zirconia ceramics doped with chromia, due to the strong interaction between zirconia and chromia, which prevents the diffusion of oxygen in zirconia [9], [60]. In fact, alumina seems to have an effect of "self-sacrifice" inducing the trapping of moisture on its surface, protecting tetragonal zirconia, at the expenses of a fast formation of oxygen vacancies in the (Cr doped) $Al_2O_3$ matrix lattice [60].

Magnani *et al* [11], also stated that the addition of chromia leads to an increase in toughness with no change in hardness for composites with different zirconia and alumina contents. When chromia is added to alumina, an isovalent solid solution is formed, since that they are both sesquioxides and present the same corundum crystal structure [11],

[62]. This factor will lead to materials with high refractoriness and chemical stability. Due to this fact, it was reported that the addition of $Cr_2O_3$ have a beneficial effect on alumina mechanical properties, with an increase of hardness, fracture toughness and tensile strength. Figure 2.13 shows the results presented by Azhar *et al* [63]. The fracture toughness of a ZTA composite (with an 80/20 wt% ratio of alumina and zirconia) increases with the amount of chromia, reaching a maximum value of 5.36 MPa.m$^{1/2}$ for 0.6 wt% of this oxide. This author also demonstrated that, with further addition of chromia, fracture toughness would result to reach to a stable value, around 5.3 MPa.m$^{1/2}$ [62]. Riu *et al* [64] also reported that the fracture strength tends do decrease with additions of chromia higher than 3 mol%.

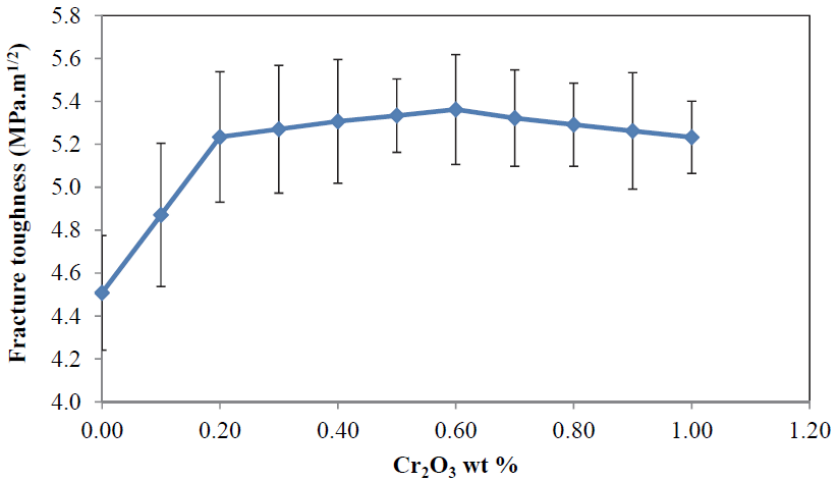


**Figure 2.13 - Fracture toughness of ZTA (80/20 ratio of alumina/zirconia) composites doped with different amounts of $Cr_2O_3$, from** [62]**.**

### 2.4.3 Pentavalent Oxides

Various authors also studied the addition of pentavalent oxides, such as $Nb_2O_5$ and $Ta_2O_5$ to ZTA materials [46], [65]. It has been reported that the addition of these oxides is positively correlated with the increase of bulk density and therefore decrease of porosity in bulk materials. Thus, with an increase of density, the mechanical properties of these composites were enhanced. The fracture toughness, bending strength and Vickers Hardness increased with the amount of $Nb_2O_5$ and $Ta_2O_5$ in the composite. However, small fractions of monoclinic zirconia were always present in the composites with both additives. The transformability of zirconia has also increased with the amount of both additives, when compared to the undoped samples, as the tetragonal phase tends to decrease

(Figure 2.14). This can be due to the annihilation of the oxygen vacancies and consequent overcrowding of the oxygen in tetragonal $ZrO_2$, which will lead to an increase of strain in the tetragonal lattice. So, these oxides increase the transformability of zirconia, which explains the enhanced mechanical properties. However, the monoclinic content may be a concern in the addition of these oxides in biomedical grade zirconia alumina composites, since this transformability could lead to a premature degradation of the ceramic. Thus, the amount of one of this pentavalent oxides should be carefully selected in order to obtain the enhanced mechanical properties without jeopardize the aging resistance.

In terms of biocompability, results indicate that niobium and tantalum are non-toxic materials and when added to Yttria Stabilized Zirconia, both can be considered biocompatible materials [66].

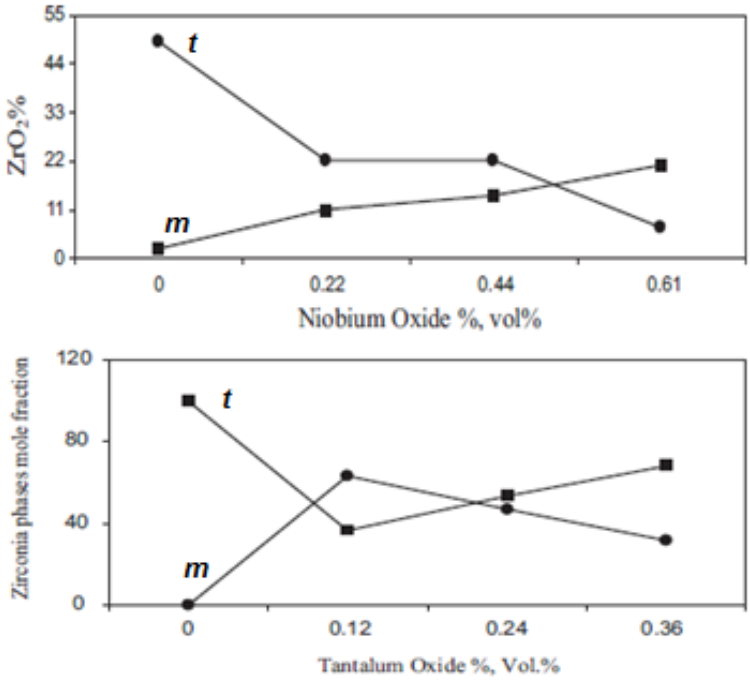


**Figure 2.14 - Effect of $Nb_2O_5$ and $Ta_2O_5$ on the transformability of fired bodies (ZTA composites with 95vol.% of alumina and 5vol.% of yttria stabilized zirconia)** [46], [65]**.**

### 2.4.4 Lanthana

In order to protect the tetragonal phase of zirconia against the Low Temperature Degradation, lanthana in dopant amounts, was also tested [50]. As previously mentioned, like $Y^{3+}$, $La^{3+}$, a ternary oxide, can decelerate the tetragonal to monoclinic transformation of zirconia since these cations with a lower valence than $Zr^{4+}$ produce oxygen vacancies

that maintain the charge balance. Because of the difference in ionic radius, these oxides also influence the grain boundary segregation, which delays the degradation [50], [67], [68].

In the study of Nogiwa-Valdez [50], lanthanum oxide and alumina were added to 3% yttria stabilized zirconia (0.1 wt% each). This doping did not result in a significant change of the mechanical properties, grain size or density; however, good results were achieved regarding hydrothermal degradation resistance. After exposure to heated steam (180ºC and ~900 kPa), the first detection of low temperature degradation was made by Atomic Force Microscopy, revealing that individual surface grains displayed monoclinic symmetry. The degradation progressed, in adjacent grains, forming monoclinic clusters that grew in radial direction and circular shape. It is reported that, after 24 hours of exposure, the surface of the control sample (with undoped zirconia) reached saturation, and, after 72 hours, the surface delaminated and material fractured. However, the addition of alumina and lanthana stopped the degradation progress and thus, the failure of the ceramic. The addition of both these oxides reduced substantially the nucleation rate and the growth of the monoclinic clusters (Figure 2.15). Cross sections of the samples were made in order to verify the bulk progression of the degradation. In comparison with the control material, the addition of lanthana and alumina significantly stopped the progression after 72 hours of exposure, showing a monoclinic layer with 4.6 µm, against 41 µm presented by the undoped stabilized zirconia.

The same authors also reported that, the addition of lanthana also changed the transformation kinetics, since the grains were only partially transformed, which led to a reduction of the surface microcracking.

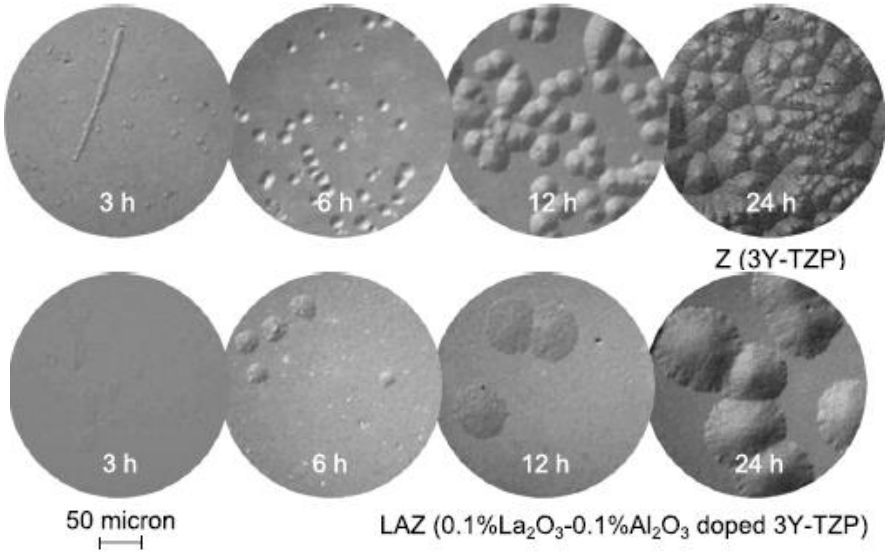


**Figure 2.15 - Optical Microscopy images of a sample of un-doped zirconia (3Y-TZP) and lanthana/alumina doped zirconia (LAZ) after hydrothermal tests** [50]**.**

In another more recent study [69], this anti-aging property of lanthana is again confirmed. It was reported that when lanthana is used as a dopant, cation segregation occurs on grain boundaries which promotes a stronger binding of the oxygen vacancies and highly contributes to maintain the stability in deleterious conditions. This dopant also inhibits the grain growth of zirconia which is concomitant with higher an aging resistance. Thus, it was also reported that the aging resistance increased with an amount of lanthana between 0.2 mol% and 0.4 mol%. Beyond this value the aging resistance starts to decrease and a secondary phase, $La_2Zr_2O_7$, precipitates for amounts higher than 1 mol%, which is even more deleterious, since a formation of a new phase is followed by a decrease in density. An aspect to take in consideration while using this dopant is the densification. In this study, when using such a little amount of lanthana as 0.02 mol%, the sintered piece (1500ºC for 2 hours) was not fully densified which affected the mechanical properties. The authors reported that, with the addition of 0.1-0.4 mol% of lanthana and 0.1-0.25 wt% of alumina, fully densified pieces can be achieved when sintered for 2 hours at 1450ºC or 1500ºC.

Regarding mechanical properties, in this study, a combination of 0.2mol% of lanthana and 0.1 to 0.25 mol% of alumina in a 3 mol% Yttria Stabilized Zirconia presents good mechanical properties when compared to a commercialized zirconia. Enhanced hydrothermal degradation resistance was also achieved in these doped composites (Figure 2.16).

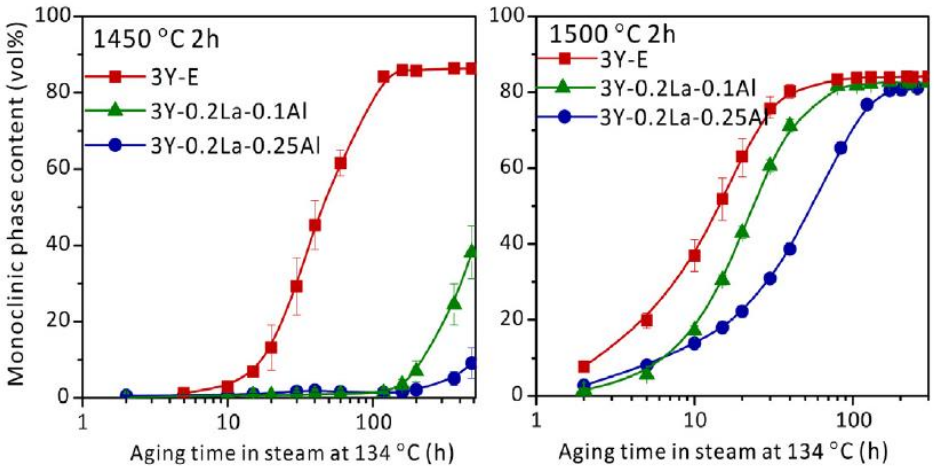


**Figure 2.16 - Aging resistance of two types of zirconia with lanthana-alumina co-doping in comparison with a commercial grade zirconia (3Y-E) with 0.25 wt% alumina, sintered at 1450ºC and 1500ºC for 2 hours** [69]**.**

### 2.4.5 Manganese Oxide

It has been reported that the inclusion of transition metal oxides, like manganese oxide, can improve the densification of zirconia and its resistance to degradation [70], [71]. The densification caused by the addition of manganese its due to the decrease of diffusion activation energy caused by the solid solution of $MnO_2$ in the $ZrO_2$ crystal. Manganese cations substitute the zirconia sites that will cause fast diffusion paths within single grains upon sintering [71]. Thus, a compact surface is observed with the addition of $MnO_2$.

Published studies from Ramesh *et al* [71], [72] showed that the addition of an amount of $MnO_2$ higher than 0.05 wt% to a 3 mol% yttria stabilized zirconia, highly increases its bulk density, at lower sintering temperatures (below 1400ºC). However, with the addition of 1 wt% of manganese, the bulk density presents the opposite results. When sintered beyond 1300ºC, the formation of the zirconia cubic phase in the tetragonal matrix is detected, which leads to a decrease in density. With the increase of bulk density, an increase of stiffness was also reported. Higher values of Young's Modulus were achieved, at low sintering temperatures. Regarding hardness, the addition of manganese oxide had a beneficial effect, since the doped samples reached higher values than the undoped ones, also at lower sintering temperatures. The maximum value of hardness (13.7 GPa) was achieved at a sintering temperature of 1400ºC, with the addition of 0.05 wt% of manganese oxide. The biggest difference is verified between the values of hardness achieved when sintering at 1250ºC, where the undoped sample achieves 9.7 GPa, and

the doped sample (with 0.5 wt% of $MnO_2$) reaches 13.6 GPa. Nevertheless, beyond 1400ºC, the hardness of all samples started to decrease. The fracture toughness did not present a significant increase, unless for the 1 wt% manganese doped zirconia, which increased from 5.3 MPa.$m^{1/2}$ at 1450ºC, to 7 MPa.$m^{1/2}$ at 1500ºC, which was due to a quick response of the metastable tetragonal zirconia grains to the induced stresses created during indentation. The aging resistance was highly enhanced with the addition of this oxide. In fact the doped sample with 0.5 wt% did not undergo phase transformation during the aging tests (180ºC/10 bar for 24 hours), which demonstrates that manganese oxide can slow the kinetics of aging, by prevent the hydroxyl reactions from occurring in tetragonal zirconia (Figure 2.17).

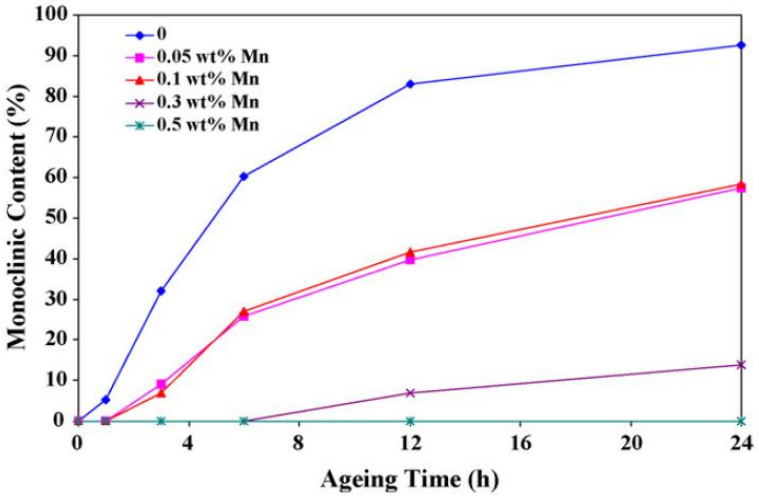


**Figure 2.17 - The effect of hydrothermal aging on the monoclinic phase development in Y-TZPs sintered at 1350 ºC** [71]**.**

Similar results were also reported by Zhou *et al* [70], where the addition of manganese to 8 mol% yttria stabilized zirconia, highly increase its relative density. Grain growth occurred with the addition of this oxide, since the average size for the doped sample with 1 wt% of $MnO_2$ was 0.3 µm, and 2.5 µm for the sample with 5 wt% of $MnO_2$. No second phases were reported, and a highly dense microstructure was achieved. Bending strength and Vickers hardness improved with the addition of manganese oxide to zirconia. Just like the results of Ramesh *et al* [71], [72], higher values were achieved at lower sintering temperatures (from 1200ºC to 1300ºC). The maximum value of hardness was approximately 1800 HV, for the 5 wt% $MnO_2$ doped sample, sintered at 1400 ºC, while the highest bending strength was approximately 230 MPa for the 3 wt% $MnO_2$ doped sample, sintered at 1300 ºC.

### 2.4.6 Ceria

Besides being tested as a stabilizer for zirconia, ceria has also been tested as a dopant, in order to improve the mechanical properties of Y-TZP. It has been found that the addition of ceria increases the fracture toughness of yttria stabilized zirconia, and zirconia alumina composites [73], [74]. However, the amount of used ceria must be carefully controlled. It was reported that, with the increase of ceria, the material porosity tends to increase, and therefore, the bulk density and strength of the material decreases [73], [75].

In the work of Ragurajan *et al* [73] the best results for fracture toughness were achieved when 0.5 wt% of ceria was added to 3 mol% of yttria stabilized zirconia, sintered at 1400ºC, reaching 6.4 $MPam^{1/2}$, against 5.3 $MPam^{1/2}$ for the undoped samples. This sample also presented the most homogeneous microstructure, with a smaller grain size. The highest value for the Vickers Hardness (1346 HV) was achieved for the sample containing 0.5 wt% ceria at a sintering temperature of 1400ºC. This sample also reached the highest value of density at this sintering temperature, which certainly explains the enhanced value for hardness.

Regarding the addition of ceria to ZTA, Rejab *et al* reported that, with an addition of ceria higher than 10 wt% to a ZTA (with 80 wt% of alumina and 20 wt% of 5.4 mol% yttria stabilized zirconia), results in a decrease of density, due to the presence of the phase $Ce_2Zr_3O_{10}$ [74]. The best results were achieved for the 5 wt% of $CeO_2$ doped ZTA, reaching 8.38 $MPam^{1/2}$ of fracture toughness, which is a result of the good solid solubility between $Ce^{4+}$ and $Y^{3+}$ in the phase $(Zr,Y,Ce)O_2$, that stabilizes the tetragonal to monoclinic transformation in the composite. Vickers Hardness also reached a maximum value (1688 HV) for this amount of ceria, which could be attributed to a higher densification.

Since ceria has also been used as a tetragonal zirconia stabilizer (previously mentioned in section 2.3 of this document), it has been reported that the monoclinic zirconia decreases with the increasing amount of ceria [76].

### 2.4.7 Magnesia

Just like ceria, been tested as a stabilizer, magnesia can be applied in zirconia alumina composites to enhance their mechanical properties. It has been reported that the addition of magnesia to alumina limits the grain growth by lowering the grain boundary mobility and surface energy of the grains, and increasing the surface diffusivity and

densification [77]. Therefore, an increase of density will indicate an increase of hardness [78], [79].

When added to a ZTA composite, an increase of hardness is also observed [63], [79]. Although the alumina grain growth in the composite is affected, the addition of MgO does not affect the yttria stabilized zirconia. However, when the content of this oxide exceeded 0.7 wt% in a ZTA (with 80 wt% alumina and 20 wt% yttria stabilized zirconia) the pinning effect of magnesia decreased, and alumina grains became larger, thus decreasing the composite density [63]. Regarding fracture toughness, it shows a decrease, with the addition of magnesia [63], [79], confirming this oxide intrinsic nature of low fracture toughness. Also, the smaller grain size of alumina, resulted in a decrease of intrinsic toughness due to the reduced load bridging capability of smaller grain bridges [80]. Thus, although an increase in hardness is observed, the fracture toughness of the composite is hindered which is not beneficial to these ceramic materials that need to be reliable.

### 2.4.8 Titania

Titania has been tested alongside with both zirconia and alumina, in order to improve its mechanical, thermal and electrical properties [81]–[83]. However, in the past few years, small additions of titania to zirconia alumina composites have also been experienced [84]–[86].

It has been reported that titania promotes the grain growth of alumina and consequent densification. This densification mechanism is a result of enhanced diffusivity created by the substitution of $Al^{3+}$ ions by the $Ti^{4+}$ ions, which creates $Al^{3+}$ vacancies [85], [87], [88]. However, if the addition of titania is increased beyond its solubility limit, from 0.15-0.35 mol%, the opposite effect is observed, due to the formation of a new phase, aluminum-titanate ($Al_2TiO_5$) [87]–[89].

This oxide also influences the mechanical properties of alumina. Wang *et al* [85] reported that the hardness of an $TiO_2$ doped alumina (that contained 5 wt% of zirconia) decreased with the increasing amount of $TiO_2$ (from 2.0 to 4.0 wt%) which was attributed to the formation of secondary phases, like $ZrTiO_4$ and $Al_2TiO_5$. Regarding fracture toughness, with the addition of 0.5 wt% of $TiO_2$, an increase of 18% has been noticed, in comparison with the undoped specimens. The same author also confirmed that the addition of this oxide to alumina, effectively lowers the sintering temperature, without significantly lose its relative density.

Concerning Y-Ti-TZP, these systems have been developed mostly in order to improve the electrical properties of stabilized zirconia [81], [90].

It has been reported that the addition of titania can also have a stabilizing effect in tetragonal zirconia, since its addition leads to a decrease of cubic zirconia formed during sintering and also lowers the sintering temperature, as occurs also for $TiO_2$ doped alumina [81]. The hardness tends to decrease with the addition of $TiO_2$ however, this difference becomes meaningless for sintering temperatures above 1650 ºC. A small increase in fracture toughness has also been reported, which can be related to the stability of the tetragonal phase, promoting the transformation toughening mechanism [81]. Also, in the work of Zhao *et al*, no monoclinic phase was detected by both X-ray diffraction and Raman spectra, of $TiO_2$-doped YSZ specimens after been submitted to tests of hydrothermal aging [82].

The addition of $TiO_2$ had been recently tested in zirconia alumina composites, and it has been encouraged since it promotes a higher grade of densification and a finer homogeneous structure, which is an important factor to take into account in these composites. However, the results are very similar than those achieved in both $TiO_2$ doped zirconia, and alumina. The densification is improved with the addition of titania, however, the formation of liquid phases for larger amounts of this oxide (8 wt%) was reported for these composites too [91]. The formation of $ZrTiO_4$ in samples with 5 wt% of titania (in a ZTA with 90 wt% of alumina and 10 wt% of 3 mol yttria stabilized zirconia) was also reported by Ormanci *et al* [92].

In a more recent work, from Manshor *et al* [84], it was observed that for a sample with 5 wt% of $TiO_2$ (in a 80 wt% of alumina and 20 wt% of a 5.4 mol% YSZ composite) the phase $Al_2TiO_5$ is detected in the X-ray diffraction spectra. This shows that titania was no longer merged into the $Al_2O_3$, since there was a reaction. Also, in this work, the solubility limit was reached at a 3 wt% of $TiO_2$ addition level, so beyond this value, the secondary phases were formed at the grain boundary, which was lead to a diminished densification. Regarding the mechanical properties of these $TiO_2$ doped ZTA composites, Vickers hardness gradually increased (approximately 6.6%), reaching a maximum value of 1616 HV for the sample doped with 3 wt% $TiO_2$. This sample also presented the highest value of density. The same was observed in fracture toughness tests, which significantly increased, and again, reaching a maximum value for the 3 wt% $TiO_2$ sample. With further addition of titania, a minor increment of the fracture toughness was also noticed (Figure 2.18). The slightly increase of fracture toughness presented by samples with more than 3 wt% of titania, was due to the formation of elongated grains of $Al_2TiO_5$ which, as

previously mentioned, compels the crack to travel in more than one plane, thus requiring more energy (Figure 2.19).

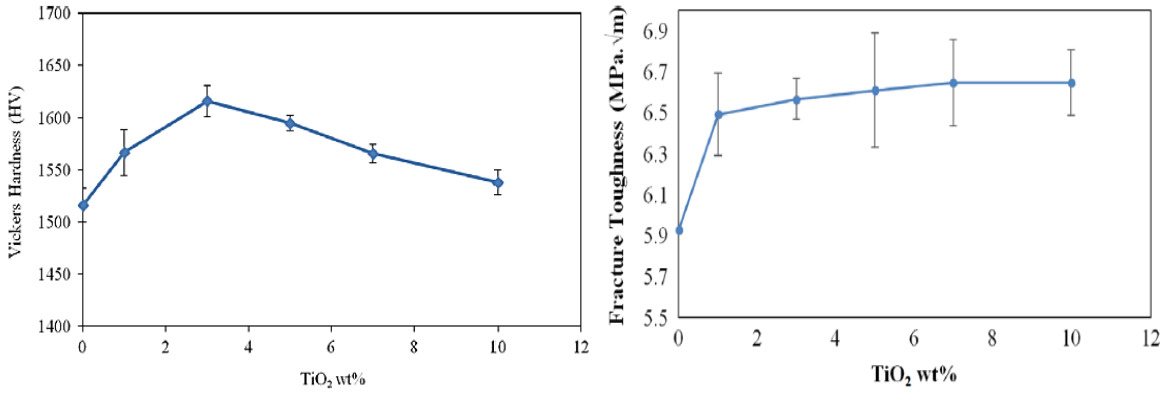


**Figure 2.18 - Vickers Hardness and Fracture Toughness as a function of $TiO_2$ content, in $TiO_2$ doped ZTA composites. Results presented by Manshor *et al* [84].**

These results are in agreement with the results published by Ormanci *et al* [92]. Besides the *in vivo* behaviour of these composites revealed that no clinical signs of inflammatory reaction such as necrosis or reddening were detected.

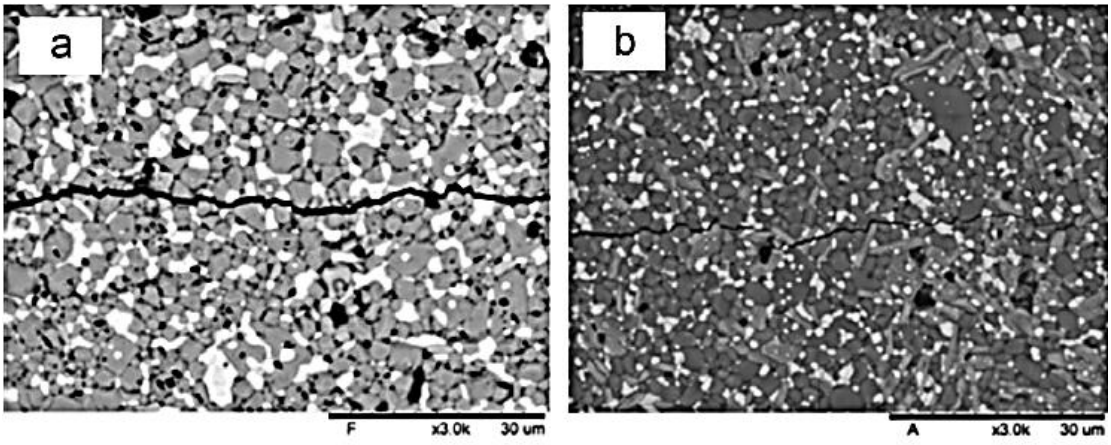


**Figure 2.19 - Microstructure of a) undoped ZTA and b) 7 wt% $TiO_2$ doped ZTA composite [84].**

### 2.4.9 Silica

Small quantities of silica had been tested as a dopant for tetragonal zirconia, in order to enhance its resistance to Low Temperature Degradation, without compromising its resistance to slow crack growth. It was reported that the addition of silica reduces the lattice strain, and therefore stabilize the tetragonal zirconia [93]–[97]. The internal stresses can facilitate the growth of monoclinc clusters, and extend the transformation to their vicinity. When silica is added to zirconia, a glassy phase at triple junctions appears, that

make the grains rounder. This consequently will lead to a reduction of the stresses at the grain corners, and a better performance against degradation.

Gremillard *et al* [94], [97] reported that, the addition of silica did not lead to an increase in fracture toughness; however, the resistance to degradation was highly improved. After 15 hours in steam environment, at 134ºC, the amount of monoclinic zirconia reached the maximum transformation (approximately 75%) in the control sample (3 mol% yttria stabilized zirconia), when the doped zirconia (with 0.5 wt% of silica) only reached 30% of monoclinic content, for the same period of time. The aging kinetics of the doped zirconia appears to be nearly constant with time, which is a result of a random transformation of grains, without inducing the transformation to neighbors [94].

Samodurova *et al* [95], achieved similar results. The additions of silica (of 0.05 wt% and 0.25 wt%) lead to the appearance of an amorphous silica phase at multiple grain junctions that made the grains rounder in shape. With the addition of either alumina or silica, the aging resistance improved with the decrease of monoclinic phase nucleation. Both transformed layers of monoclinic zirconia (formed after 24 hours of aging tests) were thinner than those presented by the un-doped zirconia sample, and presented less microcracking in the grain boundaries. However, good results were achieved when alumina and silica were combined, since they presented improved protection against aging without losing fracture toughness, before and after aging tests.

In another study conducted by Nakamura *et al* [93], it was shown that the flexural strength of samples of 3 mol% yttria stabilized zirconia doped with 0.2 mol% of $SiO_2$ increased, in comparison with the control sample of stabilized zirconia, for all the tested sintered temperatures (1400ºC, 1450 ºC and 1500ºC). This effect was also observed after aging tests, where silica doped samples were only weakened by less than 20% (Figure 2.20). The monoclinic formation rate was slower for the doped samples, in both surface and bulk, showing a thickness of monoclinic layer of only 12 µm against a layer of 36.7 µm for the un-doped sample, after 40 hours of aging.

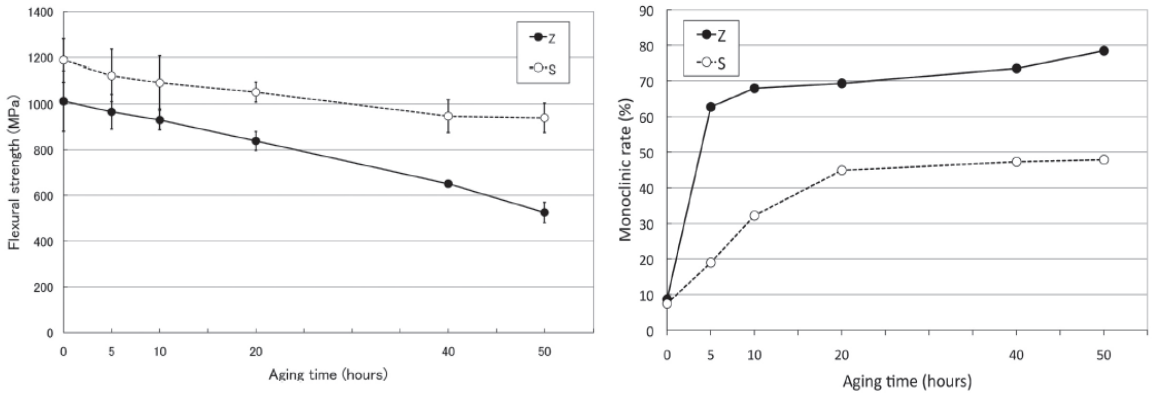


**Figure 2.20 - Flexural strength and monoclinic rate presented by samples of silica doped zirconia (S) and un-doped zirconia (Z) as function of aging time** [93]**.**

In the following Table, the researched additives for zirconia and zirconia composites are summarized, alongside with the produced effects on both mechanical properties and aging resistance.

**Table 2.3 - Additives for zirconia and zirconia composites.**

| Additive | Composition | Fracture Toughness | Hardness | Flexural Strength | Aging Resistance | *Obs.* |
|---|---|---|---|---|---|---|
| Strontia | ATZ(3 mol%yttria) + 2-5 wt% SrO [59] | 5.8 – 5 MPa.$m^{1/2}$ | 13 – 9 GPa | - | - | Density decreases with the amount of SrO |
| Chromia | ATZ(3 mol%yttria) + 0.2-0.6 wt% $Cr_2O_3$ [62] | 5.25 – 5.36 MPa.$m^{1/2}$ | - | - | $ZrO_{2(m)}$ decreases with the amount of $Cr_2O_3$ | Induces grain growth |
| | 50 wt%$Al_2O_3$ + 50 wt%YSZ( 3mol%)+ 0.5 wt% $Cr_2O_3$ [11] | 6.4 MPa.$m^{1/2}$ | 15.2 GPa | - | $ZrO_{2(t)}$ becomes more stable | - |
| Niobia | ZTA(5 mol%yttria) + 0.22-0.61 wt% $Nb_2O_5$ [98] | 5.4 - 6.19 MPa.$m^{1/2}$ | 1600 – 1792 HV | 260 – 298 MPa | For 0.51wt% of $Nb_2O_5$, there is a higher content of $ZrO_{2(m)}$ | Density increases with the amount of $Nb_2O_5$ |
| Tantalum Pentoxide | ZTA( 5mol%yttria) + 0.12-0.36 vol% $Ta_2O_5$ [65] | 5.7 - 7.19 MPa.$m^{1/2}$ | 1700 -1867 HV | 290-314 MPa | For additions higher than 0.22wt%, $ZrO_{2(t)}$ starts to increase | Density increases with the amount of $Ta_2O_5$ |
| Lanthana | YSZ(3 mol%yttria) +0.1 wt% $Al_2O_3$ + 0.1 wt% $La_2O_3$ [50] | 5.7 MPa.$m^{1/2}$ | 1305 HV | - | Enhanced protection against degradation | No considerable modifications on mechanical properties |
| | YSZ(3 mol%yttria)+ 0.1 mol% $La_2O_3$ + 0.25 wt% $Al_2O_3$ [69] | 6.02 MPa.$m^{1/2}$ | 1358 HV | 690 MPa | Aging resistances increases (until 0.4mol% of $La_2O_3$) | Mechanical properties similar to a control product |
| Manganese Oxide | YSZ(3 mol%yttria)+0.05-1 wt% $MnO_2$ [72] | 5 - 7.1 MPa.$m^{1/2}$ | 13.4 -13.7 GPa | - | Increases with the amount of $MnO_2$ | Increases bulk density at lower sintering temperatures |
| | YSZ(8 mol%yttria)+1-5 wt% $MnO_2$ [70] | - | 1400-1800 HV | 200-235 MPa | High tetragonal phase retention | - |
| Ceria | YSZ(3 mol%yttria)+0.5 wt% $CeO_2$ [73] | 6.4 MPa.$m^{1/2}$ | 1346 HV | - | - | Density drops at higher sintering temperatures |
| | ZTA(5.4 mol%yttria)+5 wt% $CeO_2$ [74] | 8.38 MPa.$m^{1/2}$ | 16.6 GPa | - | Stabilizes the tetragonal phase | Increased mechanical properties |
| Magnesia | ZTA(3mol%yttria)+ 0.7wt% MgO [63], [79] | 3.2 MPa.$m^{1/2}$ | 1710 HV | - | - | Limits the grain growth of alumina |
| Titania | ZTA(3 mol%yttria)+ 3-5wt% $TiO_2$ [92] | 5.1 - 5.3 MPa.$m^{1/2}$ | 16.7 – 17.3 GPa | - | - | Lowers sintering temperature |
| | ZTA(5.4 mol%yttria)+ 3 wt% $TiO_2$ [84] | 6.55 MPa.$m^{1/2}$ | 1620 HV | - | - | Increased mechanical properties |
| Silica | YSZ(3 mol%yttria)+ 0.25 wt% $Al_2O_3$ +0.25 wt%$SiO_2$ [95] | 4.6 MPa.$m^{1/2}$ | 14.6 GPa | - | Highly improved resistance | Don't affect the mechanical properties |

## 2.5 Biocompatibility

The lifetime durability *in vivo* of artificial hip joints generally ranges from 12 to 15 years [99] but it is expected to reach the 20 years, thanks to the improved bioceramics that have been developed through the past years [56].

All biomaterials that are intended for implantation must be strictly evaluated on multiple subjects like biocompatibility, mechanical properties, and *in vivo* scoring of the surgical outcome [56].

As previously mentioned, these implants are constantly exposed to wear, and therefore, debris are generated. These debris are the major initiating event that leads to aseptic loosening, periprosthetic osteolysis [99], decrease expression of type I collagen [100], alkaline phosphatase, osteocalcin and osteopontin by osteoblasts [101]. So in order to reduce wear, the use of nanosized particles has been advised. In fact, regarding alumina, particles with less than 100 nm present a less detrimental effect on osteoblasts function and adhesion [102], [103].

Since zirconia offers a great corrosion resistance, the ion *in vivo* release is considerably smaller when compared to metallic biomaterials that are more easily to corrode, and thus releasing ions that elicit adverse reactions in the surrounding tissue [50]. Oddly, the first results of biocompatibility studies on zirconia where firstly obtained *in vivo*, in 1969, and, only after, in 1990, results of *in vitro* tests were published [8]. Various authors verified that zirconia had no cytotoxic effect in fibroblast cell cultures, regarding different tests, like cell viability, and MTT assays [6], [104], [105]. Genotoxicity tests were also performed, and the absence of aberration in chromosomic patterns in cells cultured on zirconia was reported [8], [106].

Regarding Yttria Stabilized Zirconia, its biocompatibility has already been evaluated. It was reported that fewer bacteria accumulate around Y-TZP when compared to titanium [107], [108]. Dion *et al* [105], performed cell viability tests and MTT assays on 3T3 fibroblasts and HUVEC. It was concluded that this ceramic and its products had no harmful effect in both cell cultures and in contact with blood cells. Li *et al*, [104] reported the release of yttrium ions in *in vitro* tests, which was an indicator of material degradation. However, that effect was not reported *in vivo*.

Regarding *in vivo* studies, the biocompatibility of zirconia ceramics was evaluated by implantation in bone and in soft tissues. All tests performed on animals, in general reported the absence of local or systemic toxic effects after implantation [6].

Few papers have been published regarding *in vitro* or *in vivo* response to zirconia alumina composites. However, it has been reported. The proliferation of primary osteoblasts onto zirconia alumina composites was not significantly different than into commercial alumina samples [99]. Maccauro *et al* performed *in vitro* and *in vivo* tests on a ZTA composite. The *in vitro* results displayed no long-term carcinogenic effect [109]. Regarding the *in vivo* tests [110], where small cylinders of a produced ZTA were inserted on rabbits tibiae for 1,3,6 and 12 months, no radiolucence (which is an indirect sign of implant loosening) and nor tumors were detected. It was also verified that connective tissue was always present at the bone-implant interface. The authors concluded that the *in vivo* behavior of this material is similar to the one presented by zirconia and alumina alone. This similarity was also proved by Affalato *et al* [111]. He *et al*, reported cell adhesion and proliferation in ZTA foams, with an increase of these parameters in the surfaces that have been exposed to a soaking treatment that led to hydroxylation. Also, it was reported proliferation of fibroblasts and osteoblasts in alumina and zirconia particles in DMEM, and no cytotoxic effect [112].

## 2.6 Production Process and Commercialized Products

The current industrial production of femoral ball heads involves a series of controlled processes [14], [17], [113].

On the ceramic manufacturer, high purity raw powders are spray dryed and followed by a dry pressing stage. Cold isostatic pressing is applied to the green pieces, in order to increase their density. The sintering process suffered changes since Saint Gobain Desmarquest introduced yttria stabilized zirconia for orthopedic proposes in 1985 [14], [17]. When the recall of the hip joints occurred from 1999 to 2001, the industrial process was revised. Tunnel furnaces were used in order to reduce the processing time. However, it was found that, in 2000, these tunnel furnaces (with multiple heating chambers) influenced the reliability of the implants, since that the lots of implants sintered in these furnaces presented a higher failure rate [14]. When compared data retrieved from ball heads sintered in prior batch-type furnaces (which have a slower cooling rate) (Figure 2.21) a high failure rate was verified. It was found that, even though these furnaces provided a continuous sintering process which reduced the processing time, the applied thermal cycle and atmosphere created differences in the microstructure that lead to a lack of densification on the implant core.

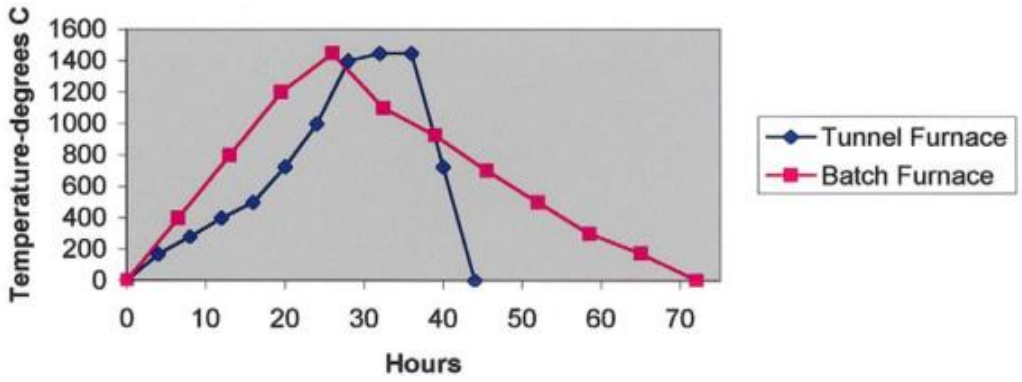


**Figure 2.21 - Sintering thermal cycles of Prozyr® BH (sintered on batch furnaces) and Prozyr® TH balls (sintered on tunnel furnaces)** [14]**.**

In order to highly increase the density and close some remaining porosity that could lead to a decrease on the aging resistance, a stage of Hot Isostatic Pressing is executed. In the machining unit, a polishing and machining stage is carried. Basically the ceramic balls are drilled so that the metallic stem can be inserted. This process must be carefully controlled because the drilling process can lead to residual stresses on the ceramic which can have a negative effect on the aging resistance and mechanical properties of the femoral head.

Sterilization and packing are the last stages before implantation in surgery environment. The sterilization is done on a gamma ultraviolet sterilizer by applying usually a minimum of 25 kGy. The sterile product package is then inspected for flaws before surgery. The various stages of this process are displayed on Figure 2.22.

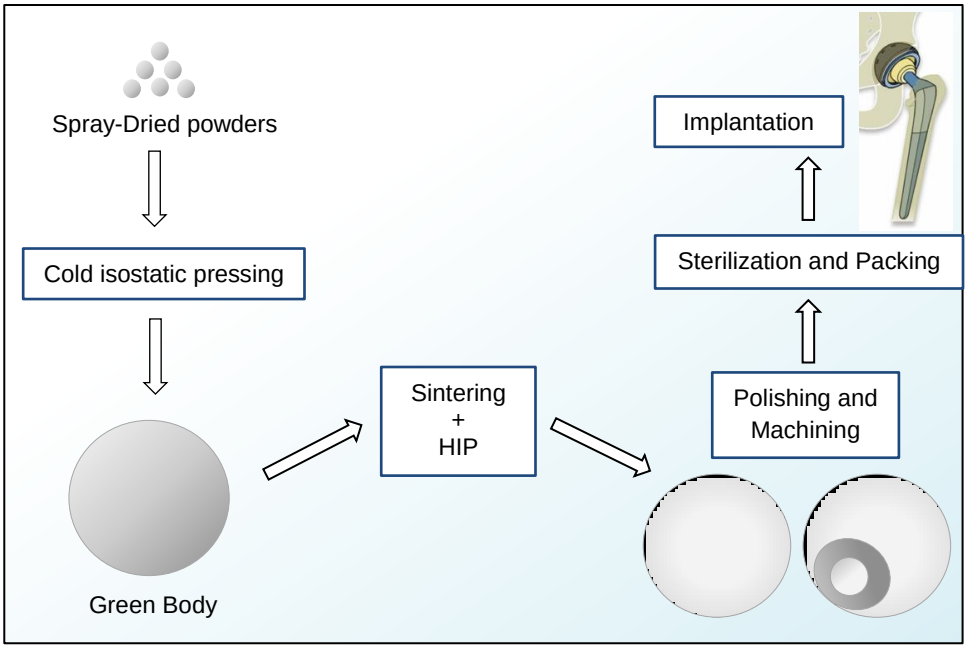


**Figure 2.22 - Synopsis of the manufacture process of zirconia ball heads, adapted from** [17]**.**

Presently, two zirconia composites for hip arthroplasty applications are produced (Table 2.3).

Commercialized by CeramTec AG (Plochingen, Germany), BIOLOX® delta was approved by FDA in 2003, and over 6 million of this femoral heads have been implanted worldwide. This manufacturer produces ZTA composites with 22.5 wt% of stabilized Zirconia, 76.1 wt% of alumina and 1.4 wt% of additives, on which chromium and strontium are included [1], [9], [58].

Another manufacturer, KYOCERA Medical (Osaka, Japan), produced a ZTA composite under the name of Bioceram®AZ209, firstly introduced in 2011. This product is currently on the market in Japan, and it contains 19 wt% of un-stabilized Zirconia, 79 wt% of Alumina and 2 wt% of unspecified additives [1], [9].

**Table 2.4 - ZTA hip implants - Manufacturers and product descriptions** [9]**.**

| Manufacturer | Product name | Availability | %Zirconia | %Alumina | Stabilizers | %Additives |
|---|---|---|---|---|---|---|
| CeramTec AG | Biolox Delta | Worldwide | 22.5 wt% | 76.1 wt% | Yttria | 1.4 wt% |
| Kyocera Medical | Bioceram, AZ209 | Japan | 19 wt% | 79 wt% | No Stabilizers | 2 wt% other (not specified) |

# Chapter 3

## Experimental Procedure

# 3. Experimental Procedure

In this chapter, the used materials and experimental work is summarized. This work can be divided in five parts: production of the composite granules by spray-drying; pressing and sintering of the composites; implementation of mechanical tests on the sintered pieces; aging tests (followed by another set of mechanical tests) and biocompatibility tests. The characterization techniques performed throughout the experimental work are also detailed. The characterization techniques used had the purpose of characterize the produced materials for their composition, structure, microstructure and mechanical behavior.

## 3.1 Materials

Two commercialized zirconia powders were used: 2 mol% Yttria Stabilized Zirconia (Innovnano) and 3 mol% Yttria Stabilized Zirconia (3YSZ, Innovnano) with a mean particle size of ~50 nm. The alumina powder (ABSCO materials, CR15: Batch 11254) was also provided by INNOVNANO.

Tantalum Pentoxide (Tantalum(V) Oxide, Sigma Aldrich, 99.99%), with a mean particle size of <20µm; and Lanthanum Oxide (Lanthanum(III) Oxide, Sigma Aldrich,>99.9%) were used as additives to the produced composites.

To adjust the pH of the suspensions accordingly to the results achieved from the zeta potential measurements, an HCl (0.5M) solution was used.

## 3.2 Preparation Methods

Aqueous suspensions of alumina and zirconia were prepared accordingly to the defined compositions for the zirconia toughened alumina and the alumina toughened zirconia composites, with and without dopants (lanthanum oxide, $La_2O_3$, and tantalum pentoxide, $Ta_2O_5$) (Table 3.1). These compositions have already been presented in section 1.1 of this document, defined accordingly to results published in literature.

**Table 3.1 - Defined compositions for the produced ATZ and ZTA composites.**

| | | Compositions |
|---|---|---|
| Undoped Compositions | ZTA | 10 wt% of 2 mol% Yttria Stabilized $ZrO_2$ and 90 wt% of $Al_2O_3$ |
| | | 15 wt% of 2 mol% Yttria Stabilized $ZrO_2$ and 85 wt% of $Al_2O_3$ |
| | | 20 wt% of 2 mol% Yttria Stabilized $ZrO_2$ and 80 wt% of $Al_2O_3$ |
| | ATZ | 10 wt% of $Al_2O_3$ and 90 wt% of 3 mol% Yttria Stabilized $ZrO_2$ |
| | | 15 wt% of $Al_2O_3$ and 85 wt% of 3 mol% Yttria Stabilized $ZrO_2$ |
| | | 20 wt% of $Al_2O_3$ and 80 wt% of 3 mol% Yttria Stabilized $ZrO_2$ |
| | | 20 wt% of $Al_2O_3$ and 80 wt% of 2 mol% Yttria Stabilized $ZrO_2$ |
| Doped Compositions | ZTA | 20 wt% of 2 mol% Yttria Stabilized $ZrO_2$, 80 wt% of $Al_2O_3$ and 0.35 wt% of $Ta_2O_5$ |
| | | 20 wt% of 2 mol% Yttria Stabilized $ZrO_2$, 80 wt% of $Al_2O_3$ and 0.1 wt% of $La_2O_3$ |
| | ATZ | 20 wt% of $Al_2O_3$, 80 wt% of 3 mol% Yttria Stabilized $ZrO_2$ and 0.35 wt% of $Ta_2O_5$ |
| | | 20 wt% of $Al_2O_3$, 80 wt% of 3 mol% Yttria Stabilized $ZrO_2$ and 0.1 wt% of $La_2O_3$ |

### 3.2.1 Preparation of the Suspensions

Before the preparation of the suspensions, the stability range for each material was determined by zeta potential measurement. The pH was adjusted in order to achieve a stabilized initial suspension for each composition.

To control the suspensions particle size, a stage of ball milling was performed. Spray drying was chosen to obtain the composite powders. The spray drying parameters were optimized during the early stages of this study.

#### 3.2.1.1 Zeta Potential

The zeta potential of the zirconia and alumina powders was measured in order to characterize the electrochemical equilibrium of the particles in the suspension in pursuance of a stabilized suspension.

This parameter gives an indication if the colloidal system is stable or unstable. For large negative or positive potentials, the particles tend to separate. Otherwise, for potentials near zero (isoelectric point) the particles agglomerate. The isoelectric point is associated to a value of pH. The appropriate pH of the medium was then determined, to avoid agglomeration of the particles on the suspension.

This parameter was measured on a Zetasizer Nano ZS (Malvern Instruments) (Fig.3.1). This equipment applies an electric field to dispersed particles, which forces them to move with a velocity related to their zeta potential. The achieved velocity is then measured by laser interferometry which allows the calculation of its electrophoretic mobility [114].


**Figure 3.1 - Zetasizer Nano ZS from Malvern, used for zeta potential measurements.**

The used dispersing medium was a solution of KCl (10 mL, $10^{-3}$M), and HCl (0.01M) and NaOH (0.1M) were added to adjust the pH of the suspension, so that various measurements of zeta potential for several values of pH could be taken, in the pH range of 3 to 10.

#### 3.2.1.2 Ball Milling

The aqueous suspensions were then prepared with the amounts of zirconia and alumina defined for each composite (wt%). From preliminary results the spray drying conditions were optimized. For the ATZ composites the aqueous suspension should have a solid content of 2%, while the ZTA composites the solid content should be 4%, in order to take advantage of the fully potential and maximum yield of the spray dryer.

The content of each powder was weighed on a precision lab scale (± 0.1 mg) in order to prepare the right amount of each material for the defined compositions.

The powders were then subjected to a deagglomeration process: distilled water was added to the powders (on the right proportion) on a nano bead mill, Dispermat® - SL12-nano (VMA) (Fig. 3.2), at 3500 rpm for 15 minutes each. This process was essential in order to achieve a controlled particle size distribution.

**Figure 3.2 - Nano bead mill Dispermat® SL-nano, available at INNOVNANO.**

The particle size distribution of the particles in aqueous medium retrieved from the mill was measured on a Mastersizer 2000 (Malvern) (Fig.3.3). After obtaining the particle size distribution, the suspensions were stored.

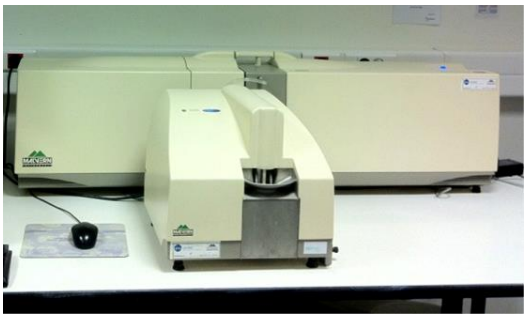

**Figure 3.3 - Malvern Mastersizer 2000, existing at INNOVNANO.**

### 3.2.2 Spray Drying Process

Before the spray drying process, the pH of the suspensions were measured, under stirring, and adjusted with HCl (0.5M) to an appropriated value (approximately 3), determined from potential zeta measurements. The composite granules were then obtained on a laboratorial spray dryer, Büchi Mini Spray Dryer B-191 with a 73 µm nozzle (Figure 3.4 - right).

Spray drying is a technical method used to dry aqueous solutions or emulsions, and it became widely used, from industrial chemistry to pharmacology research. This method basically involves the evaporation of moisture from an atomized feed, on a drying chamber, as the droplets of the spray come in contact with hot drying air. An intense heat and mass transfer occurs, and it is translated in an efficient drying process. This simple process also allows a complete control of the granule size, shape and morphology by changing some adjustable parameters like the inlet and outlet temperature, the feed rate of the peristaltic pump, and the flow rate of both spray and drying gas. The inlet temperature is the temperature of the heated drying air while the outlet temperature is the temperature of the air containing the particles at the entering of the cyclone. This last parameter can't be controlled but it is influenced by the other remaining parameters: the aspirator flow rate, the pump performance (feed rate), and the concentration of the suspension. The set of all these parameters can influence the temperature load, the final moisture of the product, the particle size and the yield of the process [115]. A schematic of this process and the used spray dryer can be seen in Figure (3.4-left).

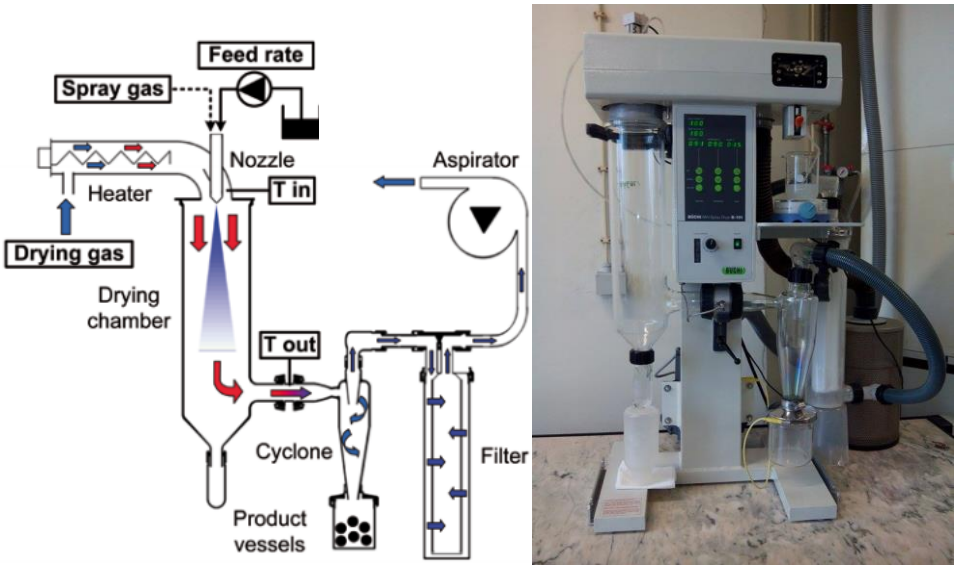


**Figure 3.4 - Left: Schematics of the spray drying process from** [115]**; Right: Laboratorial Büchi Mini Spray-dryer B-191 used.**

After a short period of optimization, the equipment parameters were adjusted in order to maximize the process yield. The stabilized spray-dryer parameters are displayed on the following table:

**Table 3.2 – Established parameters for Büchi Mini Spray-dryer B-191.**

| Parameter | Value |
|---|---|
| Inlet temperature (ºC) | 180ºC |
| Outlet temperature (ºC) | ~100ºC |
| Aspirator flow rate (%) | 95% |
| Pump Performance (%) | 20% |

The obtained powders were stored and a conformation process was followed.

### 3.2.3 Obtaining of the green bodies and sintering process

The spray dried powders were uniaxially cold pressed, in a hydraulic press, at 70 MPa. The green bodies had ~2 cm of diameter. Cylindrical powder compacts were achieved.

The obtained green bodies were then submitted to cold isostatic pressing (CIP) at 450 MPa, for fifteen minutes on a U33 high pressure system (Unipress Equipment) (Fig.3.5). An increase of the green bodies densification was expected with the performing of this additional stage of pressing.

**Figure 3.5 - CIP system used: U33 high pressure system from Unipress Equipment.**

The sintering temperature was selected after several tests. The pieces densification was analyzed after various sintering stages from 1350ºC to 1600ºC. Finally, the pieces were sintered at 1400ºC for three hours, performed in air, in a laboratory furnace. A sintering cycle with a heating rate of 2 ºC/min and a cooling rate of 5 ºC/min was applied. In Figure 3.6, a sintered piece is displayed.

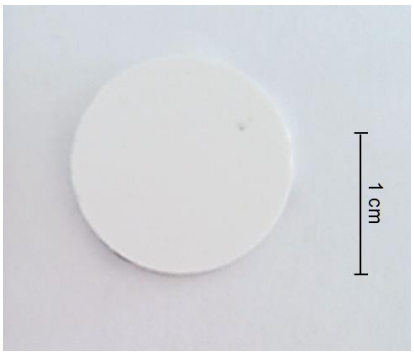


**Figure 3.6 - Superior view of one sintered piece.**

## 3.3 Mechanical tests

Mechanical tests were performed in order to fully characterize the obtained sintered pieces mechanical behavior. As previously mentioned, in the second chapter of this document, enhanced mechanical properties are essential for these ceramics for load bearing applications. Therefore, three different parameters were measured: biaxial flexural strength, Vickers Hardness and fracture toughness. Each one of these tests was performed in INNOVNANO.

### 3.3.1 Biaxial flexural strength

Biaxial flexural strength (or bending strength) is a meaningful characteristic to maintain in these ceramics. Strict requirements for this parameter are specified on ISO 13356(2008) [22]. This test allows the determination of the maximum stress and deflection of a material before its fracture.

Before this test, the sintered pieces were subjected to a fine polishing. For each composite, five pieces were used for this test.

A 3-point test (piston-on-three-ball) was performed to determine the biaxial flexural strength. A Testing Machine Zwick/Roell Z020 (Universal Materials) (Fig.3.7), was the used equipment.

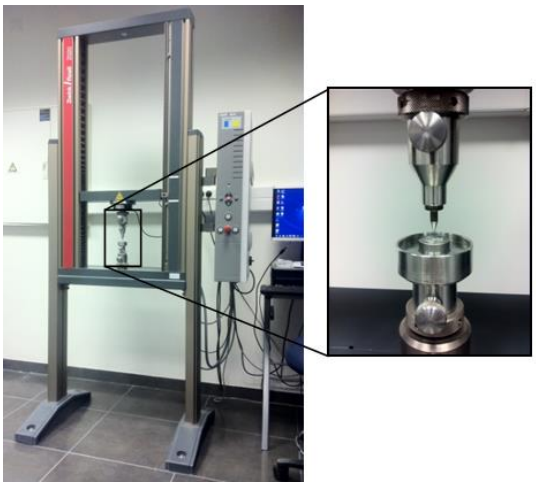

**Figure 3.7 - Biaxial flexural strength equipment: Testing machine Zwick/Roell Z020 from Universal Materials present in INNOVNANO.**

For each composite, the flexural strength values were achieved from five different measurements. The average value was then calculated.

### 3.3.2 Vickers Hardness

Indentation hardness of a material traduces its ability to resist to deformation caused by a constant compression load from a sharp object (indenter). Vickers hardness test is one of the most frequent indentation hardness test used. This test uses a square-based pyramid indenter with an angle of 136º between the opposite faces at the vertex. This indenter is pressed against the surface of the sample using a predefined force (*F*). This charge is maintained for 10 to 15 seconds. After the removal of the indenter, the diagonal lengths of the indentation are measured and the arithmetic mean is calculated. The Vickers hardness value (HV) is then given by:

$$HV = \frac{F}{A_{ind}} \qquad \text{(Equation 3)}$$

where *F* is the applied force in kgf and $A_{ind}$ is the surface area ($mm^2$) of the resulting indentation calculated from the following:

$$A_{ind} = \frac{d^2}{2sin\left(\frac{136^o}{2}\right)} \approx \frac{d^2}{1.8544} \qquad \text{(Equation 4)}$$

where *d* is the average length in millimeters of the diagonal caused by indentation. Therefore the *HV* can be calculated by:

$$HV = \frac{F}{A_{ind}} \approx \frac{1.8544F}{d^2} \qquad \text{(Equation 5)}$$

The *HV* value is then obtained by multiplying *F* by the standard gravity value (9.807 m/s$^2$) and by converting millimeters to meters.

The hardness of the sintered pieces was determined using a WIKI 100B system (Affri) equipped with Affri Fully Automatic System software (Fig.3.8). Ten Vickers indentations, using a 9.806N load, were performed in different pieces and surface points of each composite. The test force was maintained for 15 seconds in each indentation. The values were immediately obtained by software, and the average value was calculated from the ten different measurements.

**Figure 3.8 - WIKI 100B Vickers Hardness Tester available at INNOVNANO.**

### 3.3.3 Fracture Toughness

The fracture toughness ($K_{IC}$) of the composites was measured by crack indentation method. From the indentations left from the hardness tests, it was observed that the crack developed only at the corners of the indent. This type of crack which is named Palmqvist (type Pq), allowed a calculation of the fracture toughness based on Niihara equation [116], which is commonly used for the determination of this mechanical parameter on these ceramic materials. The following equation was applied:

$$3K_{IC} = 0.035\left(Ha^{\frac{1}{2}}\right)\left(\frac{3E}{H}\right)^{0.4}\left(\frac{d}{a}\right)^{-0.5} \qquad \text{(Equation 6)}$$

where *H* is the Vickers hardness, *a* is half distance of indent diagonal, *E* is the Young's Modulus, and *d* is the crack length. Optical microscopy was used to measure the crack lengths. Ten measurements were made and an average value was considered.

## 3.4 Accelerated aging tests

The aging tests were performed according to the International Standard ISO 13356(2008) [22], in order to evaluate the stability of the tetragonal phase under aggressive aging conditions, and predict the behavior of these materials *in vivo*.

This test was performed in CTCV Materials, in an autoclave, where the samples were exposed to steam under the specified conditions of temperature and pressure: 134 ± 2ºC, and 0.2 MPa. Several pieces of each composition were used, in order to achieve various times of degradation. Besides the 5 hour aging test, specified in the ISO document, the samples were exposed to this aggressive environment for 12, 24, 48 and 96 hours. The pieces surfaces submitted to aging were previously polished, using a 9, 3 and 1 μm diamond paste, on a Struers TegraPol-25 polishing machine existing at INNOVNANO.

## 3.5 Characterization Techniques

Throughout the duration of this study, several characterization techniques were used to fully characterize the produced materials. Firstly, the composite powders retrieved from spray-drying were characterized. With the implementation of conformation, sintering and aging on the initial powders, different characterization techniques were also performed. In the next section all the characterization techniques during the different stages of this study are presented.

### 3.5.1 Characterization of the spray dried powders

The obtained powders were characterized for content of crystalline phases, morphology, particle size distribution, specific surface area, density, and X-Ray fluorescence.

#### 3.5.1.1 Particle size distribution

The particle size distribution of the particles in suspension was measured on a Malvern Mastersizer 2000 (Fig.3.3). This equipment measures the size of the particles, in a well dispersed suspension, through laser diffraction. The intensity of the light scattered by the particles is measured regarding a certain number of angles and converted to a size number through an algorithm [117].

#### 3.5.1.2 X-ray diffraction

X-ray diffraction is an imperative technique to characterize the materials, since it allows the determination and quantification of crystalline phases. By this technique, other structural properties can be verified such as the lattice parameters, crystallite size and degree of crystallinity. By directing a monochromatic X-Ray beam to a material with regularly spaced atoms, each atom becomes a source of radiation. This phenomenon will create constructive and destructive interferences. A diffracted beam results from the constructive interferences. Bragg's Law expresses the relation between the diffraction angle and inter-planar spacing necessary in order to create constructive interferences:

$$n\lambda = 2dsin\theta \qquad \text{(Equation 7)}$$

where $n$= 1,2,3…$\lambda$ is the wavelength, $d$ is the inter-planar spacing, and $\theta$ the incident angle of the beam in the material. By varying the diffraction angle (2θ), the diffracted beam intensity will change and give rise to a diffractogram. The obtained diffractogram can be compared to Powder Diffraction Files (PDF files) from the International Center for Diffraction Data (ICDD).

The presence of crystalline phases was analyzed by X-ray diffraction, on a Rigaku Geigerflex D/Max-SerieC with Kα radiation (λ=1,54056 Å) in the 2θ range from 10º to 80º at room temperature.

The detected phases were posteriorly quantified on PANalytical software, X'pert HighScore Plus, with resource of Rietveld refinement and matching with ICDD files. This refinement uses a least squares approach to refine a theoretical result to a measured profile. The value of the Goodness of fit (GOF) was retrieved from the software. This value is the result of a statistic model that summarizes the discrepancy between the observed values and the ones expected under a statistical model [118]. The achieved value for

each phase quantification report was analyzed in order to understand the accuracy of this refinement.

#### 3.5.1.3 Scanning electron microscopy

Scanning electron microscopy (SEM) allows the obtaining of high resolution images of a sample surface at the nanometer scale. The obtained micrograph is caused by the interactions between the sample and the highly energetic electron beam that is emitted. Absorption, reflection and emissions of electrons occur and are detected creating contrast and therefore, an image.

The spray dried granules morphology was evaluated by SEM, on a HITACHI S-4100 microscope, provided with an electron emission system with a tungsten filament with 25 kV of acceleration, and 15 Á of maximum resolution. The powders were deposited on an aluminum sample holder, with carbon tape, and then covered with a carbon thin film, on a EMITECH K950 carbon sputter.

#### 3.5.1.4 Specific surface area

Specific surface area (SSA) is defined as the ratio $A/m$ ($m^2/g$) between the absolute surface area of a solid, $A$ (which includes all accessible inner surfaces such as pores) and its mass, $m$. In this work the SSA analysis method used was the Brunauer-Emmett-Teller (B.E.T.) method, which involves the determination of the amount of adsorptive gas required to cover the entire surface of a solid with a monomolecular layer [119]. The adsorptive gas is only physically adsorbed by van der Waals forces, and it is easily desorbed when a decrease of pressure occurs.

In this work, the specific surface area of the powders was determined using the multipoint Brunauer-Emmett-Tellerum (B.E.T.) isotherm in a Quantachrome Nova 1000e Series System, equipped with NovaWin software, present in INNOVNANO (Fig.3.9). $N_2$ was the absorbate gas used.

**Figure 3.9 - SSA equipment used: Nova 1000e Series System, from Quantachrome present in INNOVNANO.**

### 3.5.1.5 True density

To determine the true density (or more accurately the volume) of powders and bulk materials, gas pycnometers are the most commonly used equipment. This parameter is calculated from a measured drop in pressure when a defined amount of gas is allowed to expand into a chamber containing the sample. This analysis also includes closed porosity in the measured volume. A known mass of sample is placed into a cell of known volume. The introduced gas occupies the entire volume of cell (in vacuum) that is not occupied by the sample. The volume of the sample is determined, and thus the sample density. Due to its small size, helium is the most used gas [120].

Therefore, the composite powders true density was determined by this gas displacement method using an AccuPyc II 1340 (Micromeritics) helium pycnometer, available in INNOVNANO (Fig.3.10). The results achieved for each composition were obtained by the mean value of ten different cycles.


**Figure 3.10 - Pycnometer used: AccuPyc II 1340 from Micromeritics, present in INNOVNANO.**

#### 3.5.1.6 X-ray Fluorescence

X-ray fluorescence was also tested. This technique allows the elemental analysis of any kind of samples. When an incident X-ray collides with an atom from the sample, it will become unstable, inducing an ejection of an electron from low energy levels. This vacant space will then be occupied by an electron from a higher energy level. These changes in energy levels create differences of energy that will induce the release of secondary X-rays. These secondary X-rays are characteristic of the element. By analyzing these X-rays, a chemical composition analysis can be performed.

The chemical composition of each sample was assayed by a Bruker-AXS S4 Pioneer X-ray Fluorescence Spectrometer with a rhodium X-ray source, controlled by a SpectraPlus software, present in INNOVNANO (Fig.3.11).


**Figure 3.11 - X-ray Fluorescence Spectrometer (Bruker-AXS S4 Pioneer) used, present in INNOVNANO.**

#### 3.5.1.7 Dilatometry test

The thermal behavior of the samples was characterized by dilatometric analysis. This technique allows the verification of dimensional changes in a material throughout a specific temperature cycle, which allows the evaluation and selection of a proper sintering cycle. Through this analysis, the linear thermal expansion/shrinkage ($Y=\Delta L/L_0$) as function of temperature (ºC) is obtained.

This analysis was performed on a Thermoanalyse GmbH (BÄHR) with a heating rate of 20ºC/min, until 1485ºC.

### 3.5.2 Characterization of the green bodies and sintered pieces

After obtaining and characterize the powders, a conformation stage was carried out. All the techniques used for the characterization of the green and sintered pieces are described below.

#### 3.5.2.1 Density

The density of the green pieces was measured geometrically, given by the ratio between the weight and the geometric volume of the samples (geometric density):

$$GD = \frac{m}{\pi\left(\frac{d}{2}\right)^2 h} \qquad \text{(Equation 8)}$$

where *m* is the mass, *d* the diameter and *h* the height of the sample. The final green density of the samples was determined by considering a mean value for ten samples of each composition pressed under the same conditions.

The density of the sintered pieces (final density, $\rho_f$) was determined by the Archimedes' liquid immersion technique. The following equation was considered:

$$\rho_f = \frac{m_d}{m_s - m_i} \times \rho_{liq} \qquad \text{(Equation 9)}$$

where $m_d$ is the mass of the dried sample, $m_s$ is the mass of the soaked sample, $m_i$ is the mass of the immersed sample and $\rho_{liq}$ is the density of the immersion liquid. Distilled water was the immersion liquid used in this measurement. The final density value for each composition was obtained by the average of ten different pieces sintered under the same conditions.

#### 3.5.2.2 X-Ray diffraction

In order to investigate the presence of monoclinic zirconia on the sintered samples, X-ray diffraction was also made, on the same Rigaku Geigerflex diffractometer. Phase quantification was carried on X'pert HighScore Plus (PANalytical software) by means of Rietvel refinement.

#### 3.5.2.3 Scanning electron microscopy

The morphology and grain boundaries were observed by scanning electron microscopy (SEM). After sintering, the sintered pieces were polished on a Struers TegraPol-25 polishing machine, existing at INNOVNANO. To remove scratches and achieve a desired surface finish, the samples were firstly ground with abrasives, and then a fine polishing was performed using 9, 3 and 1 µm diamond paste. In order to properly observe the microstructure and grain boundaries, the samples were thermal etched in air at low temperature (100°C lower than the sintering temperature, heating and cooling rate of 10ºC/min, for 30 minutes). A ZEISS MERLIN Compact/VPCompact, Field emission scanning electron microscope (FDSEM) was used, in IPN (Coimbra) (Fig.3.12).


**Figure 3.12 - FDSEM used for observation of the samples microstructure: ZEISS MERLIN Compact/VPCompact, present in IPN, Coimbra.**

With the obtained micrographs, the grain size of each sample was measured, using the image processing tool ImageJ 1.48v, by the stereology's line interception method. A micrograph (for each sample) was used, always with the same amplification. In the following figure, the used method is presented.

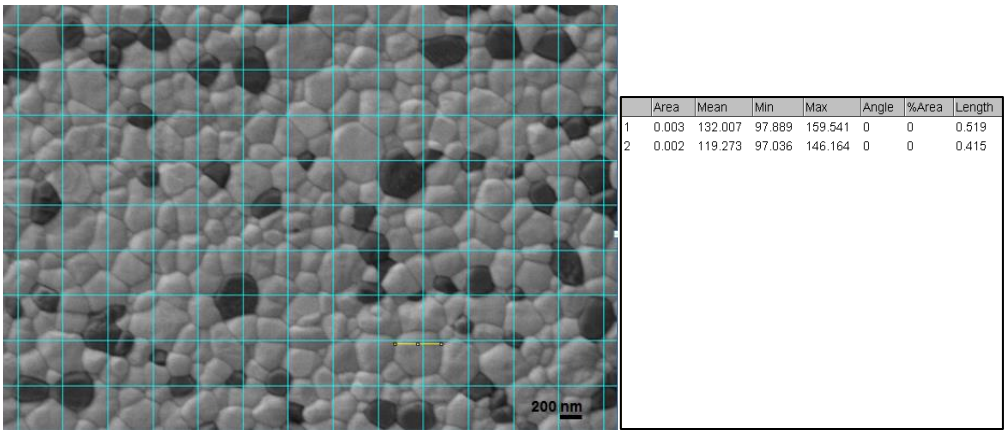


**Figure 3.13 - Grain size measurement by line interception method, on ImageJ software.**

Each grain was measured and it was assumed that the grains were spherical. The following equation was used:

$$\bar{G} = K\frac{\sum L}{N} \qquad \text{(Equation 10)}$$

where $\bar{G}$ is the mean grain size, $K$ is the correction factor which is 1.5 for spherical grains, $L$ is the length of the line interception and $N$ the total number of line interceptions. Two measurements for both zirconia and alumina were made for each micrograph used.

### 3.5.3 Characterization of the aged samples

In order to evaluate the aging resistance, the composite pieces were submitted to aging. The retrieved pieces were characterized using the techniques described below.

#### 3.5.3.1 X-ray diffraction

In order to evaluate the degradation of the samples after the aging tests, X-ray diffraction was performed on the polished surface of each piece. The diffractometer used was the same Rigaku Geigerflex D/Max-SerieC diffractometer. Phase quantification was performed on PANalytical's X'pert HighScore Plus.

#### 3.5.3.2 Scanning electron microscopy

To evaluate the extension of the degradation to bulk, a cross section view from a sample of the most degraded composition was observed by scanning electron microscopy. In order to cut the sample and expose its interior, a diamond wheel was firstly used to chip the sample. Various stages of polishing were applied to the cross section. Firstly, a rough polishing was performed to remove scratches and after that, a fine polishing was carried using 6, 3 and 1 μm diamond paste. The used polisher was a LaboPol-S, from Stuers. The HITACHI S-4100 microscope was used, and the samples were sputtered with carbon, on the EMITECH K950 carbon sputter.

## 3.6 Biocompatibility Tests

In order to evaluate the biological response of the produced composites, biocompatibility tests were accomplished. All the produced samples were submitted to these tests: the undoped ones: 80Z20A, 85Z15A, 90Z10A, 80A20Z, 85A15Z, 90A10Z and 802YSZ20A; and the $Ta_2O_5$ and $La_2O_3$ doped samples: 80Z20A+L, 80Z20A+T, 80A20Z+L, 80A20Z+T. These tests were performed at the Faculty of Dental Medicine, University of Porto (FMDUP).

The material samples were sterilized by autoclaving, and osteoblastic-like MG63 cells were used in the biological assays. This cell line is obtained from the human osteosarcoma and present similar phenotypic characteristics to osteoblastic populations. These characteristics make this cell line one of the most frequently used for cytotoxic evaluation of biomaterials in contact with bone tissue.

The materials used and the detailed procedure are described in the following sections.

### 3.6.1 Cell culture

For the cell-response assays, human osteoblastic-like MG63 cells (ATCC number CRL-1427™), of passage 25 were used. These cells were cultured in standard cell culture plates, in α-Minimum Essential Medium (α-MEM, Gibco), supplemented with 10% fetal bovine serum (Gibco), 50 $\mu g.ml^{-1}$ ascorbic acid (Sigma-Aldrich), 50 $\mu g.ml^{-1}$ gentamicin (Gibco) and 2.5 $\mu g.ml^{-1}$ fungizone (Gibco).

At 70-80% confluence, adherent cells were enzymatically released with a solution of 0.05% trypsin (Sigma-Aldrich) in 0.25% EDTA (Sigma-Aldrich), for 5 minutes at 37ºC. The cell suspension was seeded at a density of $5x10^4$ $cells.cm^{-2}$ over the materials' surface. Seeded materials were cultured for 1 and 4 days, and cell behavior was characterized for cell viability/proliferation (MTT assay) and observation by Scanning Electron Microscopy (SEM).

### 3.6.2 Cell Viability/Proliferation assay - MTT assay

MTT is a tetrazolium compound ((3-(4,5-dimethylthiazol-2-yl)-2,5-diphenyltetrazolium bromide) tetrazolium ), which is positively charged and penetrates viable eukaryotic cells. This colorimetric assay expresses the mitochondrial activity by the

reduction of a soluble yellow tetrazolium salt into a purple colored insoluble product that precipitates inside cells, with an absorbance near 570 – 600 nm – formazan [121], [122]. This change of color is due to the acceptance of electrons of oxidized substrates or enzymes (such as NADH and NADPH) from the tetrazolium salt, which converts the yellow salt into a formazan blue. When cells die, their ability of converting MTT into formazan is lost. So, every change in the number of viable cells can be detected by change of color, or, more accurately, by measuring the changes of absorbance at 570 - 600 nm on a spectrophotometer. This is possible because the quantity of formazan is presumably directly proportional to the number of viable cells.

MTT (0.5 mg/ml) was added to each well, and cultures were incubated for 3 hours at 37ºC. Following, the formazan salts were dissolved in dimethylsulphoxide (DMSO) and the absorbance (A) was determined at λ=600 nm on an Elisa reader (Synergy HT, Biotek). Results were expressed as $A.cm^{-2}$.

### 3.6.3 Scanning Electron Microscopy

The colonized material samples were fixed in 1.5% glutaraldehyde in 0.14 M sodium cacodylate buffer, pH=7.3, for 10 minutes. Then, the samples were dehydrated in graded ethanol solutions (70–100%), followed by dehydration in graded ethanol – hexamethyldisilazane (HMDS, Fluka analytical) from 50 to 100%, respectively [123]. Subsequently, samples were sputter-coated with an Au/Pd thin film, using a SPI Module Sputter Coater equipment. The prepared samples were observed under a high resolution (Schottky) environmental scanning electron microscope (Quanta 400 FEG ESEM), on FMDUP.

### 3.6.4 Alkaline phosphatase and staining

Alkaline phosphatase is a protein that presents enzymatic activity. This protein is secreted by osteoblasts and it is capable of removing phosphate groups of several molecules in basic environment. The removal of phosphate groups leads to the formation of radical phosphates. The presence of this enzyme is a marker of the osteoblastic differentiation, which leads to the beginning of mineralization. So, this test gains importance for bone related materials [124].

ALP is measured after the reaction that catalyzes the cleavage of phosphate from p-nitrophenyl phosphate (*p*-NPP, colourless) to form p-nitrophenoxide. The pH of the solution rearranges to alkaline and acquires a yellow color. The production of *p*-

nitrophenoxide is proportional to enzymatic activity and leads to a highly absorbance at 400 nm.

Alkaline phosphatase (ALP) activity was evaluated in cell lysates (0.1% Triton X-100, 5 min) by the hydrolysis of *p*-nitrophenyl phosphate in alkaline buffer solution (pH~10.3; 30 min, 37 ºC) and colorimetric determination of the product (*p*-nitrophenol) at 400 nm in an ELISA plate reader (Synergy HT, Biotek). ALP activity was normalized to total protein content (quantified by Bradford's method) and was expressed as nmol/min.µgprotein$^{-1}$.

The colonized samples were also stained for the presence of ALP. Fixed cultures (1.5% glutaraldehyde in 0.14 M sodium cacodylate buffer, pH=7.3, for 10 minutes) were incubated during 1 h in the dark with a mixture, prepared in Tris buffer (pH=10), containing 2 mg/ml of Na-α-naphtyl phosphate and 2 mg/ml of fast blue RR salt; the incubation was stopped by rinsing the samples with water. The presence of ALP was identified by a brown stain.

### 3.6.5 Contact Angle and Wetting properties

To evaluate the wetting properties (hydrophilicity or hydrophobicity) of the material samples, measurements of the contact angle were performed. The wetting properties of the material can affect the protein and cell attachment, and it is established that usually hydrophilic materials are more prompt to a good protein adsorption and favor cell adhesion. The measuring equipment used was the SL200HT contact angle system from Kino. A drop of water of 1.5 µL was placed on the materials surface and the contact angle was measured by the UEye software. The image processing was carried out using CAST 3.0 software and four measurements were performed on the sample material. An average value was considered.

### 3.6.6 Statistical Analysis

The presented results regarding the biological characterization with cell cultures are the outcome of three independent experiments. In each experiment, three replicas were accomplished for the biochemical assays and two replicas for the qualitative assays. Results are presented as mean ± standard deviation (SD). One-way analysis of variance (ANOVA) was used in combination with Bonferroni's post-hoc test to data evaluation. Values of $p \leq 0.05$ were considered significant.

# Chapter 4

## Results and Discussion

# 4. Results and Discussion

## 4.1 Undoped Zirconia Alumina Composites

Throughout this study, from the initial powders to the final sintered pieces, several tests were accomplished in order to fully characterize the different produced composites. On the next sections the results achieved for the undoped ATZ (80Z20A, 85Z15A, 90Z10A) and ZTA (80A20Z, 85A15Z, 90A10Z) composites are presented.

### 4.1.1 Suspension Stability

The zeta potential of alumina and both 2 mol%Yttria Stabilized Zirconia (2YSZ) and 3 mol% Yttria Stabilized Zirconia (3YSZ) was measured in order to determine the ideal pH and then achieve a good electrochemical balance of the particles. In the following figure the obtained curves are presented.

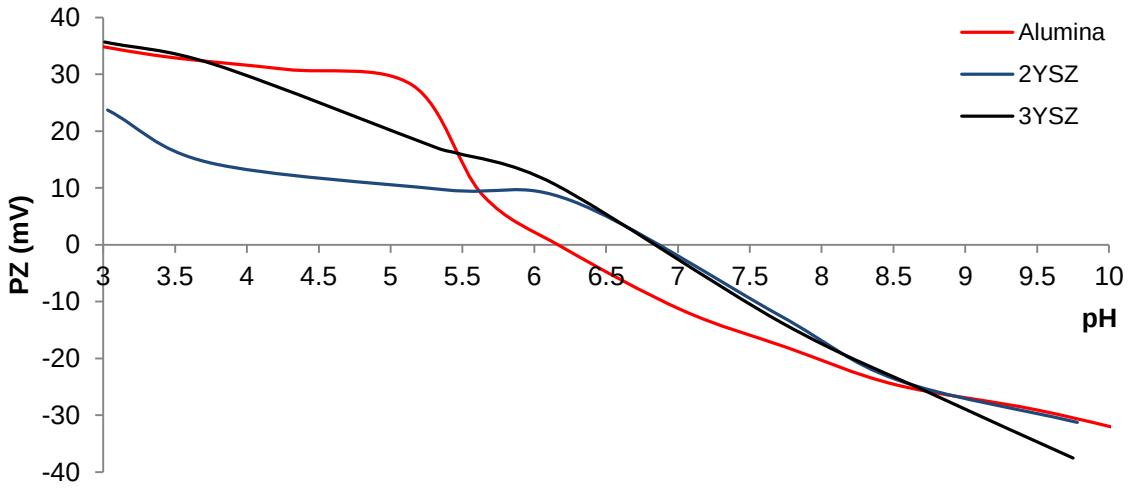


**Figure 4.1 - Zeta potentials obtained for each commercial powder.**

According to the isoelectric points presented by each material, the chosen pH to adjust the six different suspensions was approximately 3. At this pH, the suspensions were stable, not presenting agglomeration or sedimentation, and a good phase distribution of the composite powders could be expected.

### 4.1.2 Particle size distribution of the suspension particles

The particle size distribution of the used commercial powders and suspension particles was determined and adjusted, in order to assure that the milling process led to a good deagglomeration of the initial particles. The obtained size distribution and the mean diameter for the different suspensions are displayed on Figures 4.2, 4.3 and Table 4.1 respectively.

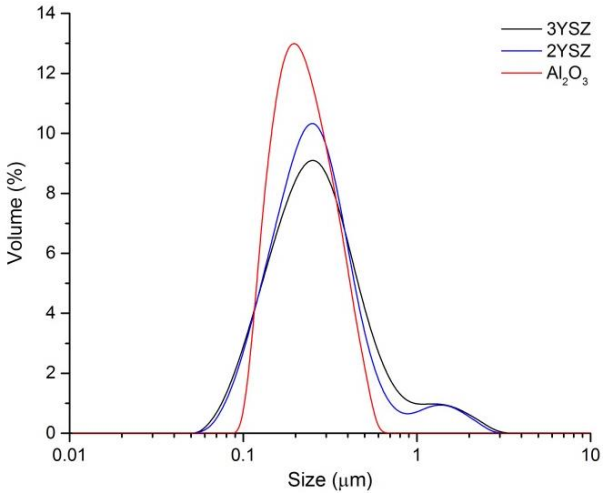


**Figure 4.2 – Particle size distribution of the commercial powders.**

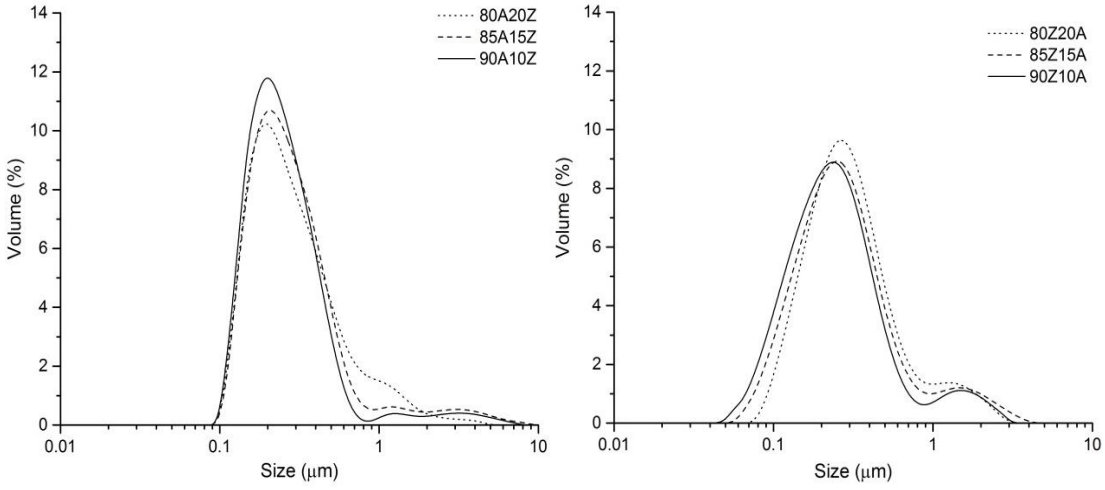


**Figure 4.3 – Particle size distribution of the ZTA (left) and ATZ (right) particles in suspension.**

**Table 4.1 - Mean Diameter of the commercial and composite particles.**

| | Composition | Mean diameter ($d_{50}$) (µm) |
|---|---|---|
| Commercial | 3 mol% YSZ | 0.257 |
| | 2 mol% YSZ | 0.247 |
| | $Al_2O_3$ | 0.216 |
| Composites | 80Z20A | 0.283 |
| | 85Z15A | 0.260 |
| | 90Z10A | 0.234 |
| | 80A20Z | 0.255 |
| | 85A15Z | 0.253 |
| | 90A10Z | 0.232 |

The obtained results confirm that the milling process successfully deagglomerated the suspension particles. This was a key factor in order to avoid obtaining a heterogeneous particle size after spray drying, thus it was important to acquire a controlled, narrow size distribution of the particles on the suspensions meant for spray drying. All the particles of the different composite suspensions possess a mean diameter of around 250 nm which is in accordance with the mean diameter of the initial powders. Both zirconias (3YSZ and 2YSZ) present a slightly bimodal distribution which explains the slightly increase in the mean diameter of the particles from the ATZ suspensions in comparison with the ZTA ones.

### 4.1.3 Characterization of the spray dried powders

#### 4.1.3.1 Morphology

Composite granules were achieved by spray drying. The obtained micrographic images of the suspension particles and the spray dried granules are displayed on Figure 4.4. The spray drying process induces an agglomeration of the powders in suspension, forming spherical morphologies and homogeneous compositions of different materials. The formed solid spheres are reported to be the ideal morphology for ceramic systems [125]. This morphology promotes a better packing of the granules during pressing which leads to a better densification process. A good densification is a beneficial aspect to

obtain ceramics with better mechanical properties. The obtained granules have a micrometric size, and it can be noticed that they are formed by agglomerates of nanometric particles (with an approximate mean diameter of 250 nm, according to the granulometric distribution) from the starting suspension (Figure 4.4-A).

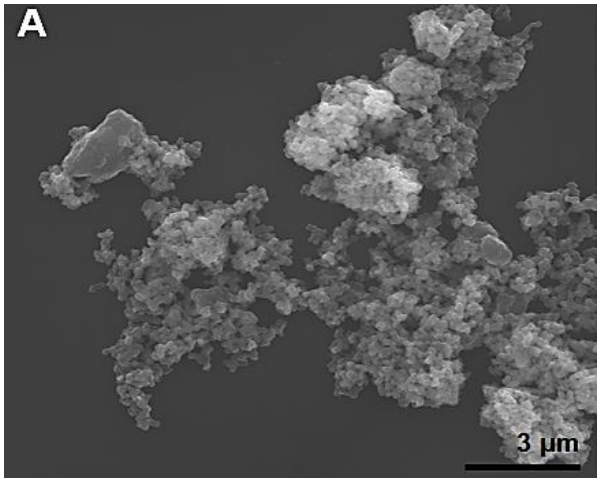


ATZ

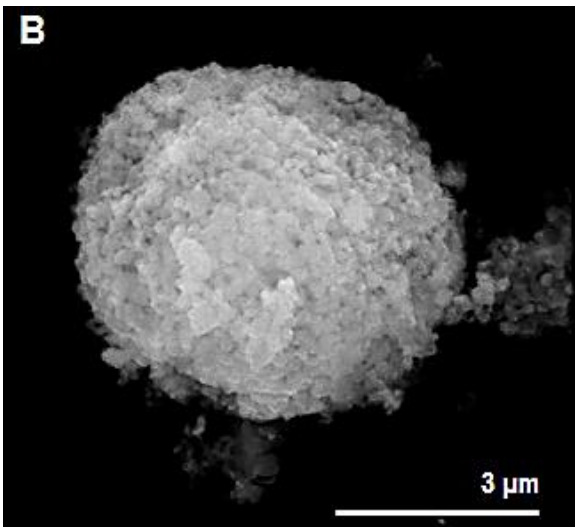


ZTA

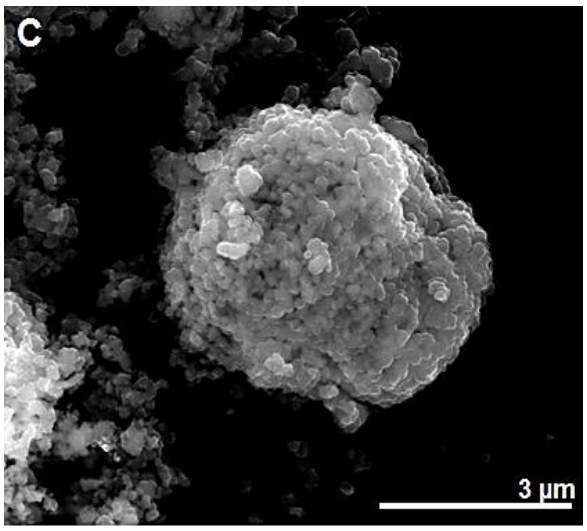

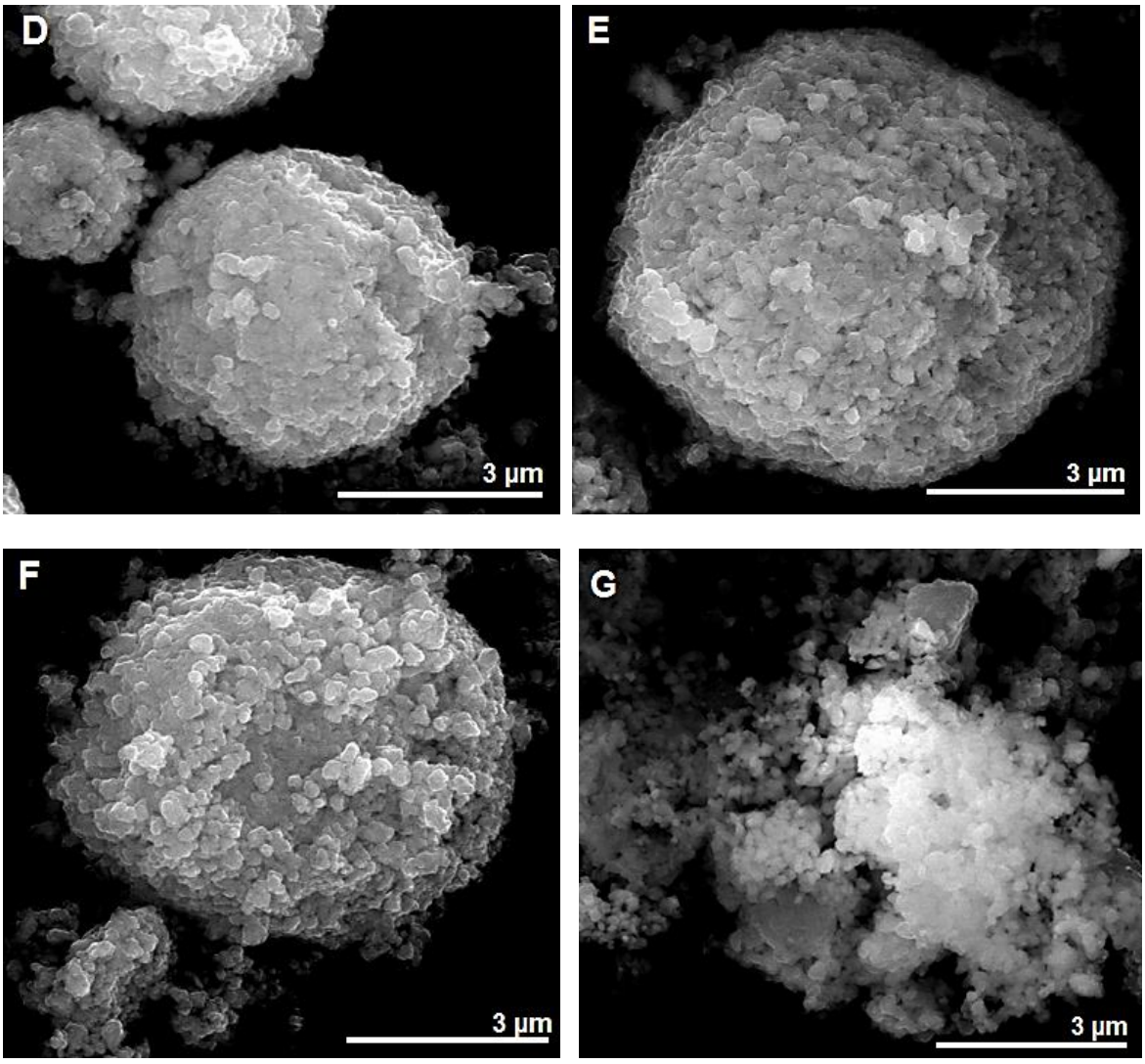


**Figure 4.4 - Obtained SEM images of the: A) Initial suspension particles; and granules of each composite: B) 80Z20A; C) 80A20Z; D) 85Z15A; E) 85A15Z; F)90Z10A; G)90A10Z.**

The formation of the micrometric granules presented on the obtained micrographs was a good indicator of suitable compressive powders that would lead to high density pieces. These granules have a diameter within the range of 4 µm to 8 µm and they are formed by nanometric particles, with a diameter within the range of the results presented by the granulometric distribution.

In general, the granules present an irregular surface, but the spherical shape can be noticed for every composition except for the 90A10Z. In Figure 4.4-G, some deagglomeration is noticed. Some alumina particles appear separated from the granule, thus not forming a granule as it is presented for the other compositions (Fig.4.4-B,C,D,E,F) which may be a signal of fragile granules.

#### 4.1.3.2 Specific Surface Area

The following table presents the specific surface area (obtained by the B.E.T. adsorption isotherm) for both commercial and composite powders obtained by spray-drying.

**Table 4.2 - Specific surface area obtained by B.E.T. isotherm for each composite.**

| | Composition | Specific Surface Area (B.E.T.) ($m^2/g$) |
|---|---|---|
| Commercial | 3 mol% YSZ | 25.6 |
| | 2 mol% YSZ | 24.9 |
| | $Al_2O_3$ | 15.4 |
| Composites | 80Z20A | 22.5 |
| | 85Z15A | 23.1 |
| | 90Z10A | 24.0 |
| | 80A20Z | 18.3 |
| | 85A15Z | 18.5 |
| | 90A10Z | 17.8 |

Both commercial zirconias (2YSZ, 3YSZ) presents a higher value of specific surface area comparing with other commercial zirconia powders [126]–[128] because they are nanostructured powders, thus having a bigger surface area and being more reactive.

The obtained values are in agreement with the ones presented by the commercial powders. Since the ATZ composite powders are mainly constituted by zirconia, their specific surface area increases with the amount of zirconia present. Therefore, the 80Z20A sample presents the lower specific surface area among the ATZ composites, while the 90Z10A, with higher amount of zirconia, achieves the highest value, 24 $m^2/g$.

The used commercial alumina presents a lower specific surface area, 15.4 $m^2/g$. The obtained values for the ZTA composite powders are similar, approximately 18 $m^2/g$. These values were slightly influenced by the amount of zirconia present, since the 90A10Z composite powders, with a lower zirconia content, presents the lower specific surface area value, 17.8 $m^2/g$.

#### 4.1.3.3 Crystal Phases Composition

The crystallographic phases present on the spray dried powders were identified by X-ray diffraction. The obtained diffractogram for each composite is presented on Figure 4.5.

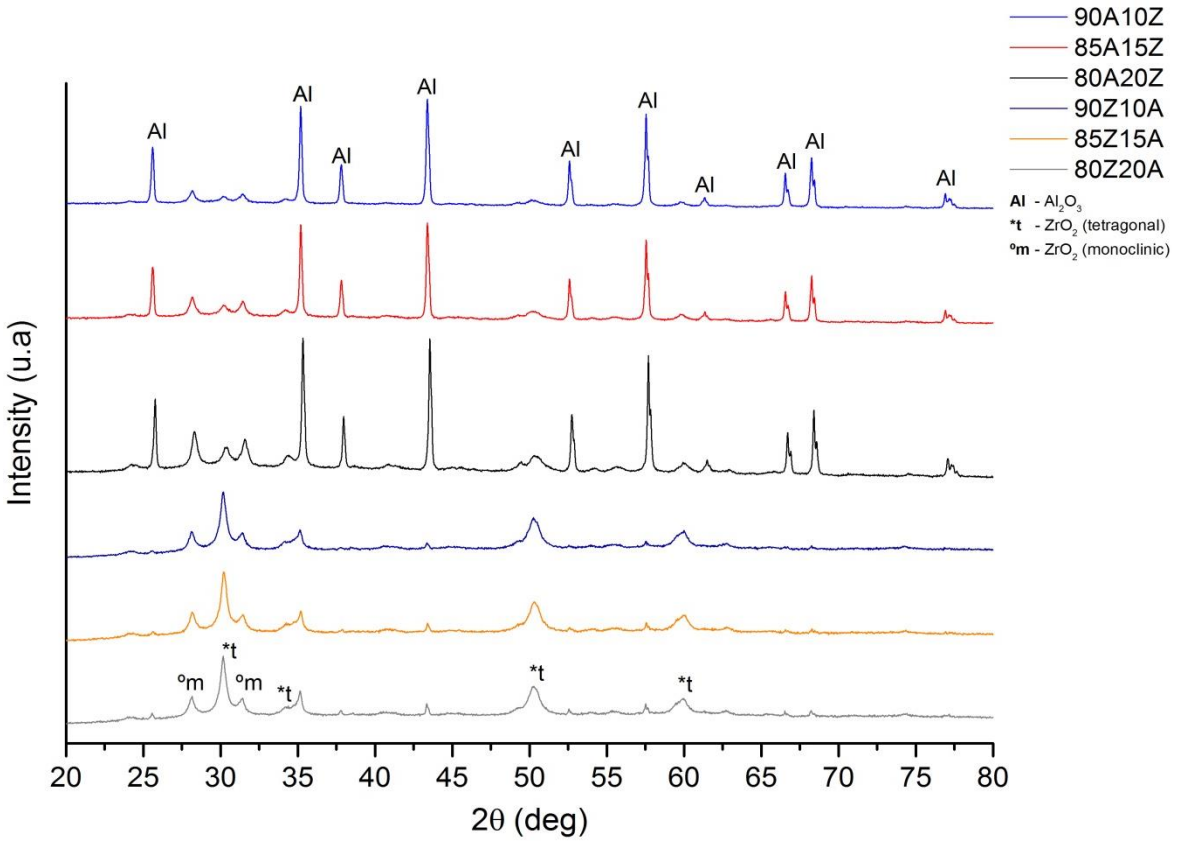


**Figure 4.5 - X-ray diffractogram obtained for each composite powder: 90A10Z, 85A15Z, 80A20Z, 90Z10A, 85Z15A, 80Z20A; obtained by spray-drying.**

This results indicate the presence of, as expected, alumina and zirconia.

Several peaks of monoclinic zirconia were detected for every composition. Phase quantification was performed by Rietveld refinement on X'pert HighScore Plus (PANalytical software) where the peak and profile data is matched with the information contained on the ICDD PDF files. The content of every phase detected is displayed on Table 4.3 below. Even tough there is a 3% error associated to this measurement, a good Goodness of Fit (GOF) value was achieved for each sample (bellow 3) and the ammount of every phase matched the expected value.

**Table 4.3 - Phase quantification of each composite powder obtained by spray-drying.**

| Composition | $Al_2O_3$ (%) | $ZrO_{2\ (tetragonal)}$ (%) | $ZrO_{2\ (monoclinic)}$ (%) |
|---|---|---|---|
| 80Z20A | 23 | 47.2 | 29.8 |
| 85Z15A | 14.8 | 49.6 | 35.6 |
| 90Z10A | 13 | 51.4 | 35.6 |
| 80A20Z | 83.5 | 4 | 12.4 |
| 85A15Z | 88.1 | 3.1 | 8.8 |
| 90A10Z | 92.2 | 1.9 | 5.9 |

The ammount of monoclinic zirconia present in these powders is due to the transformability of zirconia when in powder. The granules of zirconia present a significantly high specific surface area (Table 4.2) which makes them reactive and transformable. Thus, there is a tendency for the zirconia to reach its stable state at room temperature, which is the monoclinic phase, so the tetragonal to monoclinic transformation occurs easily. Consequently, the content of monoclinic zirconia surpasses the content of tetragonal zirconia for the ZTA samples, since the 2 mol% Yttria Stabilized Zirconia used on these composites is more transformable than the 3 mol% Yttria Stabilized Zirconia used on the ATZ composites. Thus, it is verified that for the ATZ samples the ammount of monoclinic zirconia is always lower than the content of tetragonal zirconia. The content of alumina is on the expected range.

#### 4.1.3.4 True density

The particles density was measured on a helium pycnometer. The following table presents the obtained density values for each composition.

**Table 4.4 - Particles density for each composite measured by helium pycnometry.**

| Composition | Density ($g/cm^3$) |
|---|---|
| 80Z20A | 5.055 |
| 85Z15A | 5.138 |
| 90Z10A | 5.191 |
| 80A20Z | 4.195 |
| 85A15Z | 4.043 |
| 90A10Z | 4.120 |

Since zirconia has a higher density than alumina, as expected the ZTA samples have a lower density value. On the opposite, the ATZ samples present a higher density value.

Every composition presented a particle relative density higher than 91% (considering the theoretical values of alumina, tetragonal and monoclinic zirconia) without the application of any calcination stage and it can be assumed that the obtained nanometric particles are fully dense.

#### 4.1.3.5 X-Ray Fluorescence

In order to investigate the chemical composition of each sample, x-ray fluorescence analysis was performed. This test is required in ISO 13356 (2008) [22] to detect impurities on these ceramic materials based on yttria stabilized zirconia for orthopedic implants. The chemical composition of each composition is presented on Table 4.5.

**Table 4.5 - Chemical composition for each composite by means of X-ray fluorescence.**

| Composition (%) | 80Z20A | 85Z15A | 90Z10A | 80A20Z | 85A15Z | 90A10Z |
|---|---|---|---|---|---|---|
| $ZrO_2$ | 74.78 | 78.75 | 83.35 | 16.48 | 13.84 | 10.72 |
| $Al_2O_3$ | 19.11 | 14.84 | 9.856 | 82.17 | 85.14 | 88.5 |
| $Y_2O_3$ | 4.517 | 4.746 | 5.026 | 0.8598 | 0.6715 | 0.5076 |
| $HfO_2$ | 1.49 | 1.56 | 1.65 | 0.439 | 0.319 | 0.239 |
| Other elements | 0.104 | 0.106 | 0.123 | 0.044 | 0.034 | 0.031 |

The International Standard is referred only to Yttria Stabilized Zirconia however; some requirements can be taken in consideration in these composites. According to this international standard the mass fraction of hafnia and other oxides must be controlled: the hafnia content must not exceed 5% and other oxides (except alumina and yttria in this case) must be below 0.5%.

As it can be verified the content of hafnia in all the produced composites was below 5%, as well as the other oxides, that combined did not exceeded 0.5%.

These results also show that the content of zirconia and alumina are in accordance with the defined compositions for the ATZ and ZTA composites.

#### 4.1.3.6 Dilatometric Analysis

To investigate the thermic behavior and densification kinetics of all samples and determine a sintering temperature, a dilatometric analysis was made (Fig. 4.6).

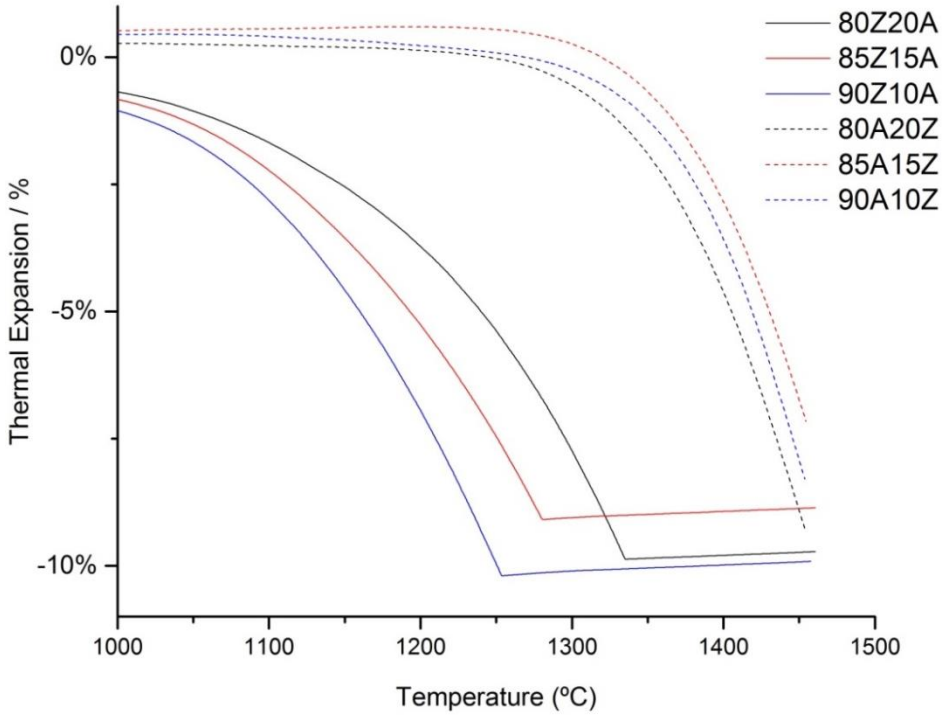


**Figure 4.6 - Dilatometric analysis performed on each composite powder.**

The ATZ samples achieve fully densification at a lower sintering temperature in comparison with the ZTA samples. With the increasing amount of alumina, a higher sintering temperature is required. This sluggish densification behavior presented by ZTA samples requires a higher sintering temperature, which leads to an excessive grain growth [129]. As mentioned on the previous chapter of this document, a refined grain size (submicrometric and nanometric grain sizes) is traduced on improved mechanical properties and aging resistance [25], [42]. In order to avoid an excessive grain growth and enhance the resistance to hydrothermal degradation, a moderate sintering temperature should be considered. A sintering temperature of 1400ºC has been reported to be an optimal sintering temperature to improve the hydrothermal degradation resistance, since materials sintered at higher temperatures tend to initiate this deleterious transformation at earlier stages [33].

The selected sintering cycle had a maximum temperature of 1400ºC during three hours, with a heating rate of 2 ºC/min and a cooling rate of 5 ºC/min.

### 4.1.4 Characterization of the sintered pieces

#### 4.1.4.1 Density of the green and sintered pieces

The composite powders were subjected to two pressing stages and sintering. First, the powders were uniaxialy pressed, and a cold isostatic pressing was followed. Finally, the green bodies were sintered. The density of the green and sintered pieces was determined geometrically, and by the Archimedes' Method, respectively. The density results are displayed in the Figures bellow.

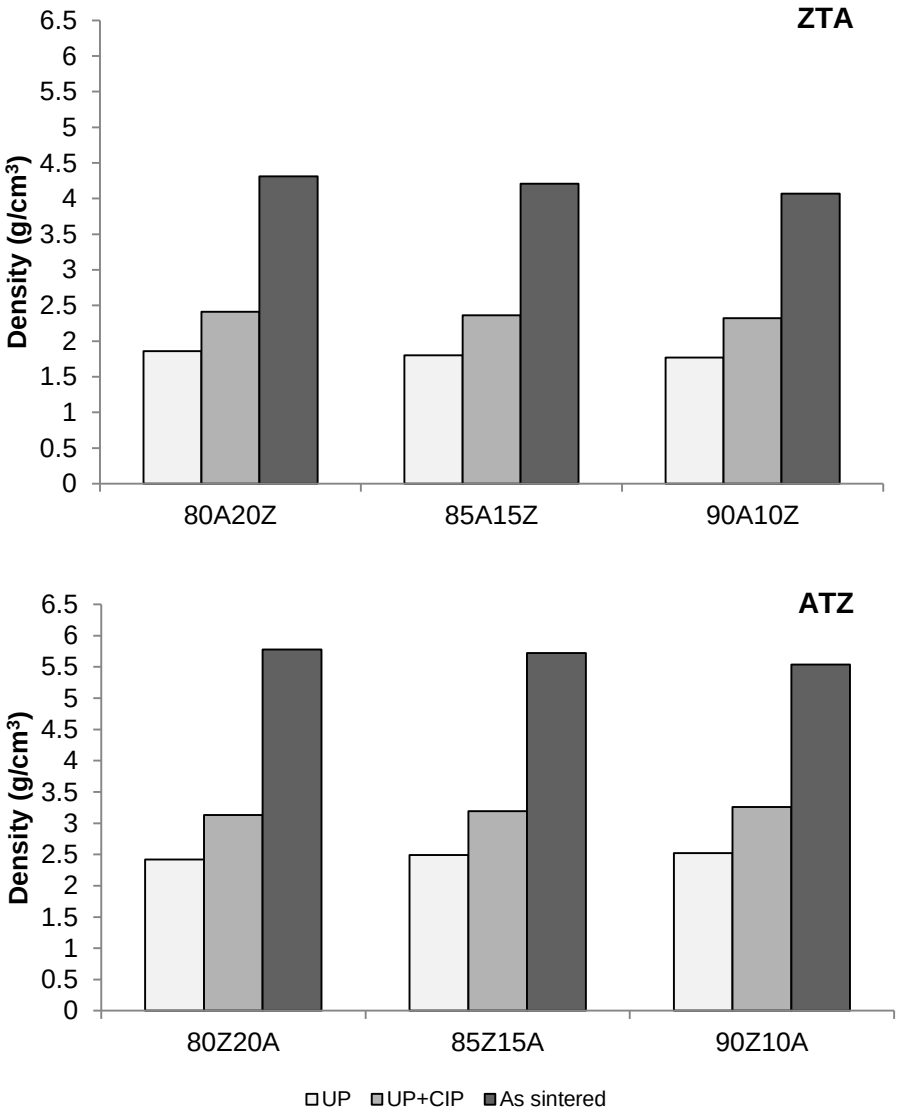


**Figure 4.7 - Density of the ZTA (above) and ATZ (below) sintered pieces, throughout the different stages of pressing and sintering.**

**Table 4.6 - Densification degree of the sintered composites.**

| Composition | Density (%) |
|---|---|
| 80Z20A | 98.47 |
| 85Z15A | 99.31 |
| 90Z10A | 98.05 |
| 80A20Z | 98.40 |
| 85A15Z | 98.59 |
| 90A10Z | 97.84 |

As it can be verified, the additional stage of cold isostatic pressing increased the density of the green pieces.

The sintering stage lead to a good densification of all samples, since the ZTA samples presented an increase of approximately 2 g/cm$^3$, and the ATZ approximately 3 g/cm$^3$. As expected, the ATZ samples have higher density due to their amount of zirconia. Compared with the theoretical values of density (Table 4.6), the achieved relative density is superior to 97%. These outstanding values of density resulted from various factors such as the spray dried powders, which were spherical, with a micrometric size and dense. A good packing of these powders during uniaxial pressing and the CIP stage improved the density of the green bodies, and the sintering stage allowed an increase of these values, at a relatively low temperature.

Some authors reported that spray drying of deflocculated suspensions can lead to the production of hollow granules and consequently give rise to porous ceramics with flaws, upon sintering [125], [130]. However this is not verified in this study. The density values obtained for each composition of these powders are associated to dense particles and not hollow, as it was reported by the authors. Even for the 90A10Z composite powders on where the granules appeared to be broken (Fig 4.4-G), a good value of density was achieved.

It is also important to remark that no hot isostatic pressing was applied in this study, so it can be assumed that an additional stage of hot isostatic pressing would contribute to produce sintered pieces with even higher density values (around 99% of relative density).

#### 4.1.4.2 Crystal Phases Composition

To confirm the full transformation of monoclinic zirconia to the tetragonal phase upon sintering, X-ray analysis was made on the composite samples. The obtained diffractogram for each composition is presented on Figure 4.8.

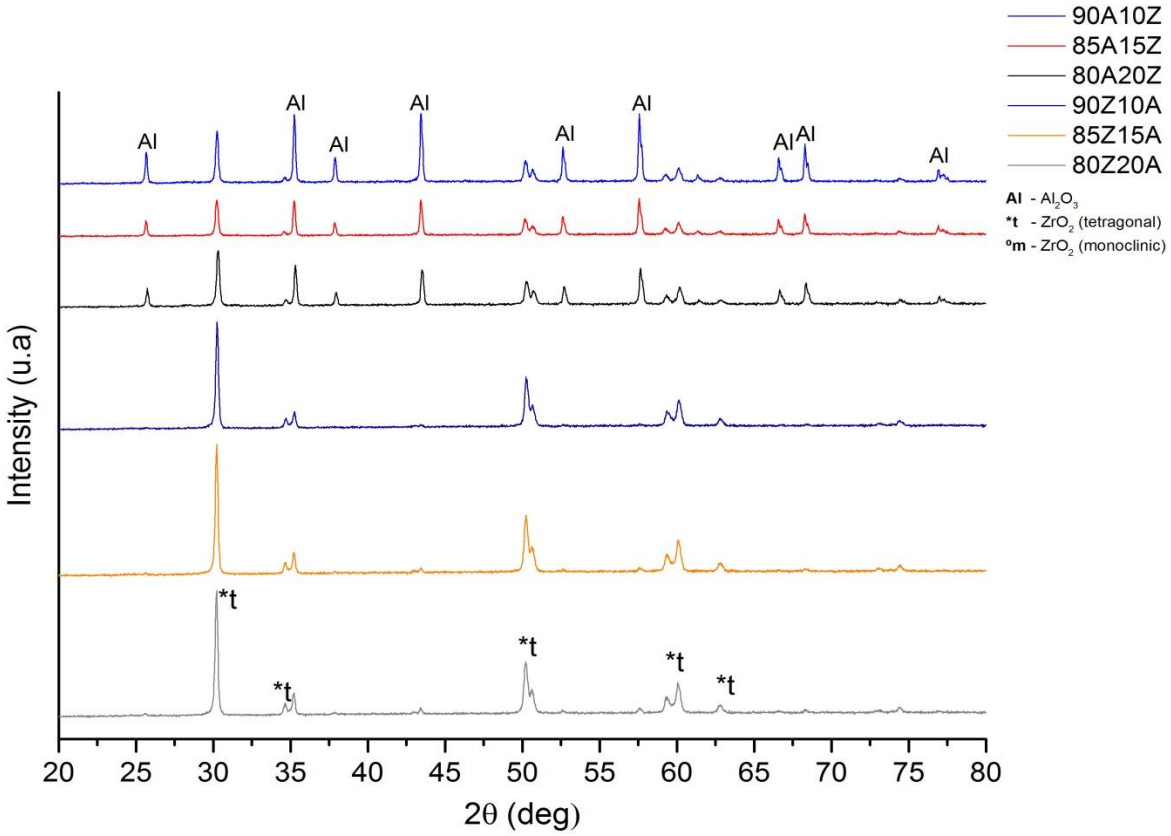


**Figure 4.8 - X-ray diffractogram obtained for each composite sintered piece: 80Z20A, 80A20Z, 85Z15A, 85A15Z, 90Z10A, 90A10Z.**

As expected, the sintering temperature carried at 1400ºC enabled the absence of monoclinic zirconia. At this temperature the monoclinic zirconia (which is stable until 1170ºC) detected on the composite powders after spray drying (Fig. 4.5), has been transformed to the benefic tetragonal phase.

Thus, it was confirmed that after sintering all the monoclinic zirconia underwent transformation to tetragonal phase, and its deleterious effects wouldn't affect the following tests.

#### 4.1.4.3 Microstructure

In order to observe the microstructure of these composites, the sintered pieces were thermally etched and observed by scanning electron microscopy. The obtained micrographs are displayed on the Figure 4.9 bellow.

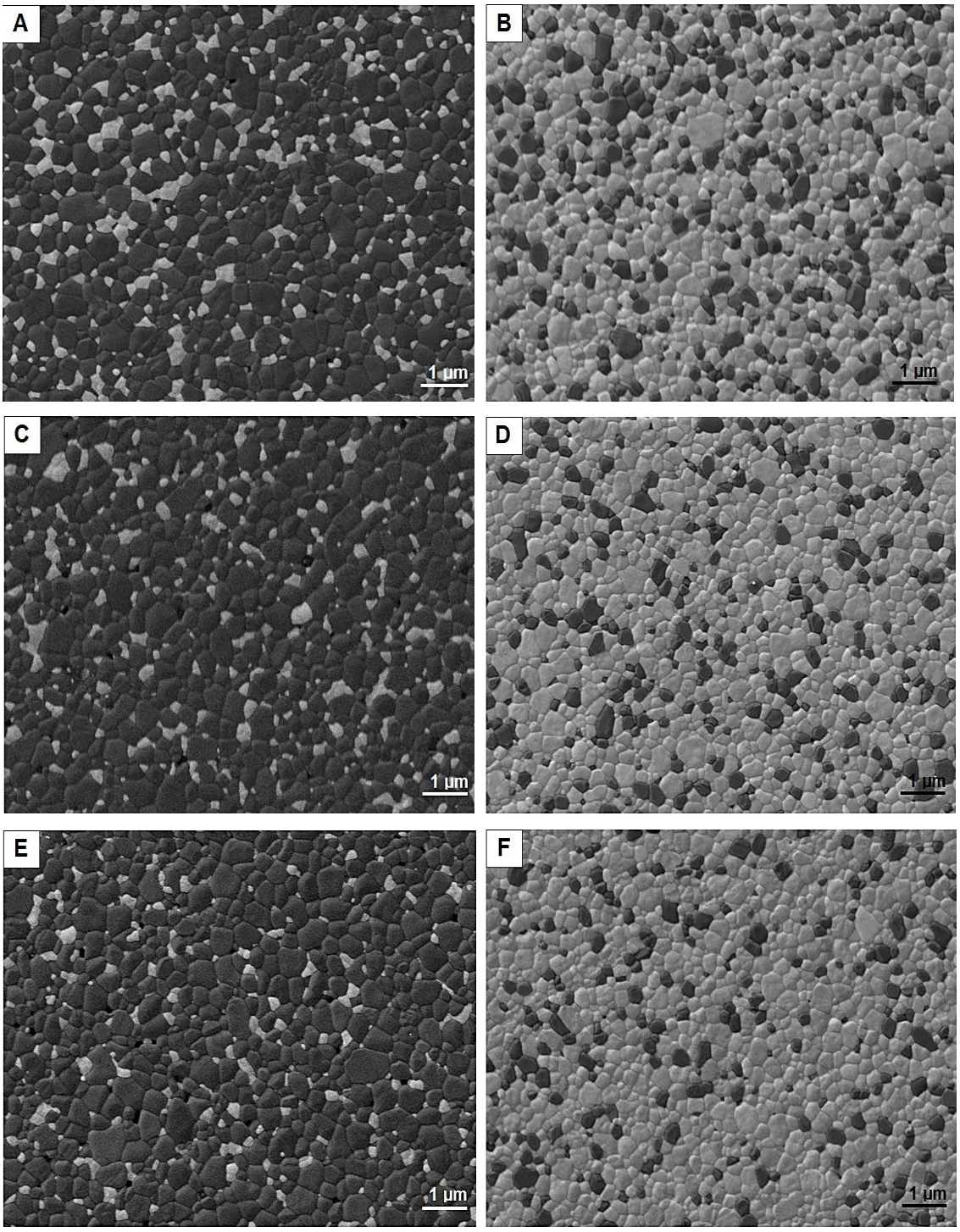


**Figure 4.9 - SEM micrographs from the thermal etched composite samples: A) 80A20Z; B) 80Z20A; C) 85A15Z; D) 85Z15A; E) 90A10Z; F) 90Z10A.**

The zirconia grains are the brighter and the alumina grains are the dark ones. As it can be observed for all the composites, a uniform microstructure was accomplished with no evident agglomeration of the least present phase. For the ZTA composites, it was reported that a limit on the zirconia content (16 vol%) would be advised in order to avoid the formation of zirconia agglomerates [1], [9], [26] (Fig.2.7, section 2.2). However, in this case, no agglomerates were detected for the 85A15Z with 15 wt% of zirconia, and even for the 80A20Z composition that has 20 wt% of zirconia. Therefore, it is assumed that the applied milling stage and spray drying successfully leads to the obtention of composites with a fine, dispersed microstructure.

Although some small pores on the ZTA samples are detected, dense sintered pieces were achieved, since the density values obtained are all above 98%.

The microstructure presented by every sample showed similarity with some published results [12], [25], [131]–[133].

The mean grain size was estimated using an interception method. The calculated values are exhibited on Table 4.7.

**Table 4.7 - Mean grain size of each composite calculated by line interception method.**

| Composition | Mean grain size (nm) | |
|---|---|---|
| | Alumina | Zirconia |
| 80Z20A | 359±12 | 353±3 |
| 85Z15A | 340±7 | 367±13 |
| 90Z10A | 356±18 | 343±21 |
| 80A20Z | 455±17 | 251±13 |
| 85A15Z | 463±10 | 234±22 |
| 90A10Z | 477±18 | 223±4 |

Alumina presents a higher grain growth during sintering than zirconia, as it grows freely, if the content of zirconia is below 5 vol% [134]. Thus, as expected alumina presented an higher grain growth than zirconia [19]. However, the selected sintering temperature did not allowed its excessive grain growth. The zirconia and the alumina present on the ATZ samples have a similar grain size, while on the ZTA side the alumina presents a higher grain growth in comparison with zirconia. This suggests that, on the high content zirconia samples, the grain growth of alumina was constrained, due to the encapsulation of its grains on a zirconia matrix. On the opposite, when alumina is in a larger amount, the grain growth occurs more freely, while the zirconia grain growth is

constrained. This pinning effect on the alumina matrix grain growth was already stated on literature, for ZTAs with a content of zirconia ranging from 5-20 wt%, on a maximum sintering temperature of 1500 ºC [12], at 1450ºC, 1550ºC [10] and 1600ºC [20].

#### 4.1.4.4 Mechanical Properties

The densification upon sintering is also a crucial factor that positively affects the mechanical properties of these materials. Accordingly to the obtained results of density for these composites, enhanced mechanical properties were expected. The sintering temperature could also provide an enhancement of hardness since it was reported that this sintering temperature of 1400ºC promotes the increasing of hardness and above it this mechanical parameter starts to decrease [19].

The Vickers Hardness (HV10), fracture toughness and bending strength were determined for all samples. The results obtained from the mechanical tests are shown on the following Figure.

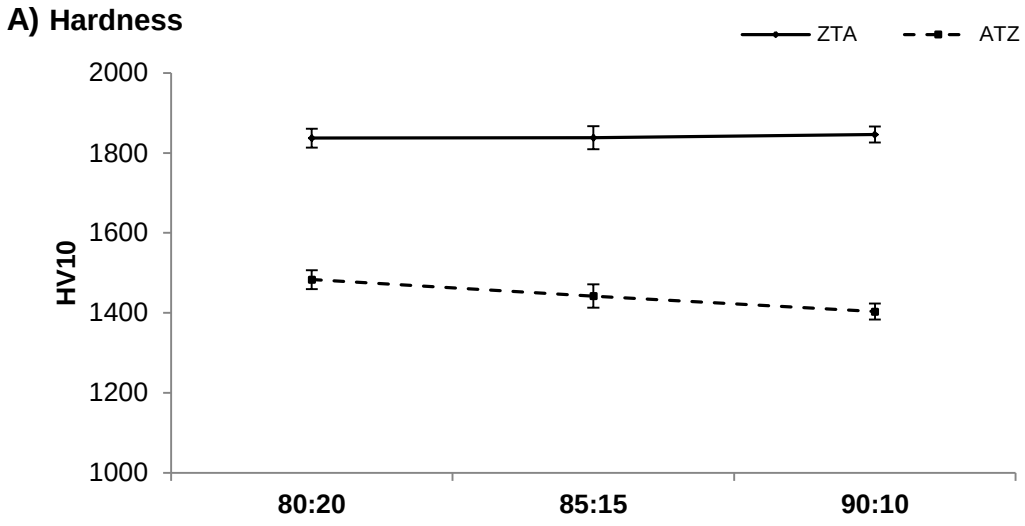

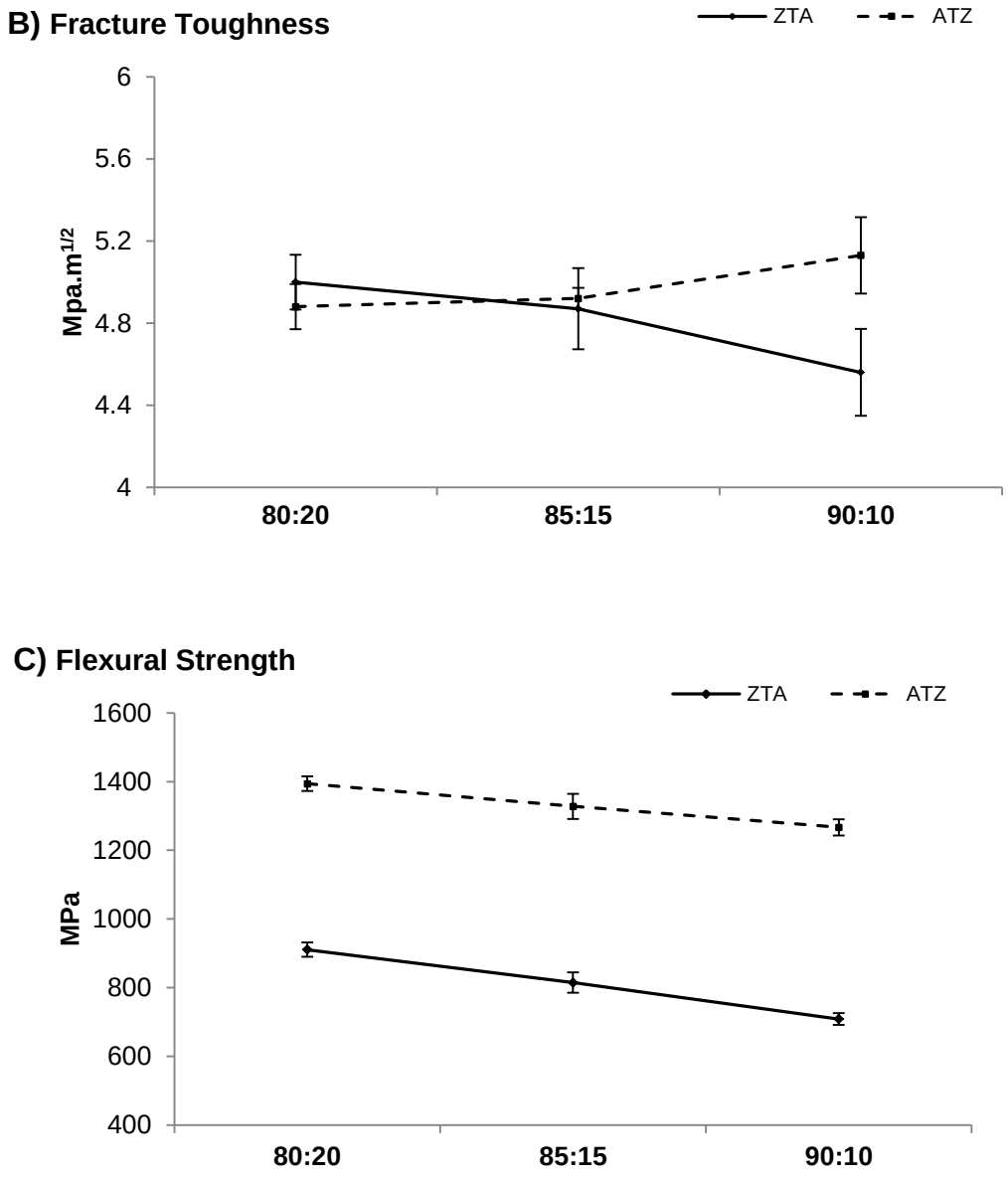


**Figure 4.10 - Mechanical properties of ZTA and ATZ composites: A) hardness, B) fracture toughness and C) flexural strength.**

Regarding the results obtained for Vickers Hardness, as expected, higher values were achieved for the ZTA samples in comparison with the ATZ samples, as a result of their higher amount of alumina, which is known to highly increase this property.

A good densification (above 97%, Table 4.6), lead to an improvement of the hardness values of the ZTA samples, where 1846 HV was reached for the 90A10Z composition. It was expected a decline on this mechanical property with the increase of the amount of zirconia; however this is not verified, since there is a linearity on the values of hardness on each ZTA composite. The 90A10Z would have the higher value of

hardness due to its amount of alumina, and 80A20Z the lowest value. However, the latter sample presents a value of 1837 HV. Thus, good results of hardness were achieved for every ZTA composition, being definitely associated to a good densification, a uniform distribution of microstructure and sintering.

Regarding the ATZ results, the hardness decreased from 80Z20A to 90Z10A, which is according to the rule of mixture [2]. For the 80Z20A composition, it was obtained a maximum value of 1483 HV; however, as it can be verified, the decrease in hardness was not significant. It can be assumed that the sintering temperature (1400ºC) and, again, a good densification (above 98%), contributed to maintaining these values despite the increasing amount of zirconia.

Although the hardness decreased with the increment of zirconia, the fracture toughness showed an opposite effect by increasing with the amount of zirconia, as it was already stated on literature [11]. The toughening enhancement is proportional to the amount of transformable zirconia present in the composite. Thus, as expected, higher values of fracture toughness were obtained for the ATZ samples.

The highest value attained was 5.13 $MPa.m^{1/2}$ for the ATZ sample with the highest amount of zirconia, 90Z10A, and as expected the lowest value (4.56 $MPa.m^{1/2}$) was obtained for the 90A10Z sample. However, the 80A20Z sample presents a slightly increase of fracture toughness in comparison with 80Z20A sample. This can be due to the different amount of yttria on the two compositions: the 2 mol% Yttria Stabilized Zirconia used on the ZTA samples is more transformable than the 3 mol% Yttria Stabilized Zirconia used on the ATZ samples. This surely contributed to this higher value for the 80A20Z sample and the similarity observed between the values presented by the 85A15Z and 85Z15A samples, indicating that, although an higher amount of zirconia was present in the ATZ samples which would indicate an higher fracture toughness of the composite, the difference of the amount of zirconia was hindered by the transformability of the ZTA sample, with the less stable zirconia. Thus, although the 80A20Z and 85A15Z samples contained less zirconia, its superior transformability allowed this enhanced values for the fracture toughness, as ZTA samples.

Similarly to fracture toughness, the flexural strength also increases with the increasing amount of zirconia, thanks to its martensitic transformation [10] and, on the contrary, with the increasing amount of alumina, this mechanical parameter shows a decrease. Thus, as expected, the ATZ samples have a higher flexural strength in comparison with the ZTA samples. The highest value achieved was 1394 MPa for the 80Z20A.

However, it would be expected an increase of flexural strength with the amount of zirconia on the ATZ samples which is not verified since a small decrease is observed between the 80Z20A and the 90Z10A samples. In ceramic materials, a decrease in fracture toughness as the flexural strength increases may occur. In this case, as the fracture toughness increases with the amount of zirconia for the ATZ samples, the opposite effect may be reflected on the flexural strength of these composites. The values of density were analyzed and it was concluded that they did not affect this mechanical property since good densification was achieved for all ATZ samples (above 96%, Table 4.6). The yttria content is the same for all the ATZ samples, thus the content of stabilizer did not affected this drop in flexural strength. It can only be assumed that the alumina content in the ATZ samples did not negatively influenced the flexural strength of the composites; on the contrary, it appears to have a beneficial effect, as the 80Z20A presents the highest value. This can indicate that a good balance of zirconia-alumina content (80:20 ratio) and a microstructural homogeneity was achieved to maximize this mechanical property. In Figure 4.11, this possibility is graphically explained.

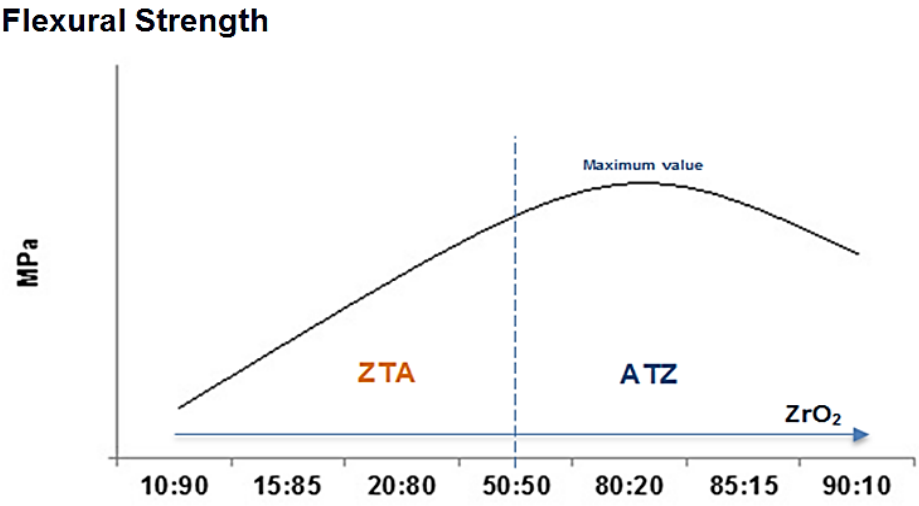


**Figure 4.11 – Evolution of the flexural strength throughout various compositions of zirconia alumina composites.**

More compositions would be needed to confirm this possibility however; the achieved results constitute a plausible explanation. In a market research for ATZ with disclosed compositions, it was verified that, one of the most used composition is in fact around 80:20 of zirconia-alumina [135], [136]. Thus it can be predicted that this composition presents the best set of balanced mechanical properties, and therefore the best results for flexural strength.

As it could be verified by the X-ray analysis (Fig. 4.8) no new phase was formed so it can be stated that the obtained results for the mechanical properties were only influenced by the amount of each material used, density and granulometric distribution.

### 4.1.5 Accelerated Aging Test

In order to verify their aging resistance, the composites were exposed to water steam in an autoclave at 134ºC at 2 bar, as specified by ISO 13358 (2008). The results obtained from phase quantification after X-Ray diffraction are displayed on the Figure 4.12 bellow.

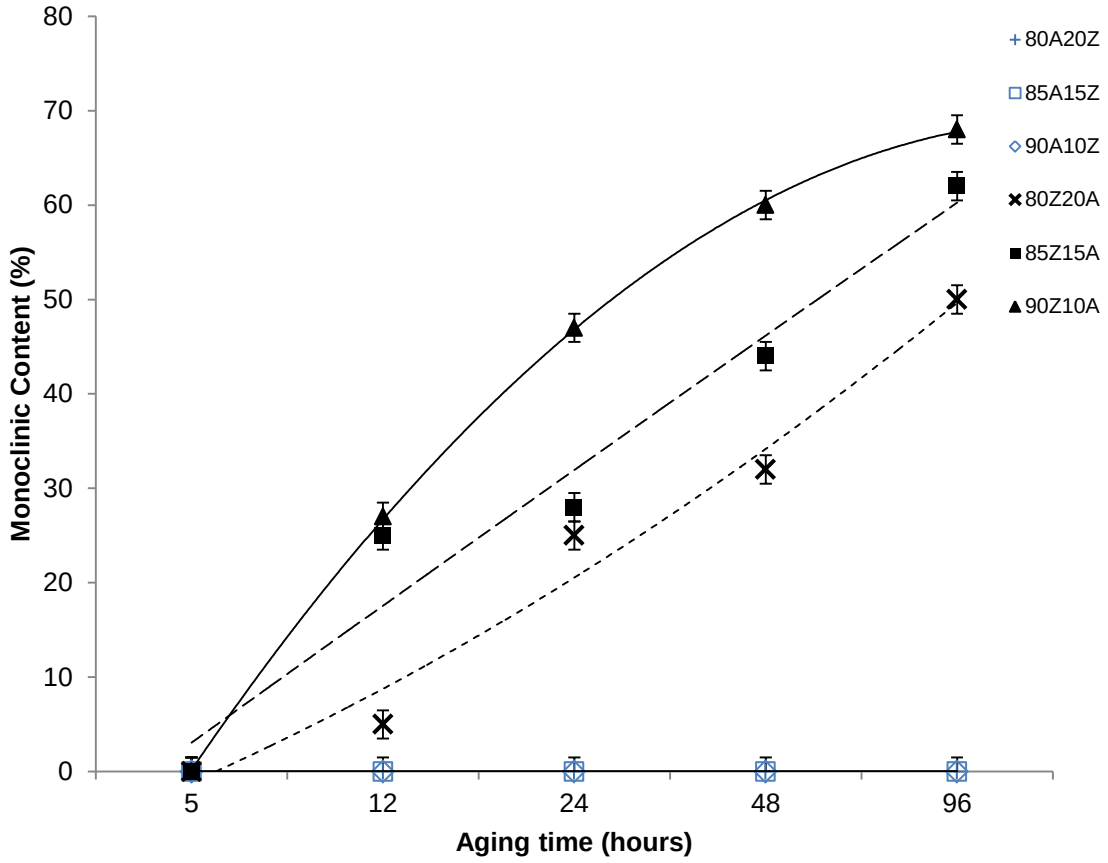


**Figure 4.12 – Change in the monoclinic content of the aged composite samples with time during accelerated aging tests in an autoclave (134ºC, 2 bar).**

It can be observed that the ZTA samples did not suffer any degradation since that no monoclinic zirconia, which is an indicator of aging, was detected throughout the duration of the test (96 hours). This is a clear indication that the presence of an alumina

matrix did not only delayed the tetragonal to monoclinic transformation of zirconia [25], [137] but completely hindered it.

As expected, the ATZ samples do not present the same behavior. It can be verified that, for these composites, the degree of degradation increased with the time of exposure and the higher amount of zirconia present on these samples made them more vulnerable to aging, reaching a maximum content of monoclinic zirconia of 68.40% after 96 hours for the sample 90Z10A. Among these samples, the best results were achieved for the 80Z20A sample, which presents the higher quantity of alumina.

Even though the zirconia on the ATZ samples have a higher content of stabilizer, it was not enough to provide a full protection against hydrothermal aging. However, the achieved values are in agreement with the ones specified on the ISO standard, that require that the fraction of monoclinic zirconia after 5 hours at 134ºC and 2 bar, must be bellow or equal 25%. The results presented on Figure 4.12 show that after 5 hours of aging tests, no monoclinic zirconia was detected for all the samples except for 90Z10A, in which was detected only 1.3% of monoclinic zirconia.

In order to determine if the aging tests affected the mechanical properties of the material, new mechanical tests were made on the aged samples. The obtained results are displayed in Figure 4.13.

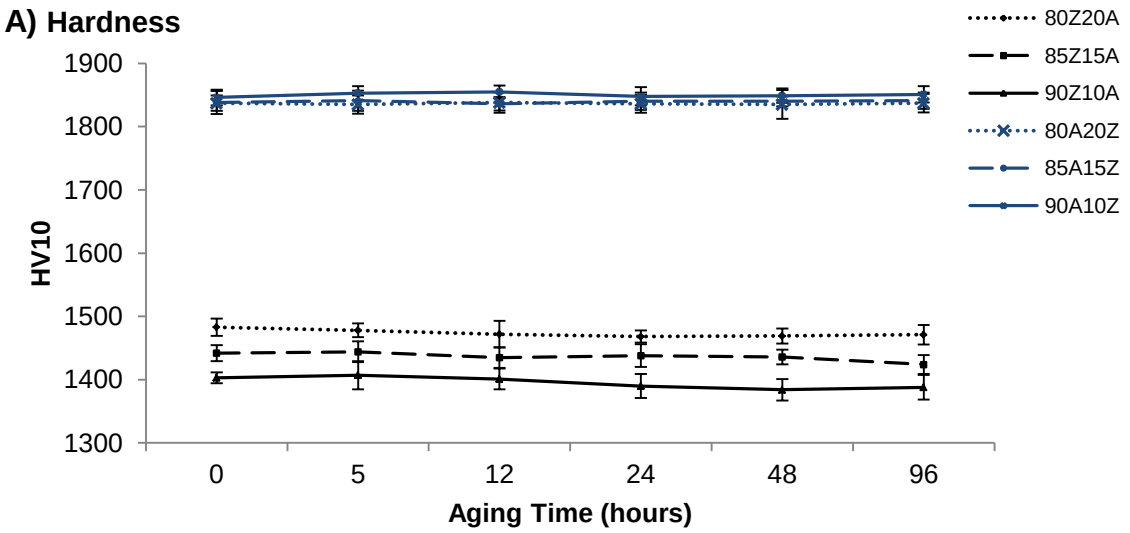

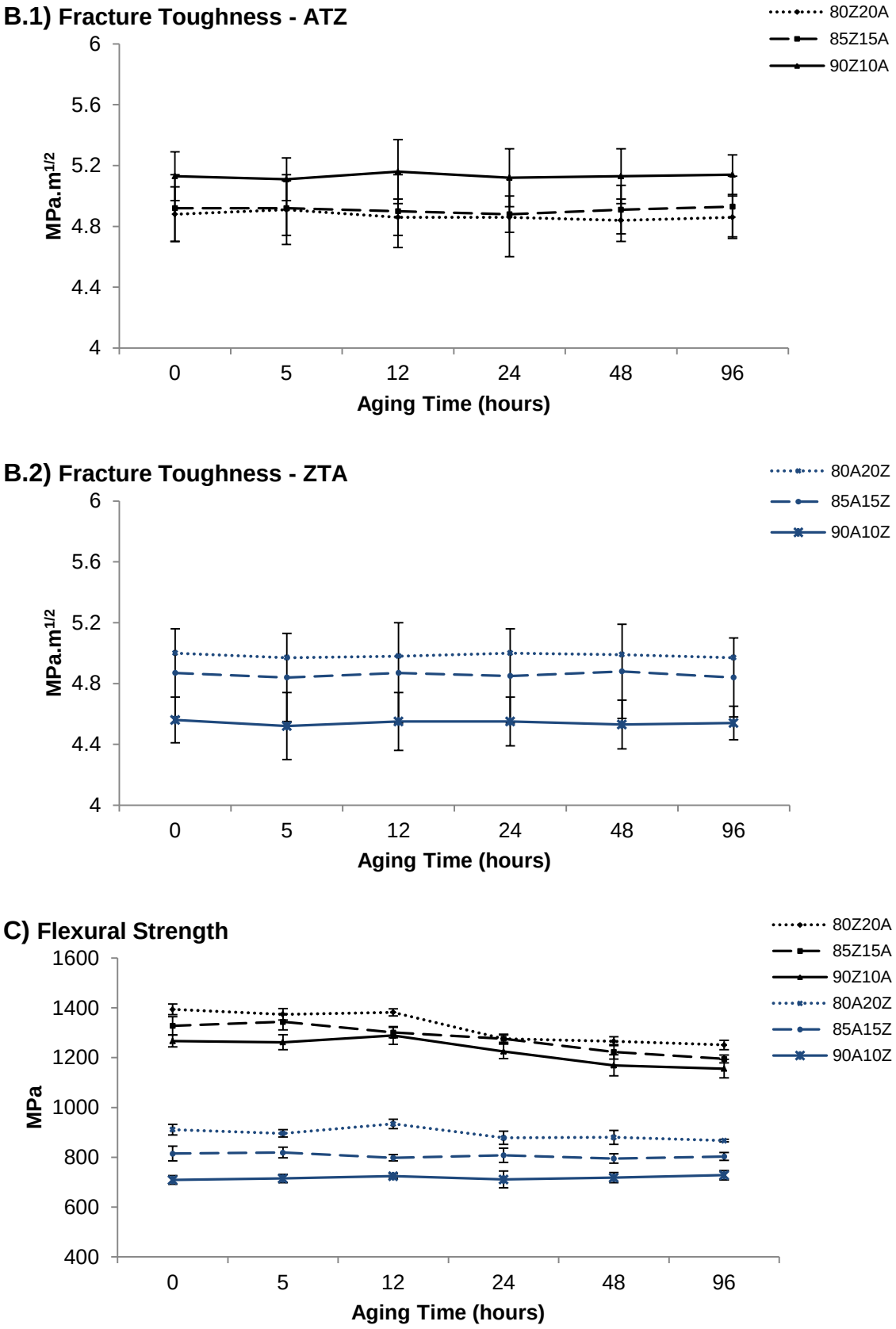


**Figure 4.13 - Mechanical properties of the aged composites throughout the duration of the aging tests: A) hardness, B,1-2) fracture toughness and C) flexural strength.**

It would be expected a decrease in the mechanical properties with the increase of the aging time since it was expected the formation of flaws like surface microcracks [25], [137]. However, in this case, for every test the values were maintained even after 96 hours of aging. Even for the ATZ samples, in which monoclinic zirconia was detected up to 68.4% (for 90Z10A sample) it was not verified a significant decline in the mechanical properties after the aging tests, since the values achieved are close to those obtained before aging tests (0 hours of aging tests). This is a clear evidence that, throughout the duration of the aging tests, the degradation did not progressed to the bulk, which have prevented the decay of the mechanical properties. So, it is assumed that, the monoclinic fraction detected on the X-ray analysis is only present on the polished surface of the samples and, remarkably, after 96 hours of degradation, no signal of serious degradation was observed.

To confirm that the degradation did not expand to the bulk, the cross-section of the sample with the highest content of monoclinic zirconia, 90Z10A after 96 hours of aging tests, was observed by SEM. Several authors have already used this technique in order to investigate the extension of Low Temperature Degradation (on zirconia and zirconia composites) [7], [33], [35], [41], [50], and thus measure the thickness of the monoclinic layer. The cross-section surface was polished, and covered with a conductive layer. The obtained micrographs for two different magnifications are displayed on Figure 4.14.

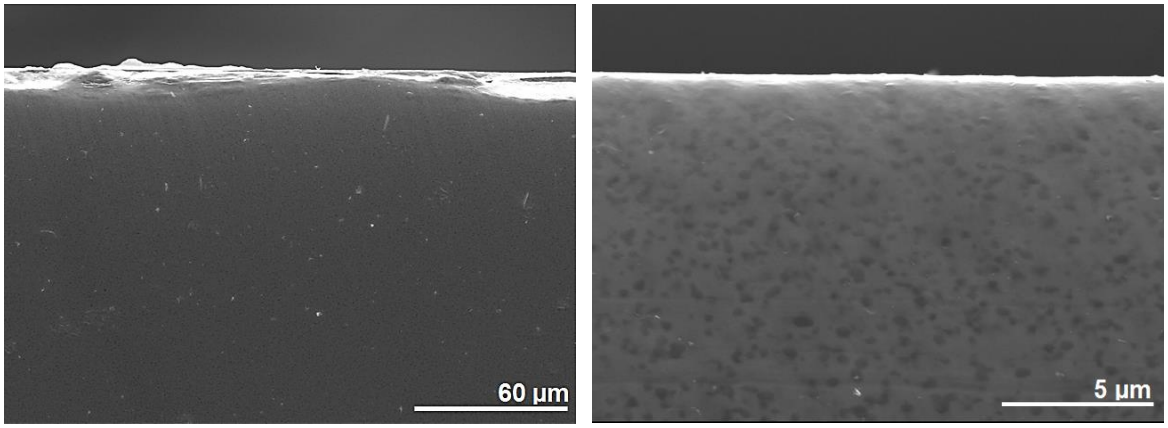


**Figure 4.14 – SEM images of the cross-section of the surface of the 90Z10A sample after 96 hours of aging tests.**

Accordingly to published results [33], [50], the monoclinic transformed region is characterized by the existence of porosity, grain pull-out and intergranular fracture. While the monoclinic region presents a disorganized, porous structure, the tetragonal fraction of the sample is dense, and presents a smooth, continuous surface. As it can be observed, the obtained surface of the cross-section is continuous, and no evident layer of porosity

and grain pull-out, characteristic of the monoclinic fraction is verified. Therefore it can be assumed that, the monoclinic zirconia detected after 96 hours of aging tests in this sample (68.4%) is present only on the surface of the sample and presumably has around 0.5 µm (which corresponds to two grain layers). This surface layer of monoclinic zirconia was not deleterious to the mechanical properties of the samples, as the results showed no significant decay in these parameters, after 96 hours of accelerated aging tests.

Low Temperature Degradation kinetics follow sigmoidal laws related to the nucleation-growth process. The surface transformation can be fitted to a modified Mehl-Avrami-Johnson (MAJ) law given by [7], [138]–[142]:

$$V_m = 1 - (\,1 - V_m^0\,)\exp[-(bt)^n] \qquad \text{Equation (11)}$$

where $V_m^0$ is the initial monoclinic phase fraction in the material before the aging test, *t* is the aging duration, *n* is the MAJ exponent (or time exponent, which is a constant and independent of the temperature) and *b* is a parameter that represents the temperature dependence of the aging effect. It is reported that the *n* constant is different according with the aging mechanisms, reflecting the proportion of nucleation or growth during this deleterious transformation [140], [143] and it depends on the microstructure and chemical composition of the material [144]. This exponent can vary from 0.3 to 4 [7], [140] and it can be derived from the logarithm form from [142]:

$$\ln\left(\ln\left(\frac{1-V_m^0}{1-V_m}\right)\right) = n\ln(b) + n\ln(t) \qquad \text{Equation (12)}$$

The *n* value can be calculated from the slope of the best regression line of the plot $\ln(\ln(1-V_m^0/1-V_m))$ versus $\ln(t)$. In order to understand these obtained results and this mechanism, the *n* constant was determined for the ATZ samples, which presented tetragonal to monoclinic transformation during the aging tests. The obtained plot is displayed on Figure 4.15.

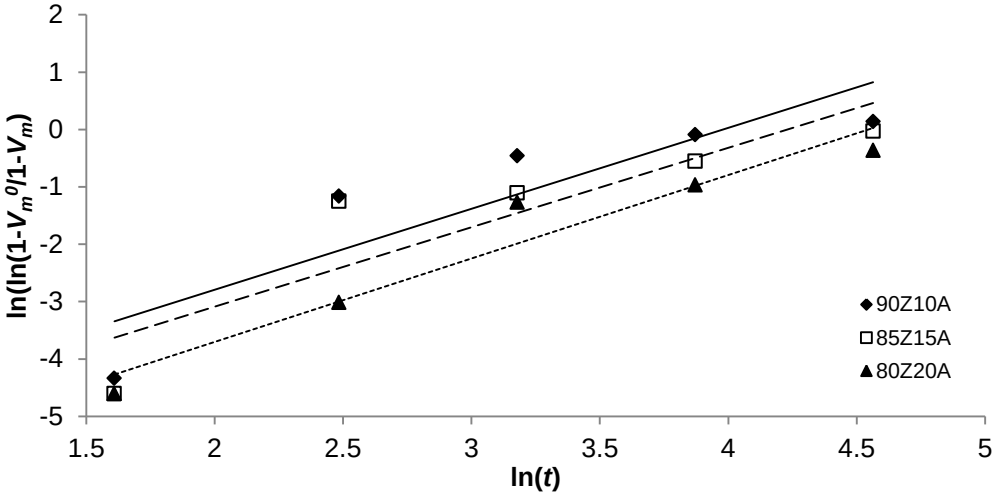


**Figure 4.15 - The ln(ln(1-$Vm^0$/1-$Vm$) vs ln(*t*) plot for each ATZ sample. For 5 hours of aging tests, a 1% monoclinic fraction value was applied for the 80Z20A and 85Z15A samples.**

**Table 4.8 - MAJ exponent obtained for each ATZ sample, from de slope of the regression lines from Figure 4.15.**

| ATZ sample | *n* |
|---|---|
| 80Z20A | 1.45 |
| 85Z15A | 1.38 |
| 90Z10A | 1.41 |

It was reported that a small value of *n* represents a higher contribution of the nucleation phase (accelerated nucleation) to aging, while for values around 4, a homogeneous nucleation and three-dimensional growth mechanism is dominant [142], [144], [145]. Thus for values of *n* between 1 and 2, the growth rate of the monoclinic phase is decelerated [144], [145], and it is also a one-dimensional process [141], [142]. The obtained values ($R^2$ >0.8) are in agreement with published results [141], [142], [144], [146] and, therefore, confirm that the nucleation process, although accelerated, occurred only in one dimension, the surface. New monoclinic nuclei were indeed formed, and detected by X-ray diffraction (Fig. 4.12) however, there was not a growth process through the bulk.

The obtained grain size, the uniform microstructure with no evident agglomeration and the beneficial sintering temperature (1400ºC) contributed to these exceptional results, since a nanometric grain size (Table 4.7) and no visible agglomerations of the least present phase (Fig. 4.9) leads to a better stabilization of the zirconia (agglomerations and bigger grains of zirconia are more prompt to destabilize and lead to further tetragonal to

monoclinic transformation). The relatively low sintering temperature applied (1400ºC) was already stated as an optimum temperature to enhance the aging resistance [19], [33].

In comparison with mechanical properties presented by the sintered samples, all the aged samples had less than 2% of decay after 5 hours and a maximum of 10% of decay was reached for 96 hours of aging, with every composite presenting a value higher than 500 MPa of flexural strength. These results are also in agreement with the requirements of the ISO standard that states that, after 5 hours of accelerated aging, the residual biaxial flexural strength should be higher or at least equal to 500 MPa and decrease no more than 20% in the sintered composites.

## 4.2 Comparative Study between the two stabilized zirconias

The results achieved for the undoped composites, increased the motivation to compare the two used zirconias, the 2 mol% Yttria Stabilized Zirconia (2YSZ) and the 3 mol% Yttria Stabilized Zirconia (3YSZ), regarding their mechanical properties and aging resistance. The objective was to compare an already existing composite with a new one, with the same proportions and a different zirconia.

The achieved results were analyzed in order to select the most promising ATZ. Since the 80Z20A sample (with 3 mol% YSZ) was the composition with a better aging resistance and the best set of mechanical properties, it was the selected composition to replicate with a less stabilized zirconia.

The objective for this additional test was to add this less stable zirconia to alumina in an new ATZ, in order to obtain enhanced mechanical properties (since it has less amount of yttria, what makes it more transformable) allied to a similar aging resistance presented by the 80Z20A, with the 3YSZ.

Therefore, a new 80Z20A sample with 2 mol% YSZ was produced under the same conditions, and submitted to the same tests and characterizations as the previously produced samples. This new composite was named 802YSZ20A (Fig. 4.16) and the obtained results were compared with the 80Z20A results (presented on the section 3.1 of this document and now named 803YSZ20A), and are showed in the following sections.

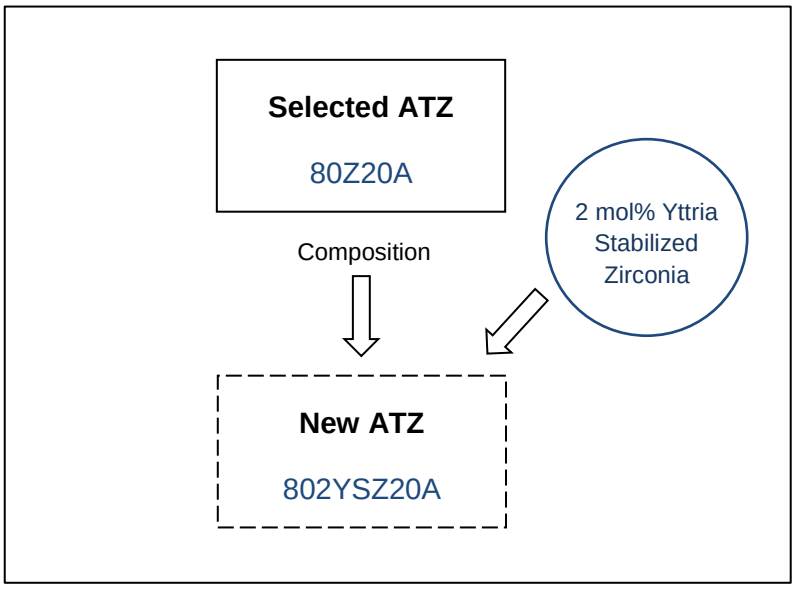


**Figure 4.16 - Addition of 2mol%Yttria Stabilized Zirconia to an 80Z20A composition previously defined (802YSZ20A).**

### 4.2.1 Particle size distribution

The particle size distribution of the new composition with the 2YSZ was determined and adjusted throughout milling to the particle size presented by its equivalent composite, 803YSZ20A. The obtained results are shown in Figure 4.17 and Table 4.9 bellow.

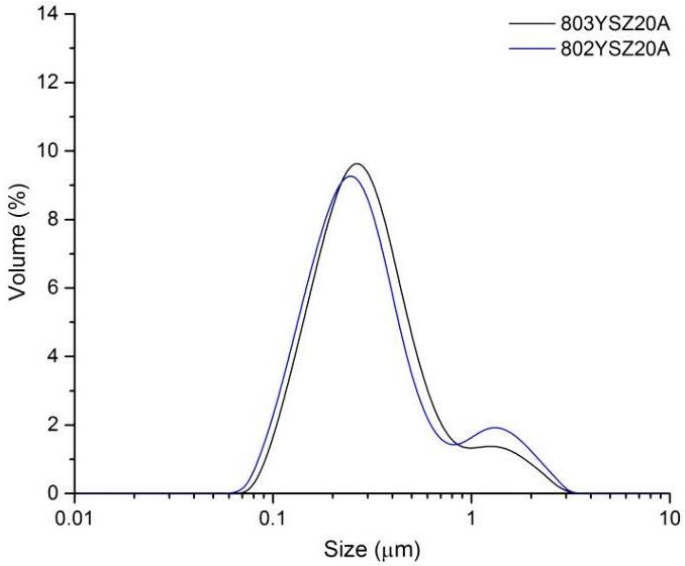


**Figure 4.17 – Particle size distribution of the 80Z20A composites with different zirconias (3 mol% YSZ and 2 mol% YSZ).**

**Table 4.9 - Mean diameter of the 80Z20A composites particles.**

| Composition | Mean diameter ($d_{50}$) |
|---|---|
| 803YSZ20A | 0.283 |
| 802YSZ20A | 0.268 |

From the obtained size distribution, it can be verified that both results are comparable, and the mean diameter of the 802YSZ20A particles is approximately 250 nm, as it would be expected since that the commercial powders and the ZTA and ATZ compositions previously characterized (section 4.1.2) present similar results.

It was then assumed that no agglomerations were present, and the suspensions were therefore prepared to be spray dried. The pH of the suspension prepared with this composition was also adjusted approximately 3 to achieve a deflocculated, stabilized suspension in agreement with the potential zeta measurements (presented in section 4.1.1).

### 4.2.2 Characterization of the spray dried powders with different types of stabilized zirconia

#### 4.2.2.1 Morphology

After the spray drying stage, the morphology of the 802YSZ20A granules was observed by scanning electron microscopy. The obtained granules were compared to the 803YSZ20A ones, already presented on section 4.1.3.1 of this document, and displayed in Figure 4.18.

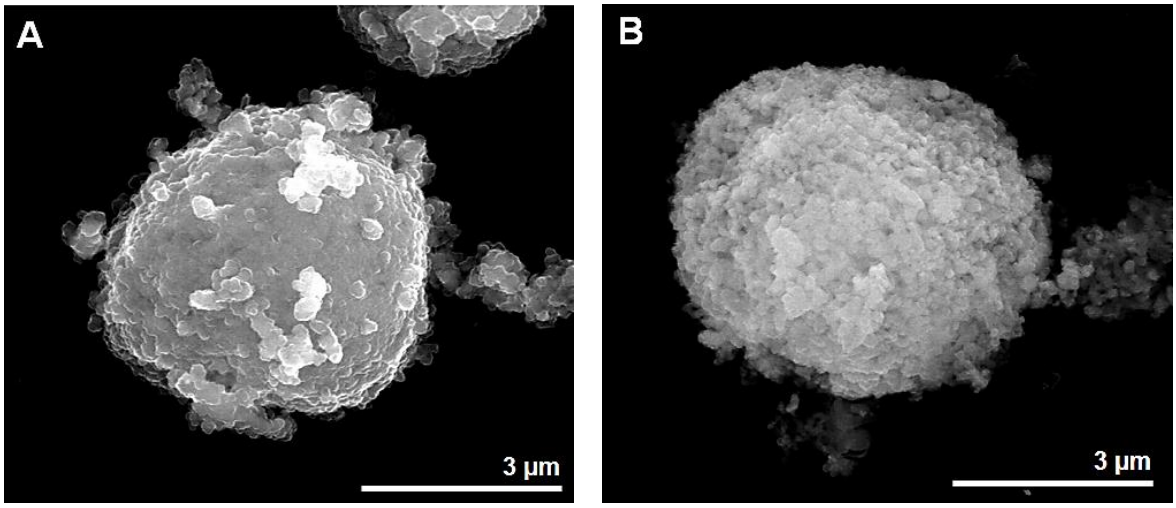


**Figure 4.18 - Obtained SEM images of the spray dried granules of each ATZ: A) 802YSZ20A; B) 803YSZ20A.**

As it can be verified, the spray drying process successfully lead to an agglomeration of the particles originated from the suspensions, by forming spherical and homogeneous granules. The obtained granules of the 802YSZ20A composition have a similar diameter to the 803YSZ20A granules (approximately 4 µm), and it can be verified that the particles which incorporate the granules are nanometric, and therefore, accordingly to the results from the particle size distribution (Fig. 4.17).

At this point it was assumed that the spray drying procedure effectively led to a good replication of the results for this new composition, and dense granules would lead to a good densification.

#### 4.2.2.2 Specific Surface Area

The specific surface area (measured by the B.E.T. adsorption isotherm) of the 802YSZ20A granules obtained by spray drying is 22.3 $m^2/g$. The specific surface area is very similar to the value presented by its homologous composite granules: 22.5 $m^2/g$ (this

value has already been presented on section 4.1.3.2 of this document). This similarity was already noticed on the values obtained the commercial powders, where the 3YSZ and 2YSZ presented 25.6 $m^2/g$ and 24.9 $m^2/g$, respectively. In comparison with these values, the addition of alumina led to a decrease in the specific surface area. Therefore, since the amount of zirconia is the same on both composites, the obtained values are in agreement with the expected ones.

#### 4.2.2.3 True Density

The obtained value of true density by helium pycnometer for the 802YSZ20A nanoparticles is 5.034 $g/cm^3$. This value is identical to the density value achieved for the 803YSZ20A particles (5.055 $g/cm^3$) and approximated to the density value of tetragonal zirconia (6.08 $g/cm^3$) as it would be expected on a ATZ composite. Therefore, it can be considered that dense nanoparticles were retrieved.

#### 4.2.2.4 X-Ray Fluorescence

X-ray fluorescence was used to confirm the composition of the 802YSZ20A sample, and assure the absence of any contamination. The results for this characterization are summarized on Table 4.10 below.

**Table 4.10 - Chemical composition of the 802YSZ20A composite powders.**

| % / Composition | $ZrO_2$ | $Al_2O_3$ | $Y_2O_3$ | $HfO_2$ | Other elements |
|---|---|---|---|---|---|
| 802YSZ20A | 76.411 | 18.986 | 2.709 | 1.326 | 0.068 |

From the obtained chemical composition, it can be observed that, the hafnia content is below 5% and all the oxides (except alumina and yttria) are below 0.5%, as it is required on ISO 13356 (2008) [22].

The content of alumina and zirconia were detected in agreement with the defined compositions.

### 4.2.3 Characterization of the composites with different types of stabilized zirconia

#### 4.2.3.1 Density of the green and sintered pieces

As it was defined on the previous produced composites, two stages of pressing (UP and CIP) besides sintering, were carried on the 802YSZ20A. The density of the green pieces was measured geometrically while the density of the sintered pieces was measured Archimedes' Method. The obtained values were compared with the equivalent sample, 803YSZ20A. The results are displayed on Figure 4.19 and Table 4.11.

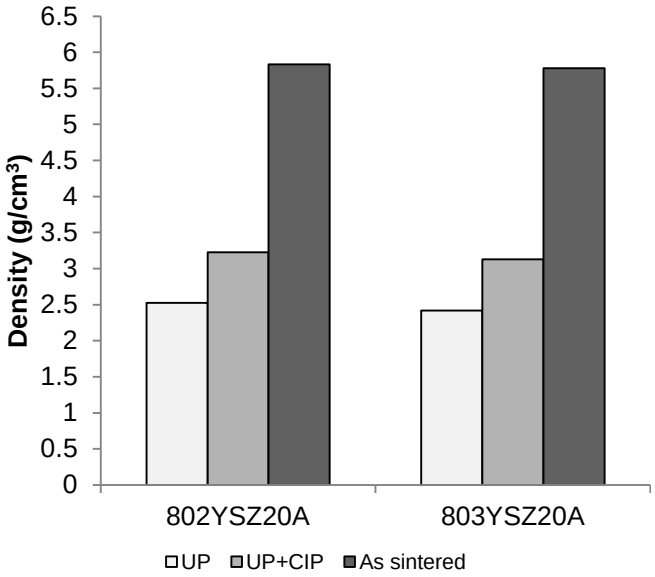


**Figure 4.19 - Density values achieved after UP, CIP and sintering for the two ATZ: 802YSZ20A and 803YSZ20A.**

**Table 4.11 - Density degree of each ATZ after sintering.**

| Composition | Density (%) |
|---|---|
| 802YSZ20A | 99.32 |
| 803YSZ20A | 98.47 |

These results confirm the similarity between the two compositions, with very close values of density (5.83 g/cm$^3$ and 5.78 g/cm$^3$ for 803YSZ20A and 802YSZ20A respectively). Once more, the sintering stage highly contributed to an increase in the densification degree that reached values higher than 98%, relatively to the theoretical values.

Since the densification values were very close, it was assumed that the density would not be a critical aspect that could influence the mechanical tests results.

#### 4.2.3.2 Crystal Phases Composition

X-ray diffraction was used to confirm the absence of other possible phases that could be formed during sintering, and verify the presence of tetragonal and monoclinic zirconia. The obtained diffractogram was compared with the one obtained for the 803YSZ20A sintered sample and displayed below.

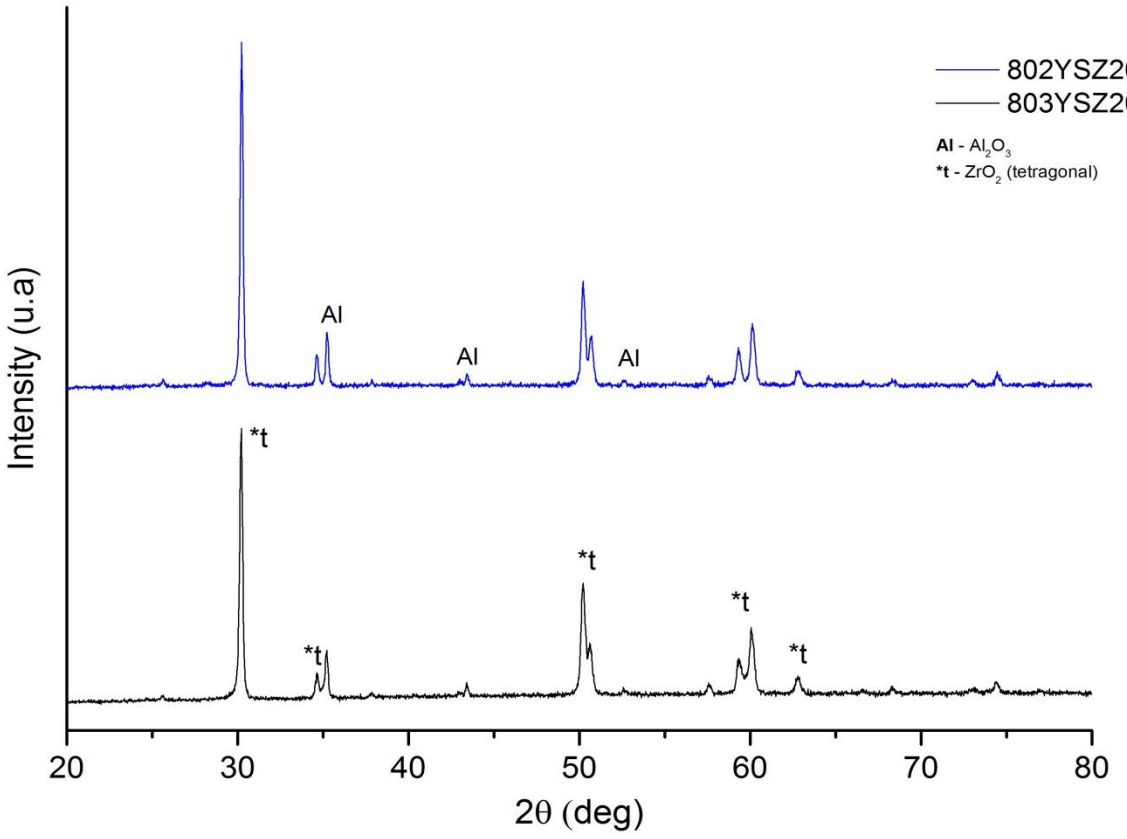


**Figure 4.20 - X-Ray diffractogram obtained for the sintered 802YSZ20A sample and compared with the obtained for the 803YSZ20A (already presented on section 4.1.4.2).**

The obtained results showed no other phase besides alumina and zirconia. It was also observed that, even though the 802YSZ20A is a more unstable zirconia, no significant peaks of monoclinic zirconia were detected (only one is nearly undetected, around 28º). However, this is not a precarious factor, since it is derivate from the highest transformability from this zirconia in comparison with 803YSZ20A.

#### 4.2.3.3 Microstructure

The 802YSZ20A sintered sample was thermally etched and observed by scanning electron microscopy, in order to evaluate its microstructure and determine its grain size. The obtained micrograph was compared with the one obtained for 803YSZ20A sample (already presented on section 4.1.4.3). The obtained images are displayed in Figure 4.21. The mean grain size was also determined by line interception method. The calculated values are shown in Table 4.12.

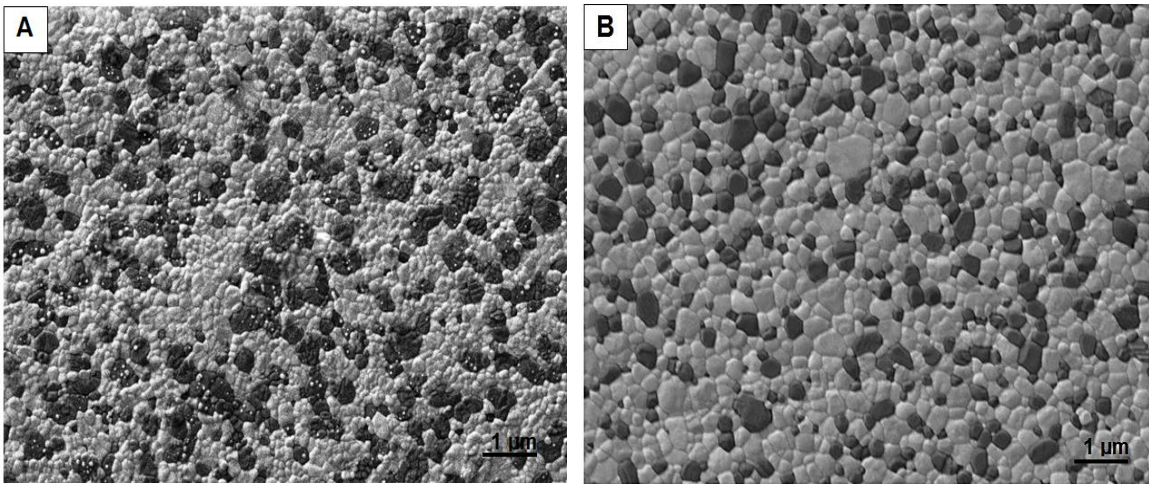


**Figure 4.21 - SEM images obtained for A) 802YSZ20A sintered sample, compared with B) 803YSZ20A.**

**Table 4.12 - Mean grain size calculated by line interception method of the ATZ composites, 802YSZ20A and 803YSZ20A.**

| Composition | Mean grain size (nm) | |
|---|---|---|
| | Alumina | Zirconia |
| 802YSZ20A | 289±6 | 221±11 |
| 803YSZ20A | 359±12 | 353±3 |

From the obtained images it can be noticed that a well dispersed microstructure was achieved, without any evident agglomerates. No porosity was also detected, as it would be expected since a good densification upon sintering was accomplished.

Regarding the grain size, the presence of zirconia as primary phase, hindered the alumina grain growth during sintering, and similar grain sizes for zirconia and alumina were achieved for both composites. However, in the new composite a decrease in grain size is detected, mainly for zirconia. Even considering this fact, good results regarding aging resistance were expected since a less stabilized zirconia is beneficiated by a smaller grain size (larger grains become more unstable [8], [30]). Therefore it was

considered that this grain size could benefit the aging resistance of the 802YSZ20A composite.

#### 4.2.3.4 Mechanical Properties

Mechanical tests were performed in order to evaluate how the yttria content would affect the hardness, fracture toughness and flexural strength of the two ATZ composites. The outcome for each test is displayed in Figure 4.22 and compared with the 803YSZ20A results. This composition attained a good densification (reaching 99.32%) which allied to its higher transformability, improved mechanical properties were expected.

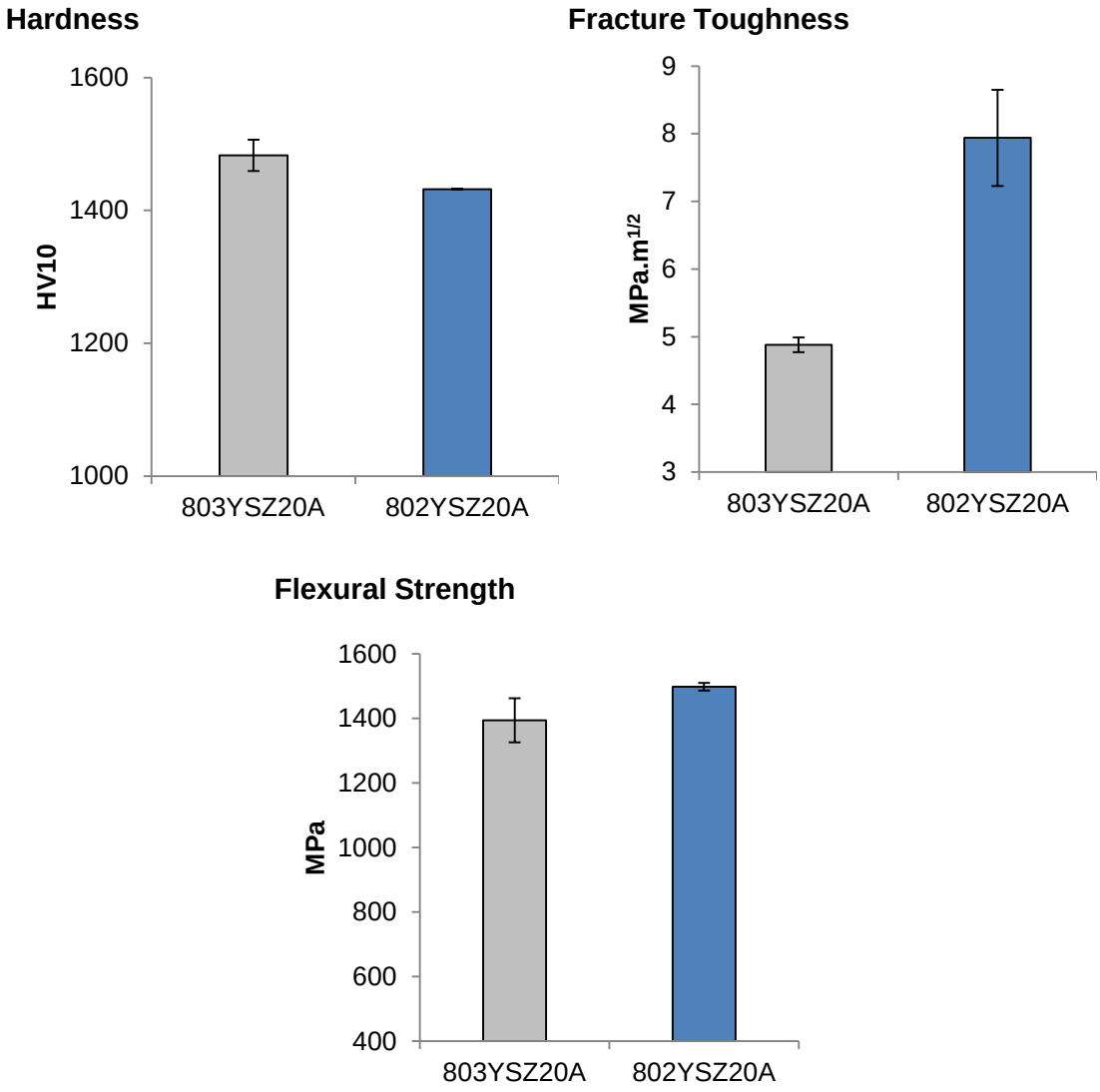


**Figure 4.22 - Results obtained for Vickers Hardness, fracture toughness and flexural strength of the 802YSZ20A and 803YSZ20A samples.**

Regarding the Vickers Hardness results, a slight decrease is verified for the less stable composite.

However, remarkable results are achieved for the fracture toughness. As expected, since that we face a zirconia with less amount of yttria, and therefore more susceptible to the tetragonal to monoclinic transformation, the fracture toughness was greatly influenced by the stabilizer content. The 803YSZ20A sample presented a fracture toughness value of 4.88 MPa.$m^{1/2}$ while the 802YSZ20A sample reached 7.94 MPa.$m^{1/2}$.

This increase in the fracture toughness can explain the decrease in the hardness values. Even though it is not significant, it is suggested that, an increase in this parameter could influence the hardness, and create a proportional decrease. Basically the improving of the fracture toughness lead to a slightly decrease in the hardness of the composite.

Regarding the results achieved for flexural strength, an increase was confirmed for the 802YSZ20A sample, since it is reported that the flexural strength also increases with the transformability of the composite [10].

From these results it can therefore be confirmed that a less stable zirconia improves the mechanical properties of the ATZ composites. The addition of the 2 mol% Yttria Stabilized Zirconia effectively improved the 80Z20A mechanical properties which was one of the objectives of this comparative study.

### 4.2.4 Accelerated Aging Test

The other objective of comparing the two types of zirconia was to analyze the aging resistance of the less stable zirconia on an ATZ composite.

Therefore, the 802YSZ20A sample was submitted to an accelerated aging test, in an autoclave (134ºC, 2 bar) for 96 hours, like it has been performed on the initial ATZ and ZTA samples. The monoclinic content was analyzed by X-Ray diffraction and the results were again compared to the 80Z20A composite (with 3 mol% Yttria Stabilized Zirconia) and they are presented on Figure 4.23.

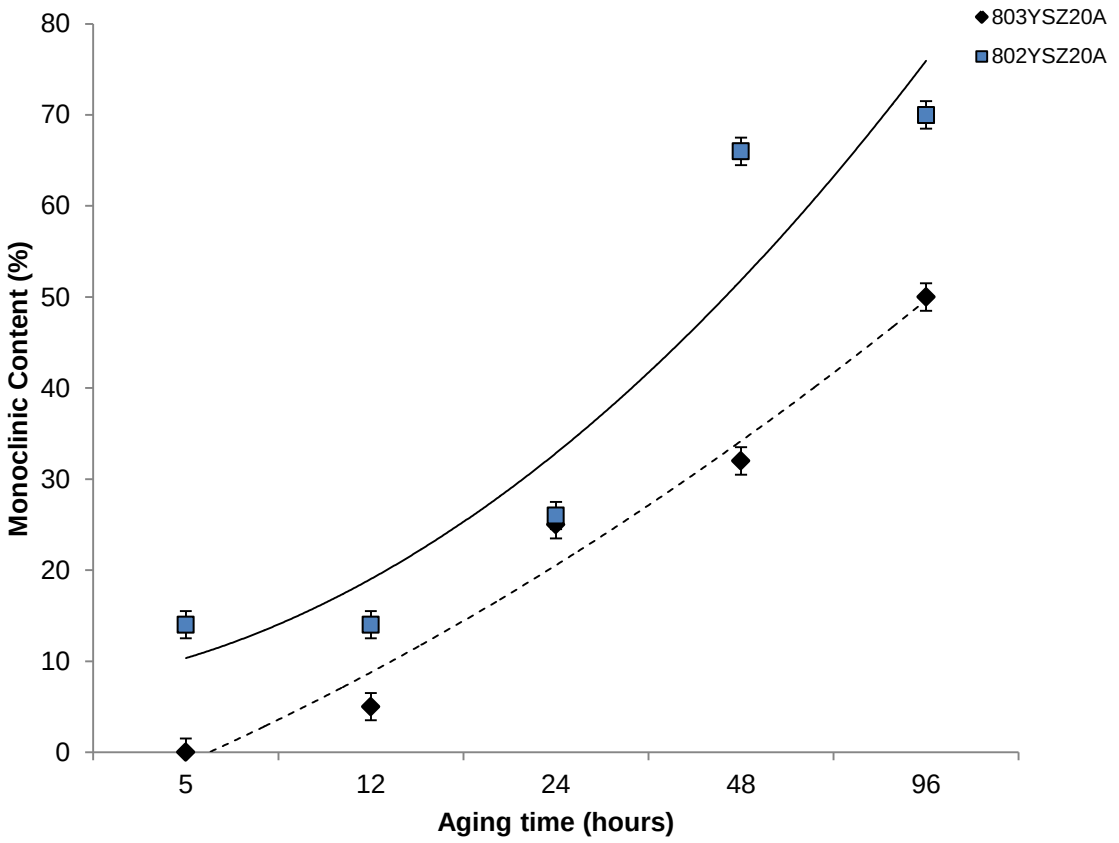


**Figure 4.23 - Change in the monoclinic content of the aged ATZ composites with 2YSZ and 3YSZ with time, during accelerated aging tests in an autoclave (134ºC, 2 bar).**

The outcome of the aging test showed that, the amount of yttria present on each composite affected the *t-m* transformation rate after several hours of aging.

As expected, the amount of monoclinic zirconia after 96 hours on aging environment was considerably higher on the 802YSZ20A, the less stable composite, reaching 70% of monoclinic zirconia. Therefore, even though 2 mol% Yttria Stabilized Zirconia was used in the composition with the highest amount of alumina, it was not sufficient to hinder the aging. However, the obtained results were comparable to the amount of monoclinic zirconia in the 90Z10A composite (68%). Thus it can be assumed that an addition of only 10% alumina added had a beneficial influence in stabilizing the 2YSZ.

The Vickers Hardness, fracture toughness and flexural strength of the 802YSZ20A composite was tested for the same period of time as the aging tests and compared with the results of the 803YSZ20A composites, presented on Figure 4.13, section 4.1.5. It was important to perform these tests, since it would give an insight of the sensibility of the 2YSZ and the extension of the degradation to the bulk. The results are shown on Figure 4.24.

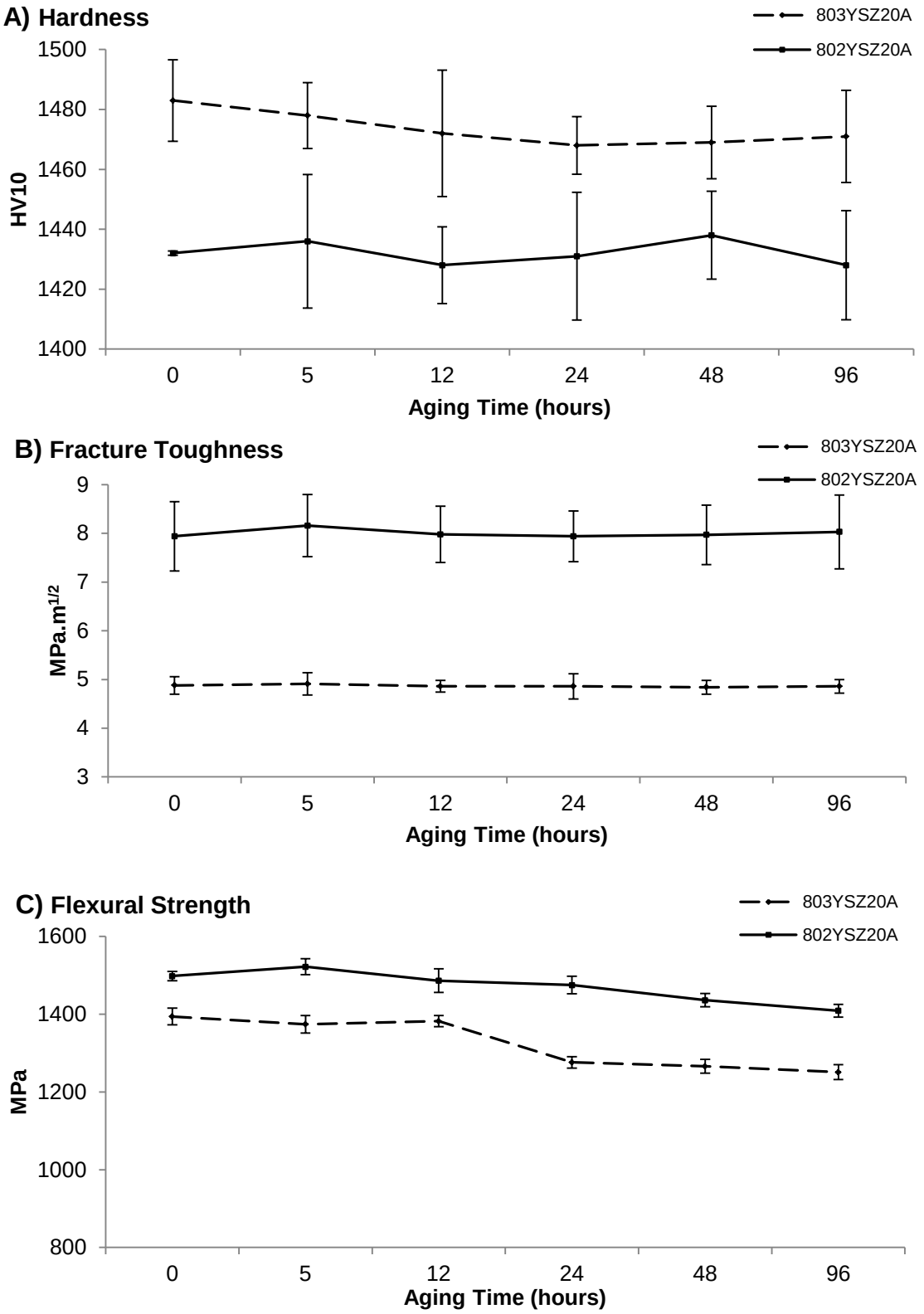


**Figure 4.24 - Mechanical properties of the aged composites with the two stabilized zirconias, 3mol%YSZ and 2mol%YSZ, throughout the aging test: A) hardness, B) fracture toughness and C) flexural strength.**

The results showed that even though the percentage of monoclinic zirconia detected by X-ray diffraction was 70%, throughout the aging test the mechanical properties of the 802YSZ20A composite did not show a significant decrease. Similarly to the obtained results for the different ATZ and ZTA compositions (Figure 4.13, section 4.1.5) the mechanical properties tested did not change during the aging tests. Only the flexural strength presented a slightly decrease, however it was not very pronounced, since only a decay of approximately 6% was noticed after 96 hours of aging.

From these results, which are similar to the ones obtained previously for the ATZ composites, it can be again assumed that the degradation on the 802YSZ20A composite did not expand to bulk. Therefore, it is considered that the detected amount of monoclinic zirconia (70%) in this composite is only present at the sample surface. It can be thus suggested that the aging resistance of this sample, which is considered less stable, is the result of a set of beneficial characteristics such as a good densification and a fine microstructure without agglomerates.

## 4.3 Doped Zirconia Alumina Composites

Two dopants were added to both ZTA and ATZ composites, with the purpose of an improvement of their mechanical properties and aging resistance. The additive selection as well as the achieved results and characterizations are presented in the following section.

### 4.3.1 Selection of the additives

After characterize the mechanical properties and aging resistance of ZTA and ATZ composites, it was decided to enhance the properties of these composites with the addition of dopants.

The main objective was to apply two additives that are known for enhancing the two crucial properties of these composites: mechanical properties and/or hydrothermal aging resistance. All the tests were repeated and the results compared with the obtained for the undoped samples to verify the behavior and changes caused by these additives. A process of selection of additives to these composites was accomplished. The theoretical background of the tested additives is presented in the section 2.4 of this document. In Table 2.3 a summary of some published results is shown.

In order to improve the aging resistance, the chosen oxide was lanthana ($La_2O_3$). This oxide has proven to highly decelerate the tetragonal to monoclinic transformation with quantities as little as 0.1 wt%. Other factor that influenced this selection was the retention of the mechanical properties, which means that even though the aging resistance increases, it has no deleterious effect in the mechanical properties. This oxide was already tested with alumina, but only in doping quantities. The goal is now to observe the changes when added to a composite with higher quantities of alumina. Also, lanthana is only now starting to be tested, differently from some stabilizing oxides that are already well stablished such as chromia [11], ceria [73], and magnesia [63], [79]. This fact increased the interest and motivation.

The selected amount of lanthana to add to the composites was 0.1 wt%, in agreement with the results obtained by other authors that reported an enhanced aging resistance with only this quantity of dopant [50].

On the other hand, to promote the increasing of the mechanical properties, tantalum pentoxide ($Ta_2O_5$) was selected. This additive promotes densification which leads to the remarkable results that have been published [65]. Higher values of hardness and fracture toughness were achieved when compared with results obtained for the addition of the

settled strontia [59], and for the titania [92], silica [95] and niobia [98]. Also, those results were achieved with a very small amount of dopant, which was a positive factor for this choice. It is also a motivation to examine the aging behavior of the composites with this dopant since it is verified an odd variation on the amount of monoclinic zirconia (Fig. 2.14) during the aging tests published [65]. Regarding these results, 0.35 wt% of $Ta_2O_5$ was the chosen quantity to add to these composites, since the tetragonal zirconia tends to increase for amounts of tantalum pentoxide higher than approximately 0.22 wt%. Considering that, the increasing quantity of this oxide maximizes the mechanical properties, the selection was relegated to a higher value.

Subsequently to the obtaining of all the results and selection of the additives, the two composites with the best set of properties, one from the ATZ side and other from the ZTA side, were elected.

Between the ATZ compositions, the 80Z20A sample was chosen, since it presented a higher aging resistance among the other ATZ samples (Fig. 4.12). Its mechanical properties were also decent, presenting the highest values for hardness and flexural strength.

All the ZTA samples did not underwent degradation during the aging tests, so the choice fell on the mechanical properties. The selected ZTA composition was the 80A20Z. The value of hardness was very consistent and both fracture toughness and flexural strength results of this composition were better in comparison with the remaining compositions.

Thus, on the basis of these results achieved for 80A20Z and 80Z20A, four new compositions were produced, 80A20Z and 80Z20A both with tantalum pentoxide and lanthana (Fig. 4.25). To investigate the effects of each dopant, these oxides were used in separate compositions.

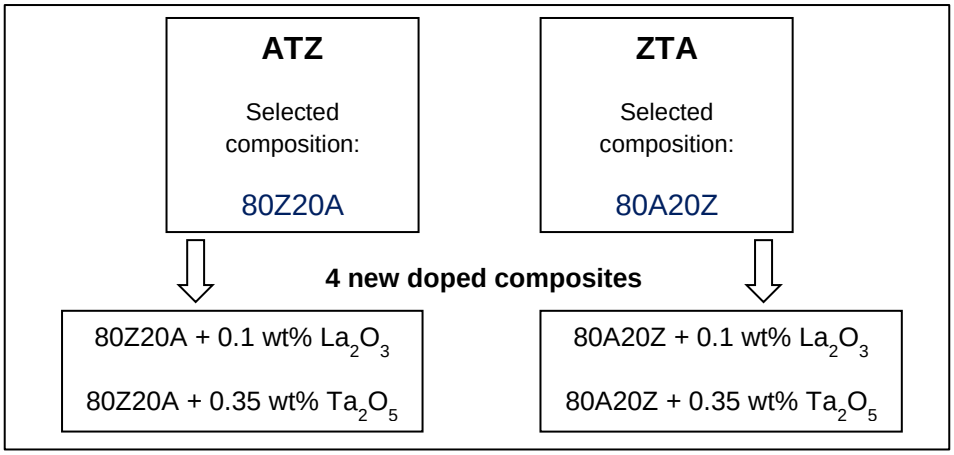


**Figure 4.25 - New doped composites derived from the results presented by the ATZ and ZTA composites.**

These new composites were produced under the same conditions and submitted to the same tests in order to compare the new results with the ones of the control group, the undoped samples.

### 4.3.2 Suspension stability and particle size distribution

The isoelectric point for the lanthanum oxide and the tantalum pentoxide was assumed from literature: for the lanthanum oxide the isoelectric point stands at a pH around 10 [147] and the isoelectric point of the tantalum pentoxide is around pH 3 [148].

Alongside with the previous results for the zeta potential of the alumina and both 3 mol% YSZ and 2 mol% YSZ (section 4.1), a suitable pH was determined for the preparation of the suspensions. Since the lanthanum oxide has an isoelectric point around 10, the suspension was stabilized at the same pH as previously (pH=3). The tantalum pentoxide has an isoelectric point around pH 3 that required that the suspension had to be slightly more basic. Thus the selected pH for the suspensions with $Ta_2O_5$ was 5.

The particle size was also adjusted to the nanometric scale. After milling, the suspension particles were analyzed and the particle size distribution of each composition was determined. The obtained curves and mean particle diameter are displayed on Figure 4.26 and Table 4.13.

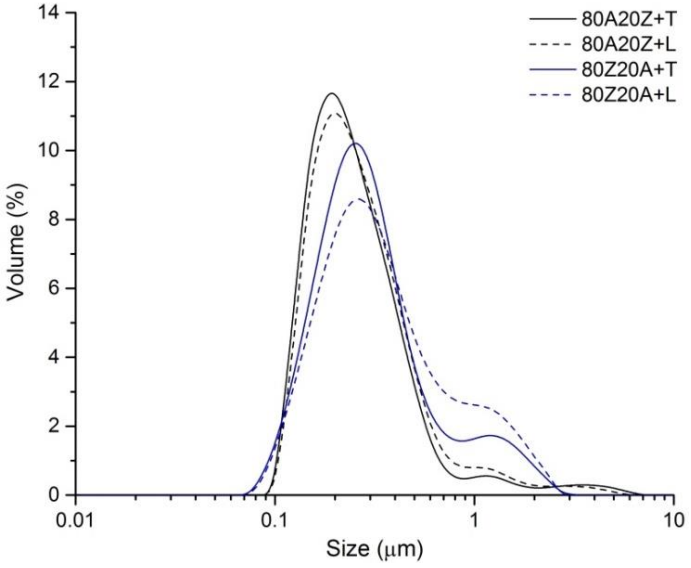


**Figure 4.26- Particle size distribution of the doped composite particles.**

**Table 4.13 - Mean Diameter of the doped composite particles.**

| Composition | Mean diameter ($d_{50}$) |
|---|---|
| 80Z20A+T | 0.274 |
| 80Z20A+L | 0.310 |
| 80A20Z+T | 0.229 |
| 80A20Z+L | 0.243 |

From these results it can be confirmed that the milling process lead to a narrow size distribution of the particles from the doped composition suspensions, within the nanometric scale (around 250 nm).

For the lanthana doped composite particles it was verified a small increase in the mean diameter which was probably due to the size of this added oxide that remained unknown. However the mean diameter remained nanometric and it was not a significant difference.

### 4.3.3 Characterization of the doped spray dried powders

#### 4.3.3.1 Morphology

To confirm the achievement of spherical granules, similar to the ones observed for the undoped composites, the retrieved spray dried powders were observed by SEM. The collected micrographs are exhibited on Figure 4.27.

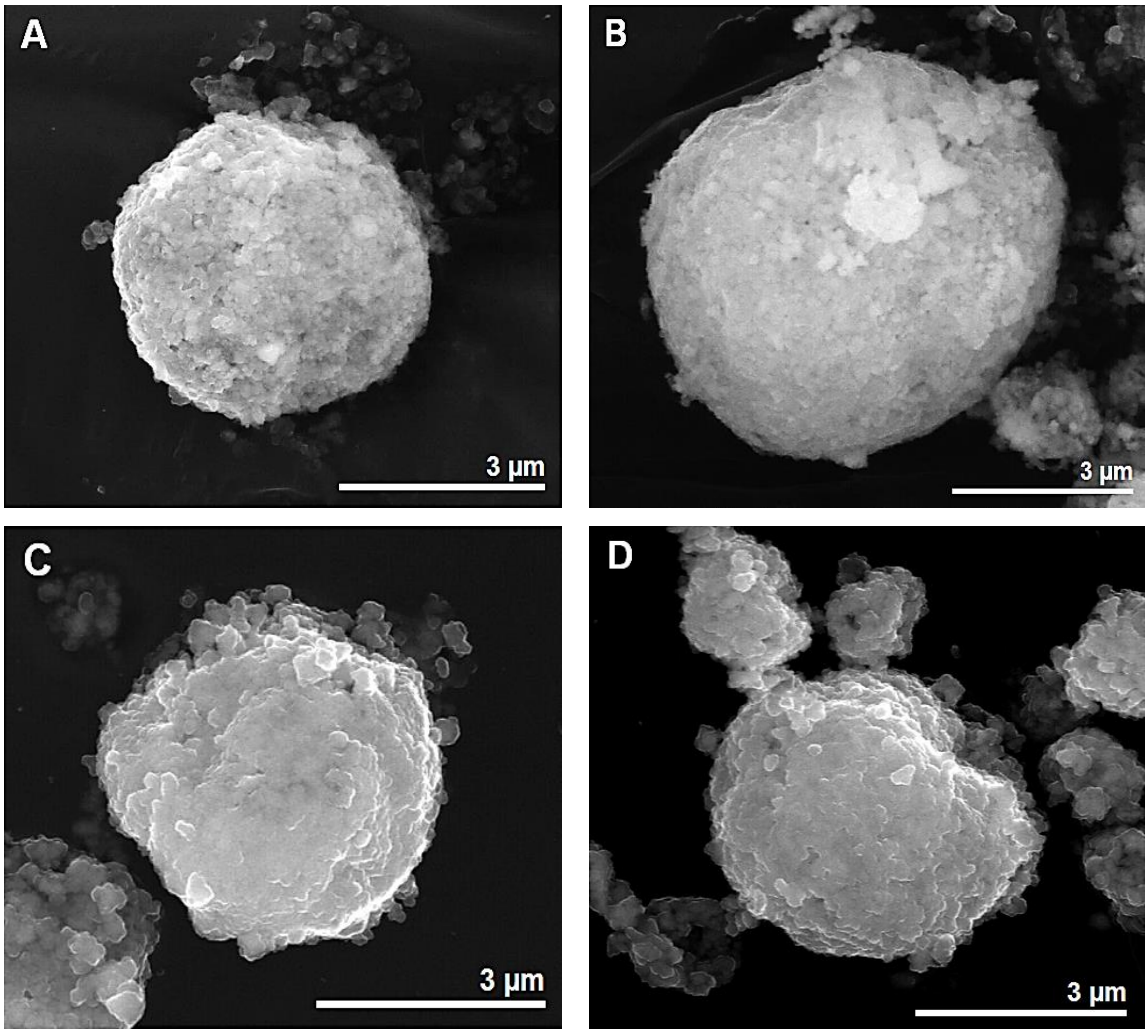


**Figure 4.27 - SEM micrographs of the granules of the doped samples obtained by spray drying: A) 80A20Z+T; B) 80A20Z+L; C) 80Z20A+L; D) 80Z20A+T.**

As it can be verified, micrometric granules were formed during the spray drying process. These granules are similar to those obtained for the undoped samples, with diameters ranging from 4 µm to 7 µm.

The granules are slightly irregular, and constituted by the nanometric particles that were present on the spray dried suspension. These nanometric particles appear to be well packed and there is also no evidence of hollow granules. However, the ZTA granules present a slightly more regular surface than the ATZ granules. No fragmented granules were noticed.

#### 4.3.3.2 Specific Surface Area

The specific surface area (SSA) of the obtained spray dried powders was determined by the B.E.T. adsorption isotherm. The SSA values achieved are presented in the following table.

**Table 4.14 - Specific Surface Area of each doped composite powder.**

| Composition | Specific Surface Area (B.E.T.) ($m^2/g$) |
|---|---|
| 80Z20A+T | 22.3 |
| 80Z20A+L | 22.2 |
| 80A20Z+T | 18.4 |
| 80A20Z+L | 18.4 |

As expected, it can be observed the ATZ powders have a higher specific surface area than the ZTA ones. Again, a specific surface area around 22 $m^2/g$ is achieved for the ATZ samples, which is in agreement with the previously obtained values (Table 4.2). Regarding the ZTA composite powders, the addition of alumina, again, caused a decrease on this parameter to, approximately, 18 $m^2/g$. Basically, these results are accordingly to the expected, and it is verified that the addition of both $Ta_2O_5$ and $La_2O_3$ did not affected this parameter.

#### 4.3.3.3 True Density

The density of the obtained particles from doped composites was measured. The attained values are summarized on Table 4.15.

**Table 4.15 - Particles density for each doped composite measured by helium pycnometry.**

| Composition | Density ($g/cm^3$) |
|---|---|
| 80Z20A+T | 5.055 |
| 80Z20A+L | 5.052 |
| 80A20Z+T | 4.035 |
| 80A20Z+L | 3.944 |

Just as expected, the ATZ nanoparticles exhibit a higher density than the ZTA ones, due to their higher amount of zirconia. The obtained values are similar to the ones presented by the undoped samples (Table 4.4, section 4.1.3.4) and thus it can be

assumed that both additives did not influence the true density of the powders. From the obtained values, it is expected that the nanometric particles (that constitute the granules) are dense.

#### 4.3.3.4 X-Ray Fluorescence

The chemical composition of the doped composites was analyzed through X-Ray fluorescence. This characterization was important to determine the presence of impurities and verify the presence of the additives in the composites. The retrieved contents of each oxide are summarized on the Table below.

**Table 4.16 - Chemical composition for each doped composite by means of X-Ray fluorescence.**

| Composition (%) | 80Z20A+T | 80Z20A+L | 80A20Z+T | 80A20Z+L |
|---|---|---|---|---|
| $ZrO_2$ | 75.599 | 75.079 | 18.837 | 19.044 |
| $Al_2O_3$ | 18.406 | 18.628 | 79.098 | 78.092 |
| $Y_2O_3$ | 4.154 | 3.663 | 1.103 | 1.073 |
| $HfO_2$ | 1.306 | 1.014 | 0.418 | 0.415 |
| $Ta_2O_5$ | 0.3321 | - | 0.3716 | - |
| $La_2O_3$ | - | 0.1086 | - | 0.0918 |
| Other elements | 0.061 | 0.063 | 0.054 | 0.046 |

From the results presented, it can be confirmed the presence of the additives, $Ta_2O_5$ and $La_2O_3$, on both ATZ and ZTA composites.

Like the previous results obtained for the undoped samples, no major contamination was noticed. The content of hafnia was below 5% for every composite and any other oxide content (except alumina and yttria) was, as well, kept below 0.5%, as specified on ISO13356 (2008) [22].

Also, the contents of zirconia, alumina and both additives, are in agreement with the defined compositions for each doped composite.

### 4.3.4 Characterization of the doped sintered pieces

#### 4.3.4.1 Density of the green and sintered pieces

A well densified material is a good indicator of good mechanical properties. Since good densification was achieved for the previously produced composites, the same two stages of pressing, uniaxial pressing (UP) and cold isostatic pressing (CIP), were repeated for the doped samples, before sintering. The density values for each doped composite, after each stage of pressing and sintering, are shown on Figure 4.28. The densification degree relative to the theoretical values of density of alumina and zirconia was calculated and presented in Table 4.17.

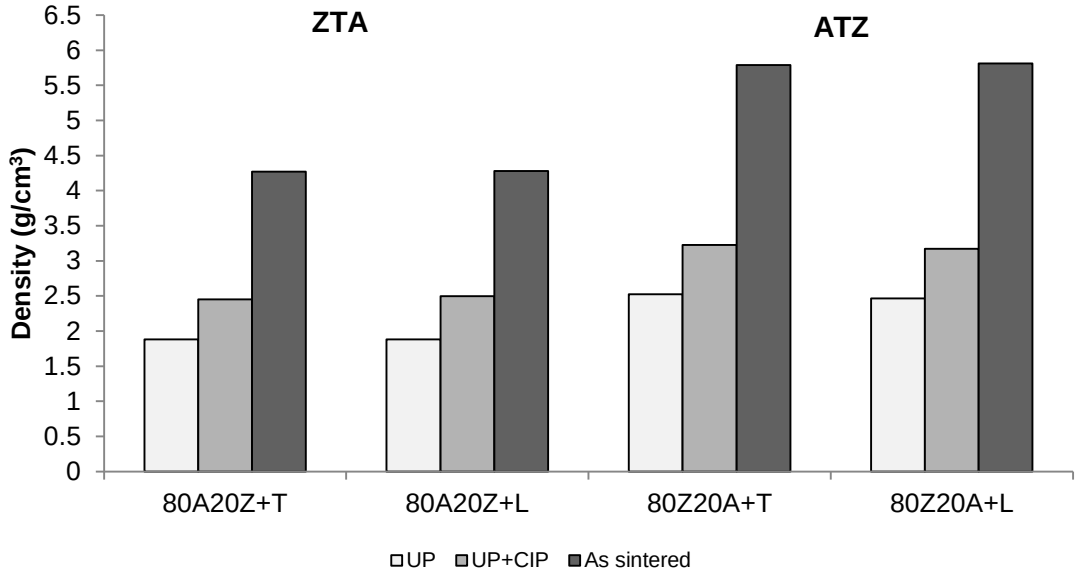


**Figure 4.28 - Density of the doped composites sintered pieces, throughout the different stages of pressing and sintering.**

**Table 4.17 - Densification degree of the sintered doped composites.**

| | Composition | Density (%) |
|---|---|---|
| Undoped | 80Z20A | 98.47 |
| | 80A20Z | 98.05 |
| Doped | 80Z20A+T | 98.64 |
| | 80Z20A+L | 98.98 |
| | 80A20Z+T | 97.49 |
| | 80A20Z+L | 97.72 |

It was again confirmed that after sintering, all the composites achieved high density values with the ATZ samples, with zirconia as the main phase, reaching the highest values (approximately 6 g/cm$^3$).

As the previous results for the density of the undoped composites (Table 4.6, and 4.11, sections 4.1.4.1 and 4.2.3.1, respectively) the calculated density degree was above 97% which confirms that the obtained composite pieces were fully dense and improved mechanical properties were anticipated.

An increase in density was reported with the increasing amount of $Ta_2O_5$ [65], however, in this case it was not noticed.

Regarding the lanthana doping, no variation of the density [50] or even a poor densification after sintering at 1500ºC for 2 hours was reported [69]. This however was not verified in this work, since a good relative density (higher than 97%) was achieved for both doped compositions.

#### 4.3.4.2 Crystal Phases Composition

X-ray diffraction was performed on the sintered doped samples to confirm the absence of new crystalline phases, and also verify the zirconia phases present. The obtained diffractogram for each doped composite is exhibit in the Figure 4.29, below.

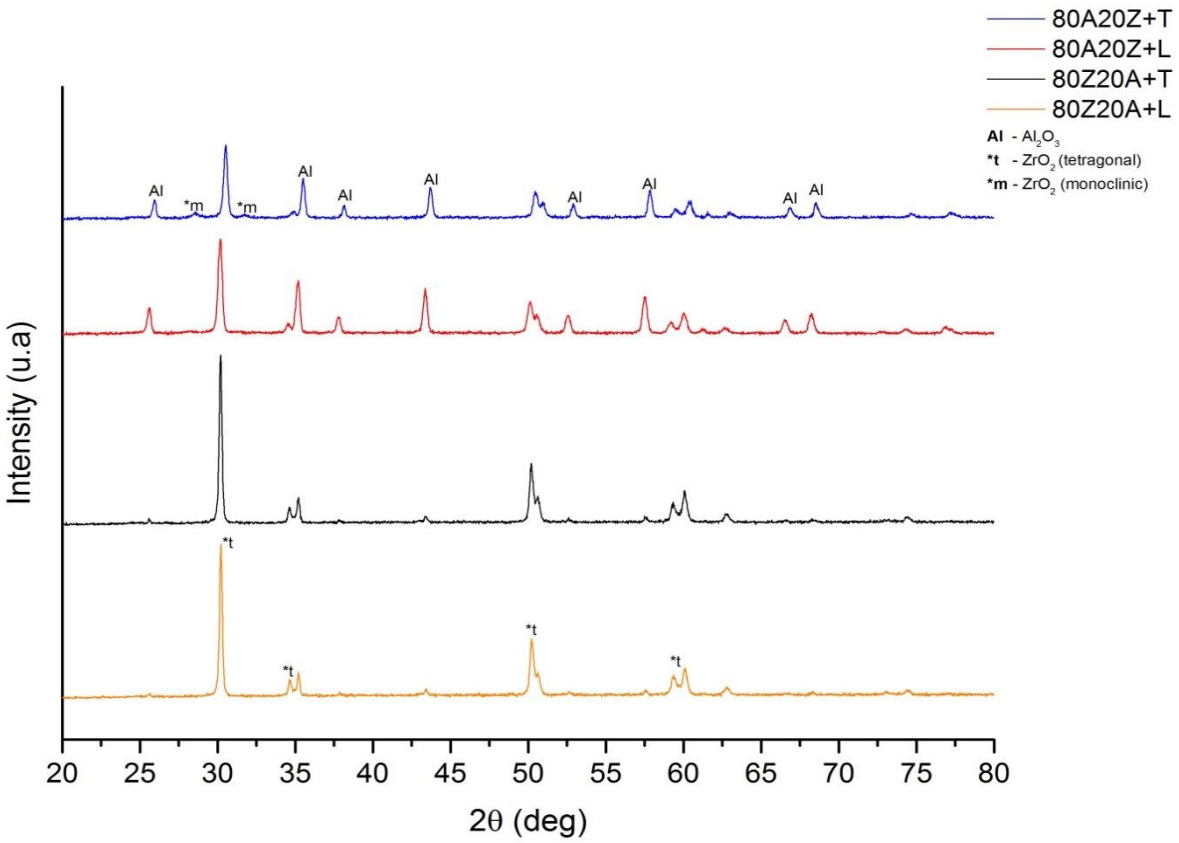


**Figure 4.29 - X-ray diffractogram obtained for each doped composite after sintering.**

From the obtained results, it can be confirmed that no other phase is present in the doped composites besides alumina and zirconia.

However, monoclinic zirconia is detected for the 80A20Z doped with $Ta_2O_5$. It was reported that this dopant increases the transformability of zirconia [65]. The presence of $Ta_2O_5$ causes an increase of the lattice distortion that destabilizes the tetragonal phase of zirconia [149], [150]. Since it was used the less stabilized zirconia (2YSZ) in the 80A20Z+T composite, it could happen that, the addition of this dopant could have destabilized the tetragonal zirconia. This was not verified in the ATZ doped with $Ta_2O_5$, 80Z20A+T that, in fact, have a larger amount of zirconia. In this case it can be assumed that the 3 mol% Yttria Stabilized Zirconia used in the ATZ doped composite was less susceptible to the destabilization caused by $Ta_2O_5$ and the tetragonal phase remained stabilized. Yet, this destabilization on the 80A20Z+T composite was not alarming since it was determined, by Rietveld refinement, that the content of monoclinic zirconia is around 4.4%, and therefore just an outcome of the composite enhanced transformability.

#### 4.3.4.3 Microstructure

The doped composite sintered pieces were thermally etched and observed by scanning electron microscopy. The obtained images for the ATZ and ZTA doped composites are displayed in Figure 4.30 (A-D).

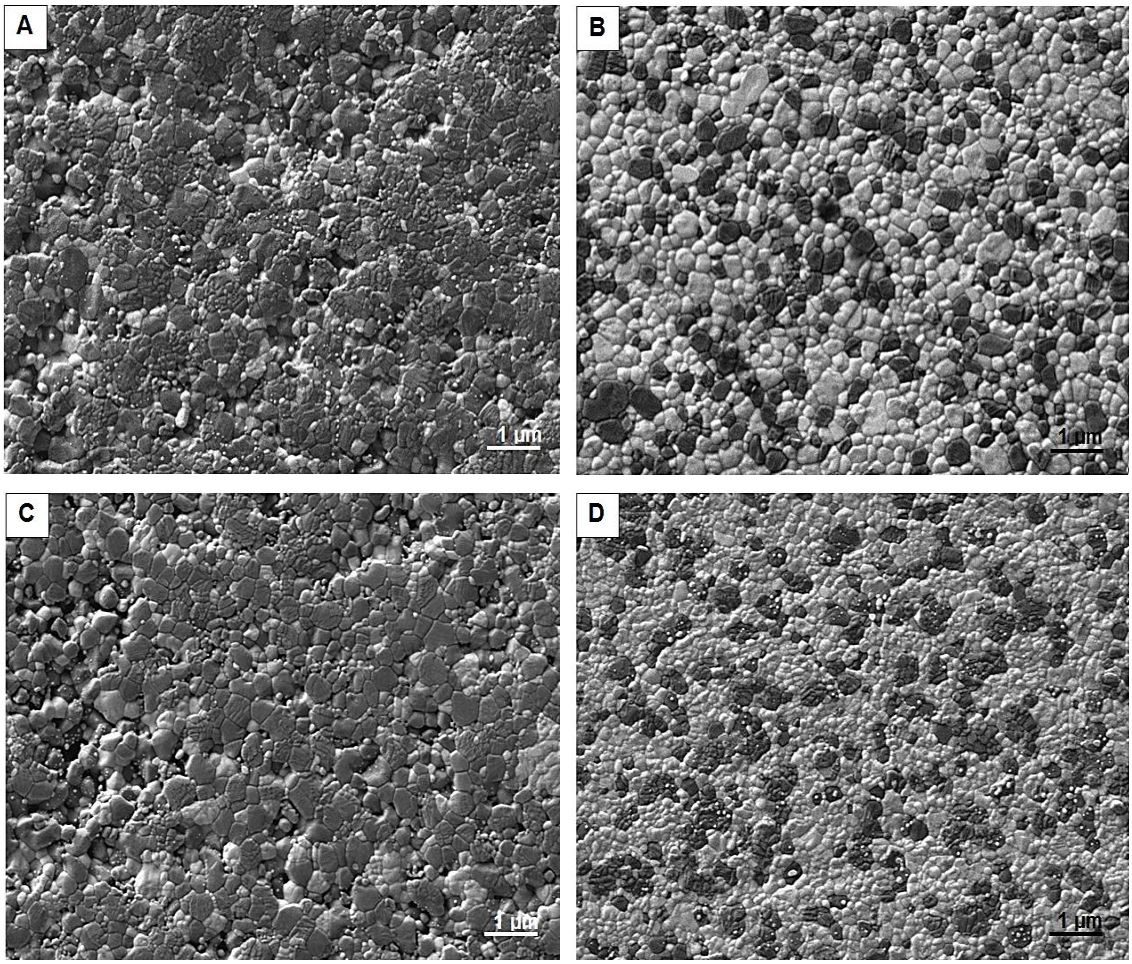


**Figure 4.30 - SEM micrographs from the thermal etched doped composites: A) 80A20Z+L; B) 80Z20A+L; C) 80A20Z+T; D) 80Z20A+T.**

From the obtained images it is clearly noticed that the ZTA doped samples present an irregular surface. The density of the ZTA samples reached slightly lower values (around 97%) in comparison with the ATZ ones (higher than 98%). However, this value is still an indicator of a good densification. Therefore it can be assumed that this porosity was present only at the surface of the material.

From the obtained SEM micrographs, the mean grain size was calculated. The outcome of this determination is summarized in Table 4.18.

**Table 4.18 - Mean grain size of each doped composite calculated by line interception method.**

| Composition | Mean grain size (nm) | |
|---|---|---|
| | Alumina | Zirconia |
| 80Z20A+T | 289±18 | 244±13 |
| 80Z20A+L | 357±14 | 341±7 |
| 80A20Z+T | 393±15 | 280±2 |
| 80A20Z+L | 319±19 | 248±19 |

As expected and verified for the undoped samples (Table 4.7, section 4.1.4.3), on the ZTA doped samples the alumina grain growth stands out, and consequently hinders the zirconia growth.

In the ATZ samples, the mean grain size remained similar for both alumina and zirconia. This effect was also verified in the undoped ATZ composites. Regarding the lanthana doping, it was reported that, such as density, it does not cause a significant variation of the grain size [50] or decreases the zirconia grain size, due to the segregation of $La^{3+}$ at the zirconia grain boundary [69]. However, in this work, the ATZ doped with $La_2O_3$ presented a coarser grain size than the $Ta_2O_5$ doped one.

The alumina grains in the 80A20Z+T composite reached the highest mean grain size (~393 nm) which confirms that the addition of this additive had a little effect in the alumina size [65]. However, no excessive grain growth was noticed. In fact, the alumina in the ZTA samples is smaller in comparison with the undoped ZTA composites, which present values (higher than 400 nm), while the zirconia grains achieve higher grain sizes. So it can be assumed that, in the ZTA samples, the pinning effect is present however it is less pronounced, allowing zirconia grains to grow a bit more than what was previously verified.

When faced with the surface porosity presented by the doped ZTA samples (Fig. 4.30 - A,C), a thermal analysis for each composite was performed to verify if the applied sintering temperature (1400ºC) was still adequate after the addition of this two dopants. Even though the selected sintering temperature was suitable to the undoped samples, it might have changed with the addition of $La_2O_3$ and $Ta_2O_5$ and 1400ºC was not enough to fully densify and close the remaining porosity of these composites. The results from the dilatometric analysis of these two ZTA composites were compared with the ones from the undoped one (80A20Z, Fig.4.6, section 4.1.3.6) and they are present in the Figure below.

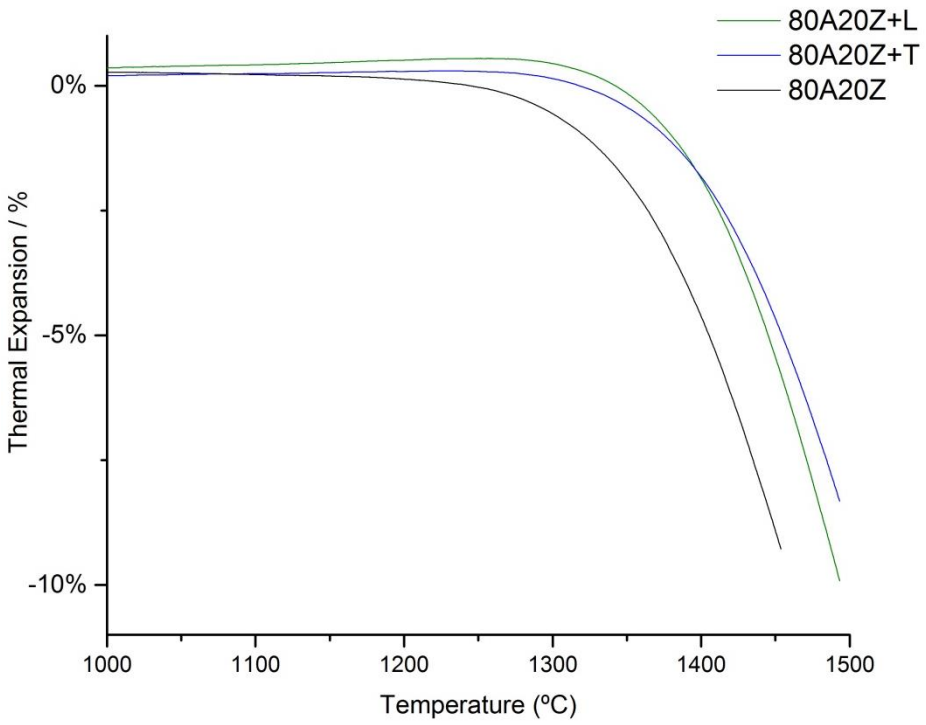


**Figure 4.31 - Dilatometric analysis performed on the doped ZTA composite powders.**

From the obtained results it is confirmed that, a slightly higher sintering temperature would have a beneficial effect on eliminating the surface porosity of the ZTA doped composites. To achieve the same densification degree of the undoped ZTA samples, it would be necessary a sintering temperature higher than 1450ºC. However, the achieved the densification degree was still acceptable (higher than 97%).

#### 4.3.4.4 Mechanical Properties

To allow the comparison of the mechanical properties between the undoped and doped composites, mechanical tests were performed under the same conditions. The Vickers Hardness, fracture toughness and flexural strength results obtained for the doped composites are shown and compared with the respective results for the undoped ones, in Figure 4.32.

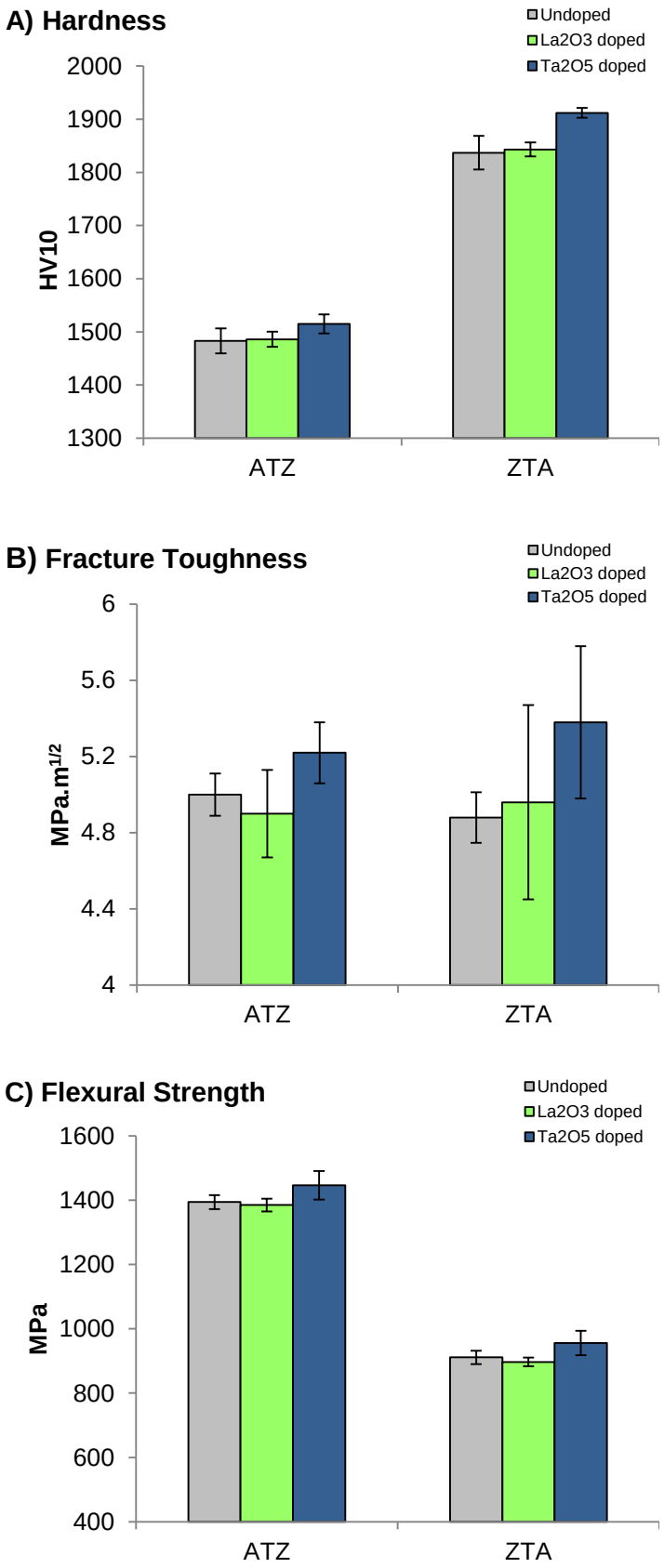


**Figure 4.32 - Mechanical properties of the undoped (80Z20A and 80A20Z) and correspondent doped composites: A) hardness, B) fracture toughness and C) flexural strength.**

From the analysis of the obtained results, as expected, the ZTA composites, with the higher amount of alumina, present the highest values for hardness. In contrast, the ATZ composites have the highest fracture toughness and flexural strength, which is characteristic of zirconia.

Regarding the achieved results for Vickers Hardness, a slight increase was verified on both ATZ and ZTA composites doped with $Ta_2O_5$. This is in conformity with results from a previous study that reports the increase of hardness with the amount of this oxide (in a ZTA composite) [65]. In this work, the hardness enhancing is also verified in the ATZ composites. It is reported that the $Ta^{5+}$ nano-size ions improve the cohesion between grains [65], and consequently the hardness of the material.

The same tendency is also verified for the fracture toughness which highly increases with the addition of $Ta_2O_5$. The same behavior is observed for both ZTA and ATZ composites. It was previously mentioned that, the inclusion of this additive increases the transformability of tetragonal zirconia. Since the enhanced fracture toughness presented by zirconia has origin in the tetragonal to monoclinic transformation this was a beneficial effect to this mechanical property. Surprisingly, the highest value of fracture toughness was achieved for the ZTA composite: 5.38 $MPa.m^{1/2}$ against 5.22 $MPa.m^{1/2}$ for the ATZ doped sample. This effect might be related to the amount of stabilizer in zirconia. The 2 mol% Yttria Stabilized Zirconia used on the ZTA composites could have been more easily destabilized by the presence of $Ta_2O_5$, which highly increased its transformability. Therefore, even though only 20 wt% of zirconia was present in this composite, the addition with this dopant was enough to enhance this mechanical property that increased from 4.88 $MPa.m^{1/2}$ (on the undoped ZTA) to 5.38 $MPa.m^{1/2}$.

The flexural strength is also slightly influenced by the transformability of zirconia [10]. The addition of this dopant promoted a small increase in the flexural toughness of the ZTA composites (from 911 MPa to 956 MPa) which present lower values of this property, due to their amount of alumina. In the ATZ composites even though the flexural strength is higher in comparison with the ZTA ones, no significant increase was verified with the $Ta_2O_5$ addition.

In relation to the $La_2O_3$ doped composites, it was reported that this oxide does not have a considerable effect in the mechanical properties, since it is reported to significantly increase the aging resistance of zirconia [50], [69].

Regarding hardness, the obtained values are comparable to the attained results for the undoped composites. The same trend is observed for both fracture toughness and flexural strength. The obtained fracture toughness, in fact presents a slightly decrease in

the ATZ (from 5 to 4.9 MPa.$m^{1/2}$) and increases in the ZTA composites (from 4.88 to 4.96 MPa.$m^{1/2}$). Therefore the obtained results are in agreement with published results, and it is confirmed that the addition of lanthanum oxide does not significantly affect the mechanical properties of both ATZ and ZTA composites.

### 4.3.5 Accelerated Aging Test

The aging resistance was expected to be affected by the addition of these additives. The lanthanum oxide was expected to improve the aging resistance of the material by slowing down the tetragonal to monoclinic transformation during the aging tests. On the other hand, since the addition of $Ta_2O_5$ increases the transformability of tetragonal zirconia, a slightly increase in the monoclinic zirconia would not be a surprising fact.

The doped composites were submitted to aging tests, under the same conditions applied for the undoped samples (134ºC and 2 bar) for several hours. The monoclinic content was quantified by X-ray diffraction after 5, 12, 24, 48 and 96 hours on aging environment. The obtained amount of monoclinic zirconia for each time period was compared with the results obtained for the undoped samples (Fig. 4.12, section 4.1.5). The results obtained for the ATZ and ZTA samples are presented on Figure 4.33.

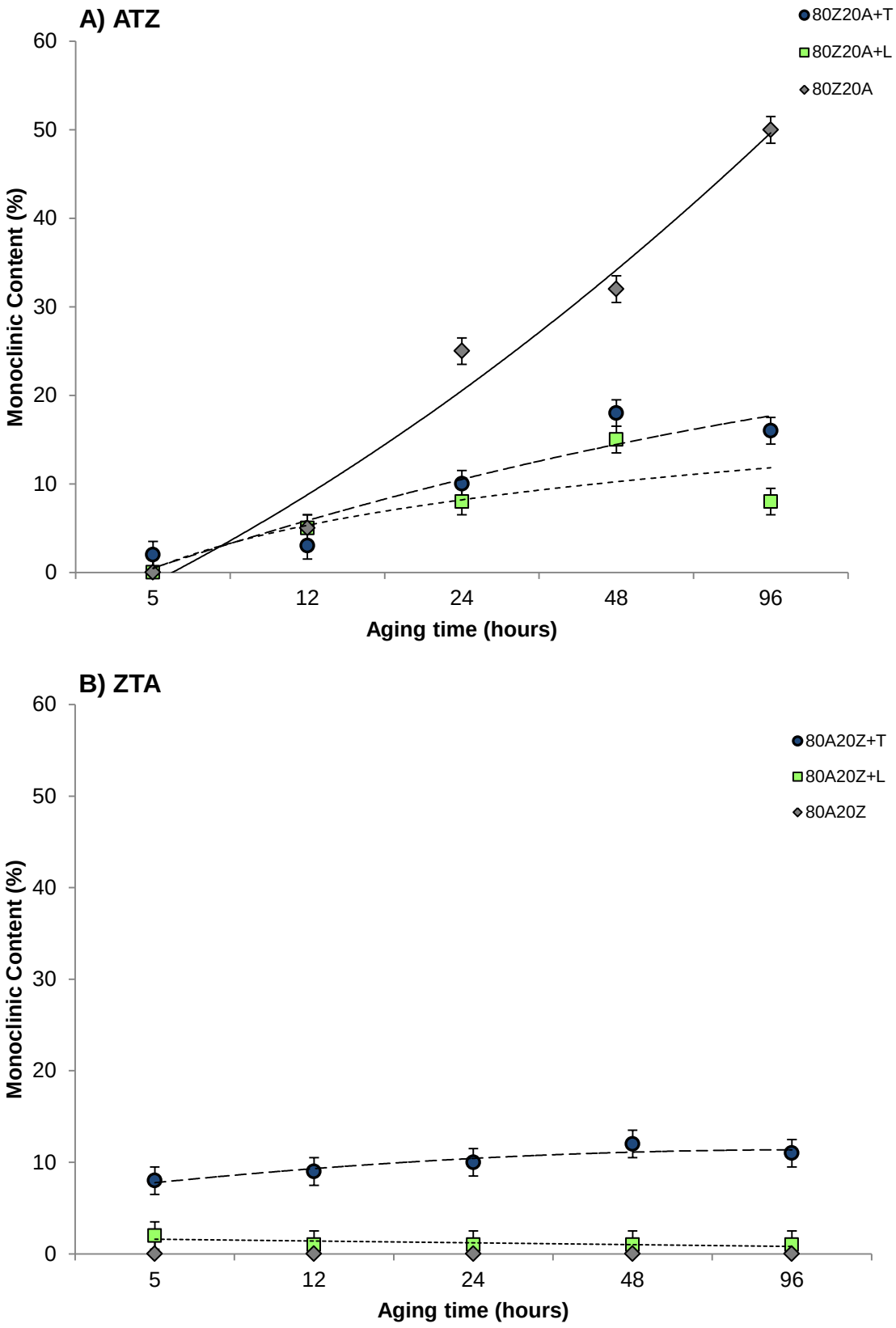


**Figure 4.33 - Change in the monoclinic content of the aged A) ATZ and B) ZTA doped composites with time, during accelerated aging tests in an autoclave (134ºC, 2 bar).**

Regarding the results obtained for the ATZ doped samples, it can be verified that both additives were successful in delaying the deleterious transformation upon aging. All the doped samples presented less than 20% of monoclinic zirconia after 96 hours of aging tests, which is 30% less than the monoclinic amount detected by the undoped composite.

As expected the lanthana doped composites presented the lowest amount of monoclinic zirconia throughout the aging test. This additive was used in these composites for this reason since it has been reported that this ternary oxide, $La^{3+}$, like $Y^{3+}$, can decelerate the tetragonal to monoclinic transformation by producing oxygen vacancies [50], [68].

However, this resistance to aging is also verified in the $Ta_2O_5$ doped composites. It would be expected that these samples would be more vulnerable to aging since it is reported that the $Ta^{5+}$ promotes a decrease in the concentration of oxygen vacancies, and therefore causing an increase of the transformability of zirconia. This characteristic explains the enhancement of the mechanical properties, especially the fracture toughness of the composite. However, this mechanism is not clear. It was also reported that doping zirconia with both $Ta^{5+}$ and $Y^{3+}$ (an stabilizer oxide) leads to an increase of both tetragonality and stability [149]. In another study, it was also found that $Ta^{5+}$ stabilized zirconia to its tetragonal form. The authors suggested that the Ta-O bonds formed are strong enough to stabilize the tetragonal phase upon transformation, by hindering the atomic rearranging [151]. Thus in this case, for the ATZ composites, the addition $Ta_2O_5$ promoted a stabilizing effect on the 3YSZ present. In this case, the grain size might have also affected this property, since the zirconia presented a finer grain size in comparison with the $La_2O_3$ doped and undoped ATZ that presented zirconia grain sizes higher than 300 nm (Fig. 4.30, Table 4.18 and section 4.1, Fig. 4.9, Table 4.7). Thus it is also suggested that, the grain size could have beneficially affected the aging resistance, since smaller grains are more difficult to destabilize than bigger ones.

On the other side, in the ZTA composites, the tantalum doping clearly created a destabilization on zirconia. From the X-ray data achieved for the sintered samples (Fig. 4.29) some monoclinic zirconia was already detected for the $Ta_2O_5$ doped ZTA composite. Throughout the aging test, that monoclinic amount increased, and stabilized around 10%. Adding to the fact that the ZTA contain 2YSZ, it was observed that both doped composites presented a slightly lower density than the undoped ZTA composites (Table 4.17 and 4.6 respectively). Also, the obtained SEM images of these samples (Fig.4.30 A,C) present some porosity at the surface. Thus, one plausible explanation to the detection of monoclinic zirconia in this doped ZTA composite is that, upon the aging test, the water

species infiltrated easily through the pores, into the material. Even though the pores were just superficial, the 2YSZ present on the surface was more easily destabilized, and transformed to the monoclinic phase.

Since the $La_2O_3$ has a stabilizing function in zirconia, the same behavior is not verified, and the monoclinic phase remained insignificant despite the surface porosity. The addition of this oxide successfully stabilized the 2YSZ present on the ZTA samples even in the presence of surface porosity. After testing the co-doping of alumina and lanthana, it is then confirmed that this property is also maintained in the presence of an alumina matrix, since no significant degree of degradation was detected on the ZTA composites doped with this additive.

Again, to verify the extension of the degradation the remaining mechanical properties of the doped samples after the degradation tests were analyzed. The results obtained for Vickers Hardness, fracture toughness and flexural strength, are shown in the Figure below.

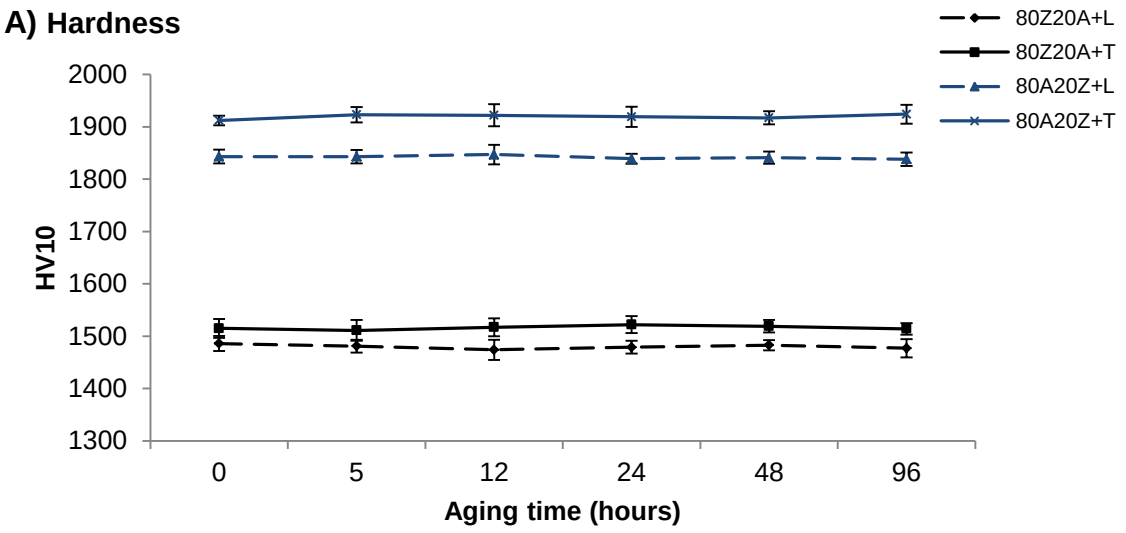

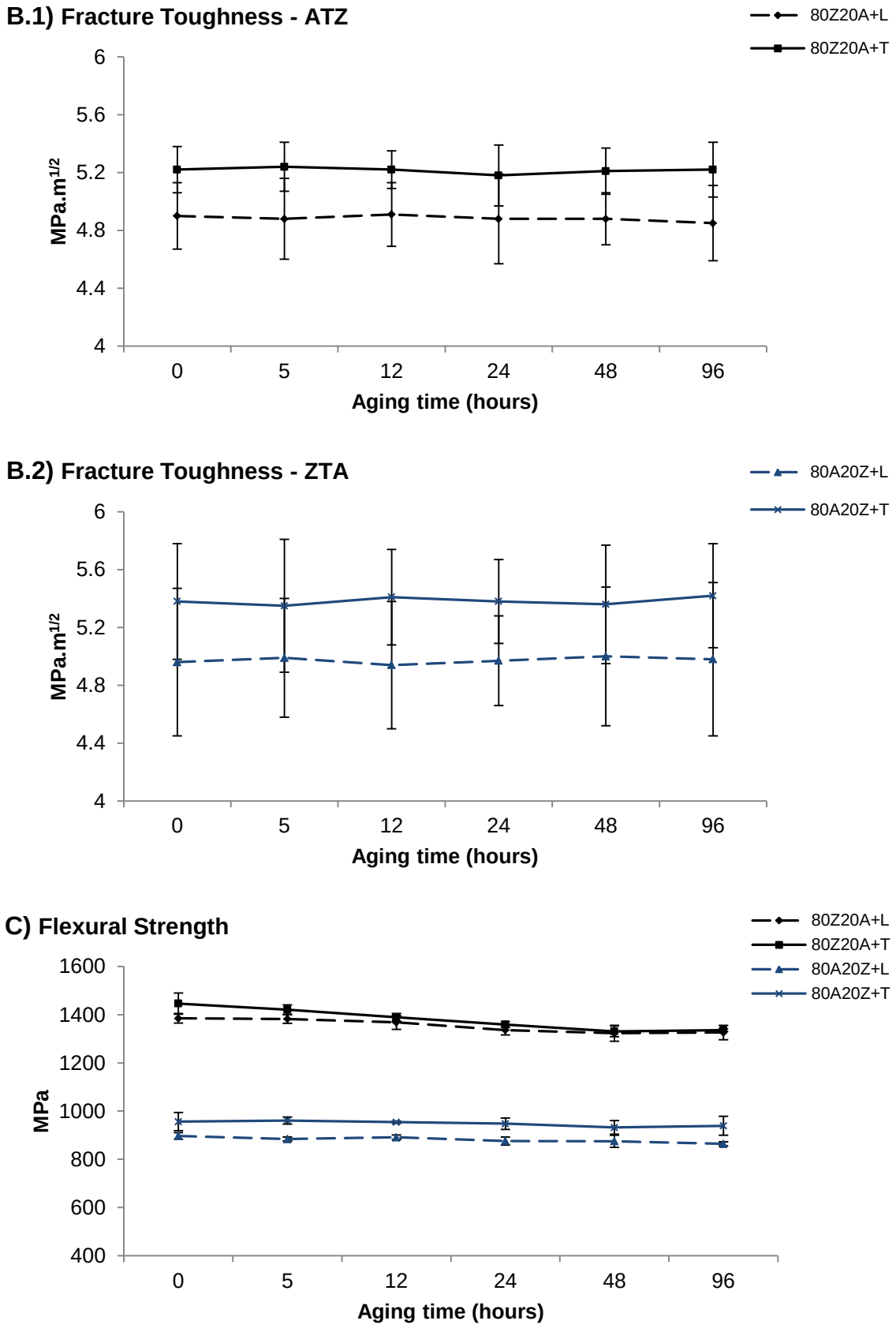


**Figure 4.34 - Mechanical properties of the aged doped composites throughout the duration of the aging tests: A) hardness, B.1-2) fracture toughness and C) flexural strength.**

Similarly to the previous results, it is verified that the mechanical properties of the tested composites are kept throughout the aging tests. Even the $Ta_2O_5$ doped ZTA, in which it was detected 10% of monoclinic zirconia, maintained all its properties until 96 hours of test. This is a clear evidence that, even though lower density and surface porosity were achieved, it did not jeopardize the material's integrity, and the degradation was successfully stopped and restricted only to the surface material. These results support the previous clarification, since a significant decrease in these properties would be expected if the degradation expanded to the material bulk.

The flexural strength of the ATZ presented a highest decrease for the ATZ samples however, it did not surpassed 8% of decay after 96 hours in deleterious environment.

Thus, from these results it can be verified that the $La_2O_3$ doping in fact increased the aging resistance in comparison with the undoped samples. On the other hand, the $Ta_2O_5$ doping lead to outstanding results regarding the mechanical tests, and also provided some aging resistance to the ATZ composites, which contained 3YSZ and have higher density. Finally, thanks to a set of characteristics and used preparation methods, such as the initial spray dried powders, pressing and sintering, the mechanical properties were maintained after 96 hours of aging tests.

## 4.4 Biocompatibility Tests

The biocompatibility behavior of these zirconia alumina composites was also tested. Cell viability and proliferation assays were performed under the same conditions for every composite produced in this study. The obtained results are presented in the following sections.

### 4.4.1 Undoped samples

The cell viability/proliferation evaluated by MTT assays of MG63 cells for 1 and 4 days in the undoped samples is presented in Figure 4.35. This colorimetric assay measures the changes in absorbance produced by a change of color proportional to the number of viable cells.

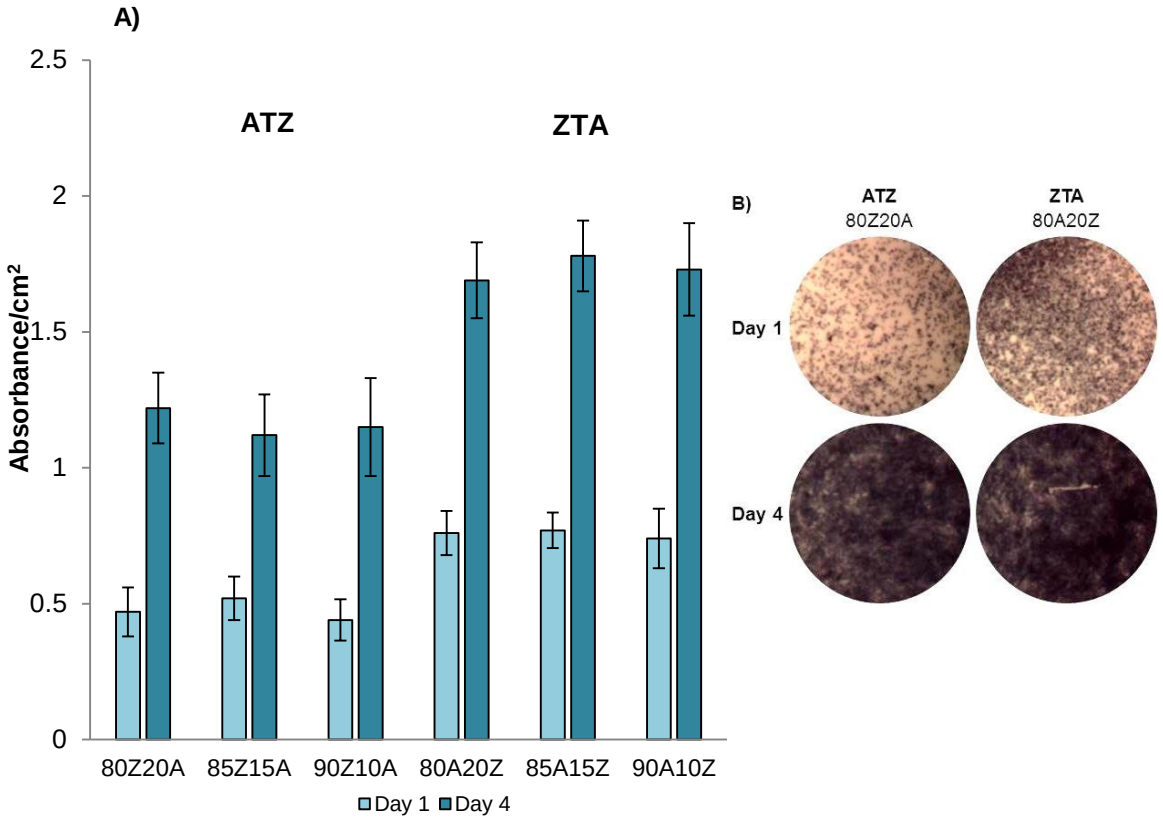


**Figure 4.35 - Cell viability/proliferation of MG63 cells cultured on the undoped samples, for 1 and 4 days, evaluated by the MTT assay. A) Quantitative evaluation; B) Representative images of the colonized composites, showing the formation of the insoluble dark blue formazan compound by viable cells.**

From the obtained results it can be verified that cell viability/proliferation increased significantly from day 1 to day 4 for all the undoped samples, showing a high growth rate during the culture time.

The achieved values were similar in the three ATZ compositions analyzed and on the ZTA compositions as well. Therefore it can be assumed that, from the separate analysis of the ATZ and ZTA compositions, the differences in the zirconia and alumina content did not induced changes in the cell viability/proliferation. However, when comparing the results presented by the ATZ and ZTA composites, it can be verified an increase in the cell viability in the ZTA ones.

MG63 cells grown on the ATZ and ZTA composites show the ability to produce alkaline phosphatade (ALP), an important osteoblastic marker. Results are shown in Figure 4.36. ALP activity, normalized to the total protein content, increased from day 1 to day 4 in all composites. At day 1, the obtained values were similar in the ATZ and ZTA samples, however, at day 4 ALP was slightly higher in the ZTA composites (Fig.4.36-A). The histochemical staining of the enzyme (Fig.4.36-B) provided similar information. ALP is a membrane-bound enzyme that begins to be synthesized earlier on the osteoblastic differentiation pathway, showing a significant increase later, in more mature cells, playing a significant role in the onset of matrix mineralization [152].

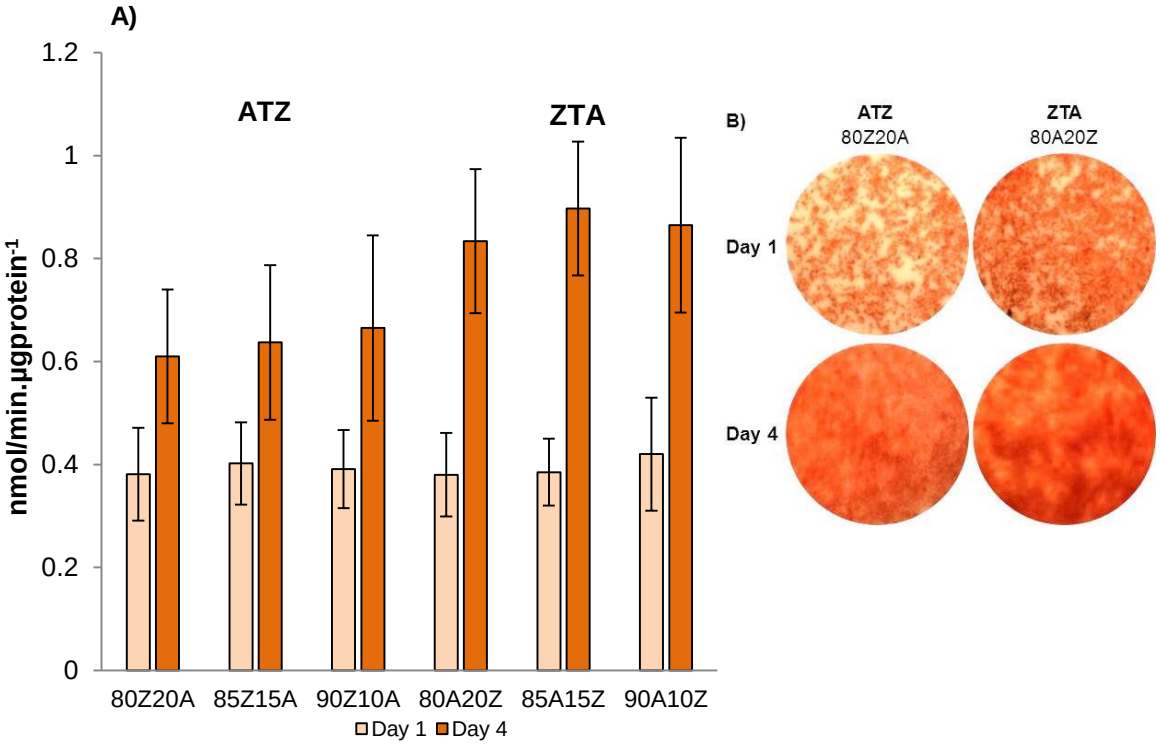


**Figure 4.36 – A) Alkaline phosphatase (ALP) activity of MG63 cells cultured on the undoped samples for 1 and 4 days; B) Representative images of the colonized composites stained for the presence of ALP.**

The seeded materials were also observed by scanning electron microscopy and the obtained micrographs at different magnifications are displayed below, Fig.4.37, 4.38 and 4.39.

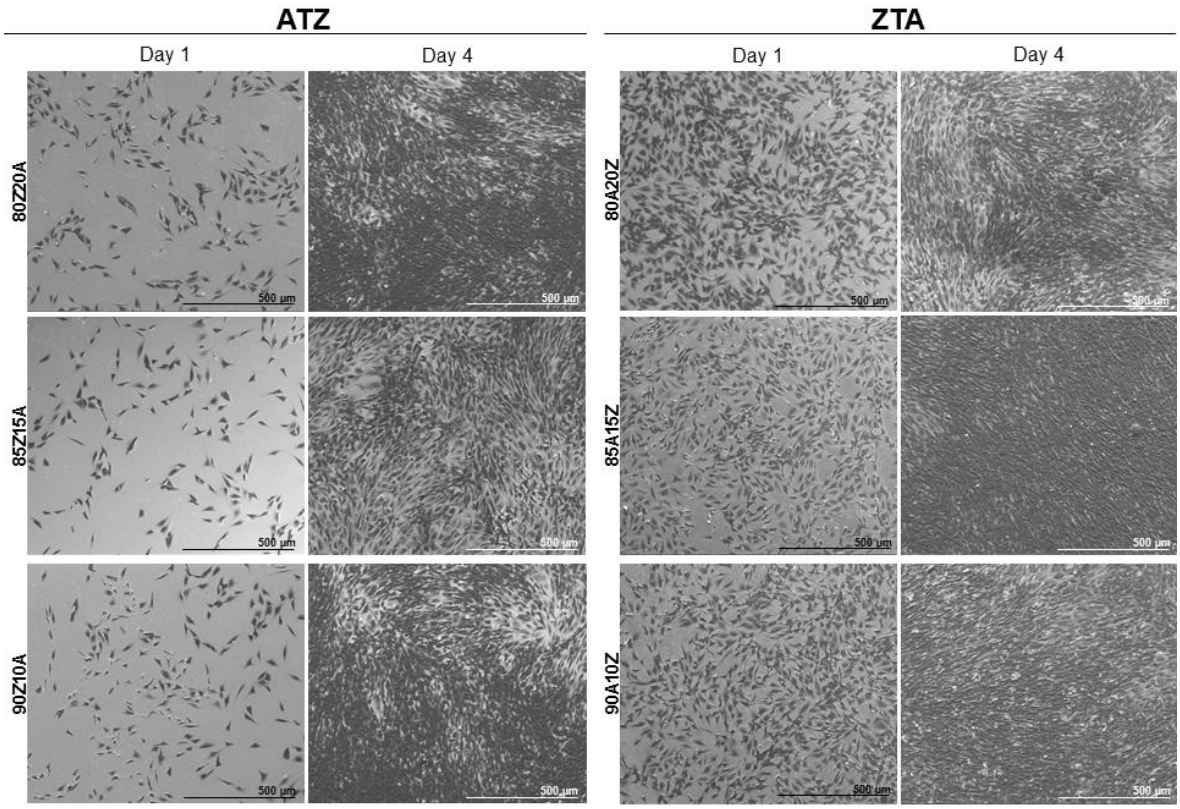


**Figure 4.37 - Representative SEM images of the undoped material samples cultured with MG63 cells for 1 and 4 days (Bar=500 µm).**

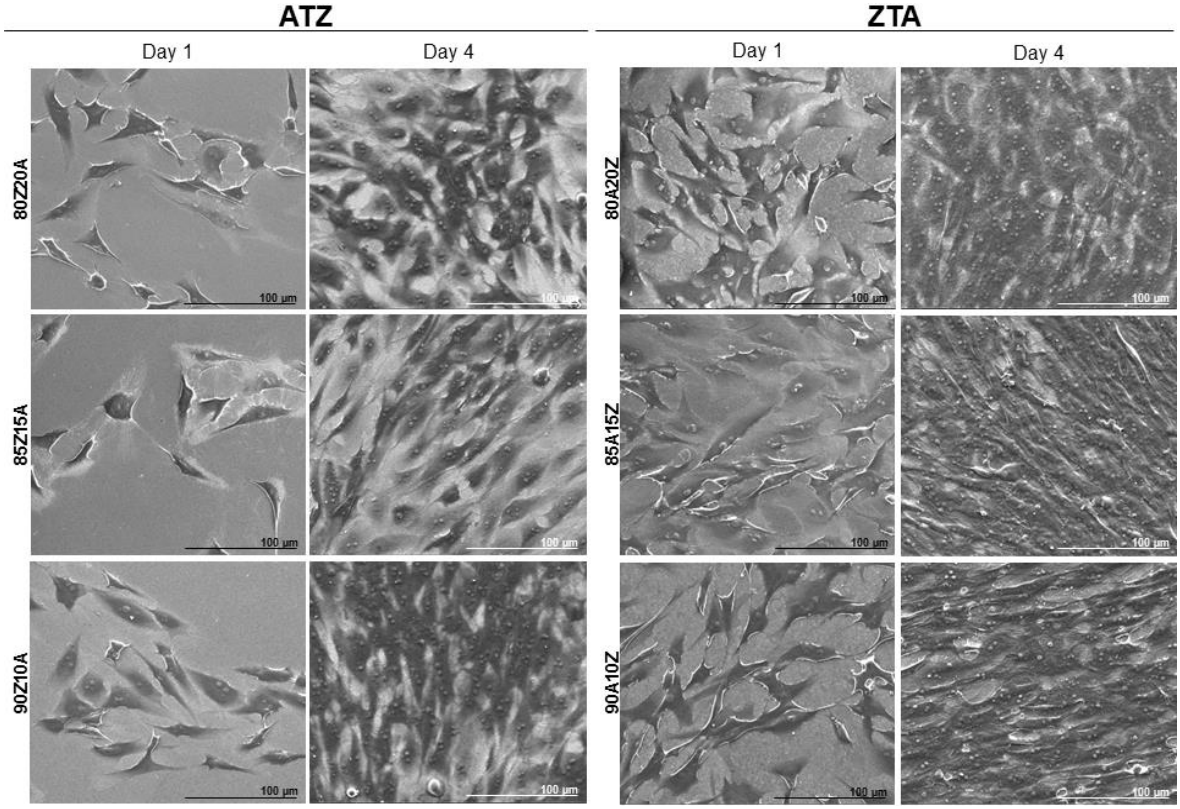


**Figure 4.38 - Representative SEM images of the undoped material samples cultured with MG63 cells for 1 and 4 days (Bar=100 µm).**

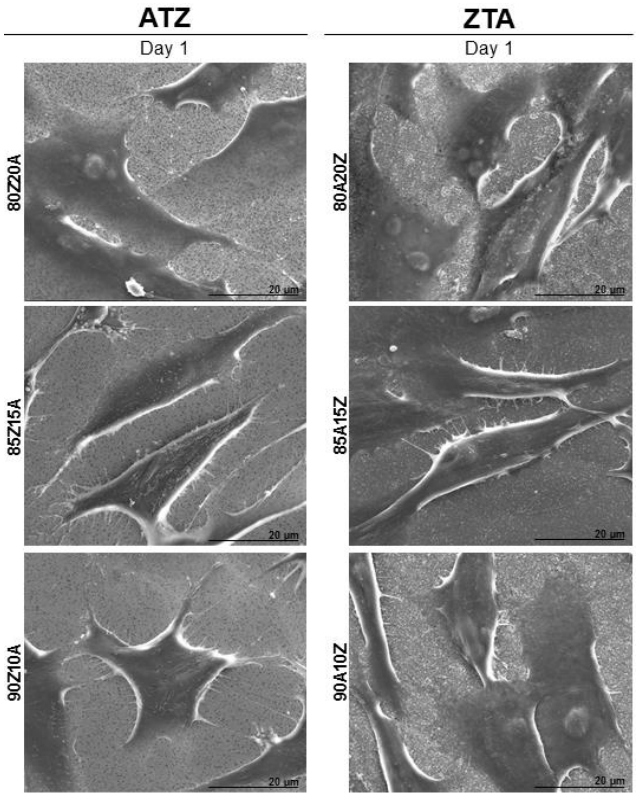


**Figure 4.39 - Representative SEM images of the undoped material samples cultured with MG63 cells for 1 day (Bar = 20 µm).**

The acquired SEM images of the colonized materials were in agreement with the results observed in the MTT assay. The cell adhesion and the pattern of cell growth were similar in all samples (Fig. 4.37 and 4.38). Cells were able to adhere to the material surface, as seen in the images of day 1. Cells were randomly distributed on the material surface and presented an elongated morphology. At day 4, a confluent and well-organized layer of elongated cells was observed on the surface of all samples. The higher number of adherent cells on the ZTA samples was clearly evident. High magnification images showed that they established numerous cell-to-cell contacts and also a close interaction with the material surface (Fig. 4.39).

Overall, these results are in agreement with the known biocompatibility of zirconia and alumina ceramics, from both *in vitro* and *in vivo* studies [153]. Regarding ZTA and ATZ composites, the few reported *in vitro* studies also points for a favorable cell response, despite the diversity of experimental cell protocols and composite composition. Thus, no deleterious effects were noticed on the proliferation and osteoblastic parameters of MG63 cells cultured on ZTA foams [112] and polished ZTA discs [99]. Also, MG63 cells grown on polished samples of alumina and on a ZTA composite showed similar behavior for cell morphology, cell proliferation and ALP activity [154]. Further, comparison of ATZ

composites and titanium substrates yielded equivalent biological response regarding HOS cells [155] and human osteoblastic cells [156].

However, comparative studies addressing ZTA and ATZ composites using the same experimental cell protocol have not been reported. The results observed on the behavior of MG63 osteoblastic cells cultured on the ZTA and ATZ composites prepared in this work showed that cell adhesion on the ZTA composites was higher than that on the ATZ composites.

Adherent cells, as the osteoblastic cells, are highly sensitive to the physicochemical profile of the material surface. Alumina and zirconia are generally considered bioinert materials. However, several changes occur at the microstructural level upon the producing process of alumina and zirconia composites, depending on the relative percentages of the two compounds. Thus, in the ZTA composites, the mean grain size of the alumina particles was around 460 nm and that of the zirconia particles varied from 251 to 223 nm (80A20Z to 90A10Z). Comparatively, on the ATZ composites, the mean grain size of the alumina grains decreased to around 350 nm and that of zirconia particles greatly increased attaining values around 350 nm. These changes would be reflected on the surface roughness and topography of the composite as well as in the wettability, parameters that are determinant factors in cell-material interactions. Additionally, the zirconia granules were stabilized with 3 mol% of yttria on the ATZ composites and with 2 mol% of yttria on the ZTA composites, which is another variable that might affect cell behavior, as will reported bellow. Further, high magnification SEM images of the polished samples used in the cell culture experiments showed differences on the surface of the ATZ and ZTA composites (Figure 4.40 below).

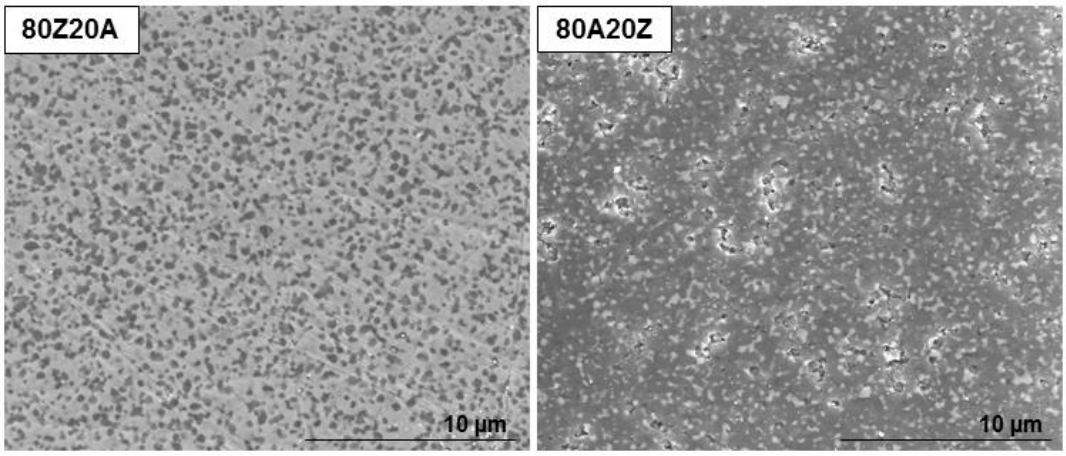


**Figure 4.40 - Representative SEM images of the surface appearance of ATZ (80Z20A) and ZTA (80A20Z) undoped material samples after 1 day in cell culture medium (Bar=10 µm).**

ATZ composites presented a very homogeneous and smooth surface while the ZTA samples exhibited some surface porosity, and therefore the presence of abundant pitting features. The ZTA topography is expected to offer increased anchorage possibilities to the initial surface protein adsorption, the molecules that provide the polypeptide cues for the cell adhesion through cell-surface receptors. This might contribute for the better cell adhesion on the ZTA composite, a determinant factor for the subsequent proliferation and differentiation events. However, the exact explanation for the relatively better cell response to the ZTA composites was not identified, but the several factors mentioned above might play a role.

A better characterization of the surface properties of both composites will be helpful to clarify this issue.

### 4.4.2 Comparison between the two stabilized zirconias

The cell viability/proliferation and ALP activity of the ATZ composites with different zirconias (803YSZ20A and 802YSZ20A) were also tested in order to investigate the role of the content of yttria in this biological response. The outcome of these assays is displayed on Figures 4.41 and 4.42.

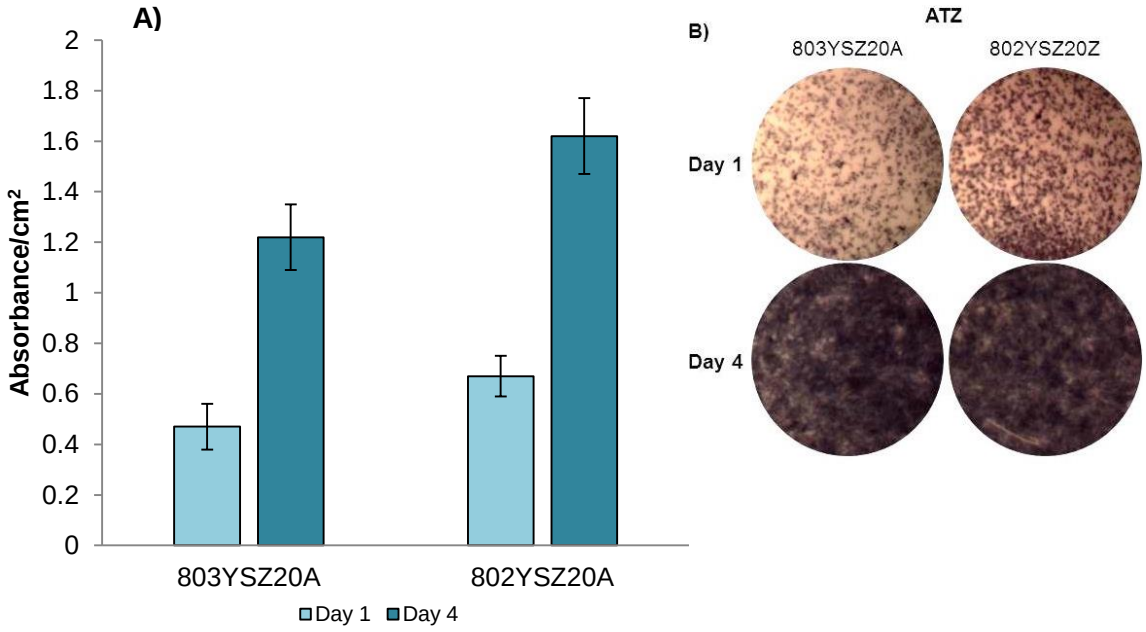


**Figure 4.41 - Cell viability/proliferation of MG63 cells cultured on the 803YSZ20A and 802YSZ20A samples for 1 and 4 days, evaluated by the MTT assay. A) Quantitative evaluation; B) Representative images of the colonized composites showing the formation of the insoluble dark blue formazan compound by viable cells.**

It can be assumed that the amount of yttria may affect the cell viability and proliferation of the samples. The 802YSZ20A sample, which contains less yttria, presents higher cell viability after one and four days in comparison with the ATZ with more yttria, 803YSZ20A. Also, ALP activity is slightly higher on the 802YSZ20A composite, at day 4, as shown on Figure 4.42.

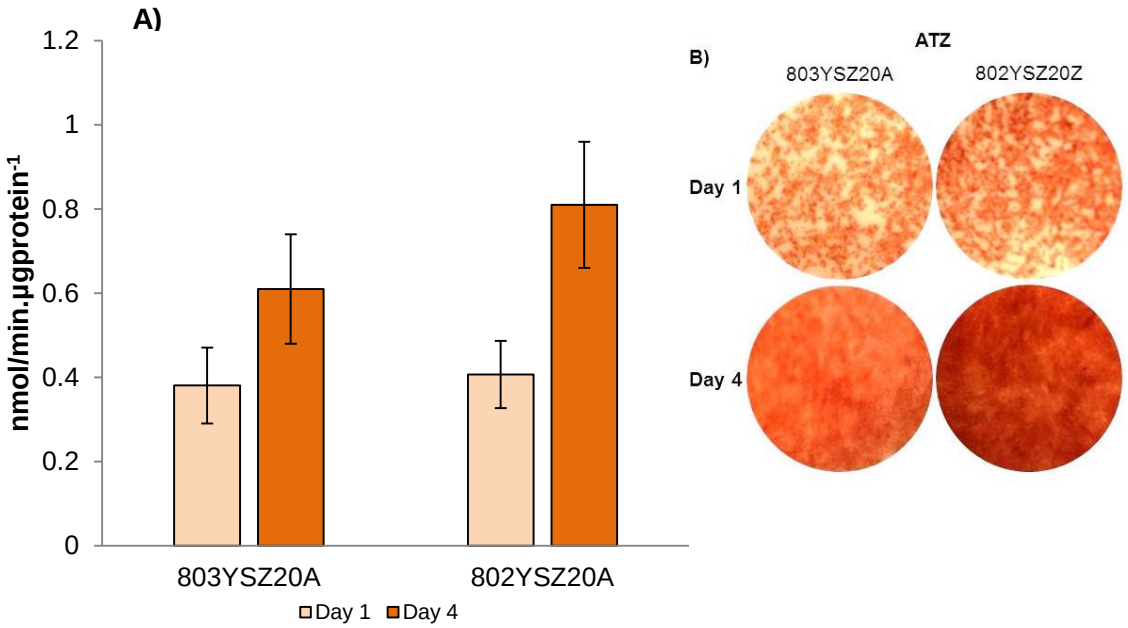


**Figure 4.42 – A) Alkaline phosphatase (ALP) activity of MG63 cells cultured on the 803YSZ20A and 802YSZ20A samples for 1 and 4 days. B) representative images of the colonized composites stained for the presence of ALP.**

The seeded materials were also observed by scanning electron microscopy after one and four days in culture. The obtained Figures are displayed below.

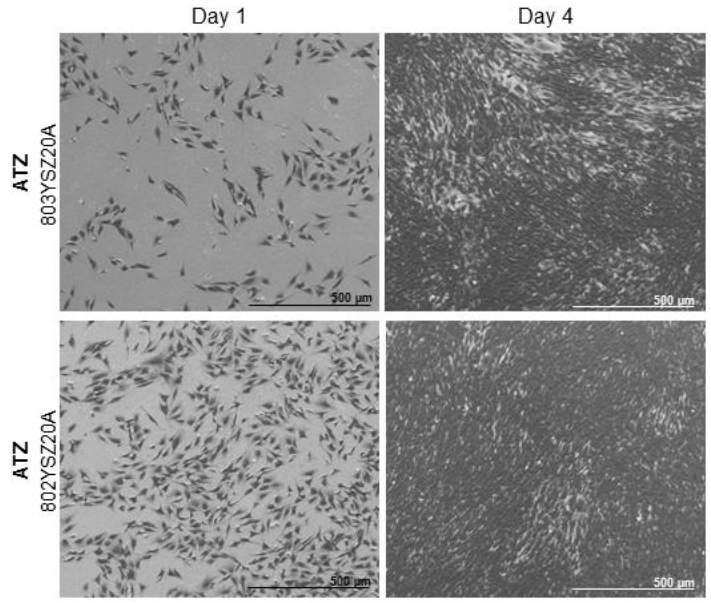


**Figure 4.43 –Representative SEM images of the 803YSZ20A and 802YSZ20A material samples cultured with MG63 cells for 1 and 4 days (Bar=500 µm).**

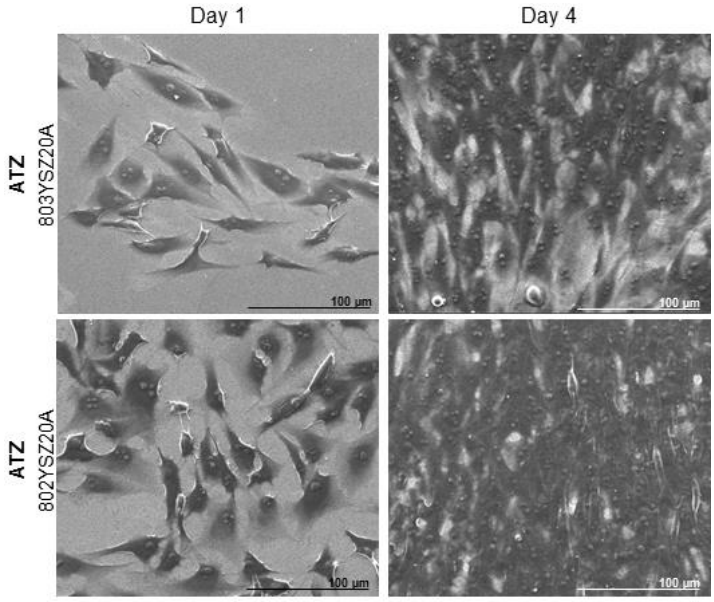


**Figure 4.44 - Representative SEM images of the 803YSZ20A and 802YSZ20A material samples cultured with MG63 cells for 1 and 4 days (Bar=100 µm).**

From the SEM images it is possible to observe a difference in the cell adhesion between the two ATZ composites. The images are in conformity with the MTT assay results, since after one day, the cell adhesion is more pronounced in the ATZ with less yttria (802YSZ20A).

As described previously (section 4.2.3.3), the decrease on the percentage of yttria from 3 mol% to 2 mol% in order to stabilize the zirconia greatly affect the microstructure of the composites. The mean grain size of the zirconia particles in the 803YSZ20A is

significantly higher (353 nm) than that observed in the 802YSZ20A (211 nm). This change in the microstructure is expected to influence the surface properties, which would be relevant in terms of cell response. The results suggest that the surface profile of the 802YSZ20A appears to be more attractive for the cell behavior.

### 4.4.3 Doped Composites

The MTT assay was also made on the doped composites, in order to investigate any influences in the cell viability caused by the used additives. The achieved results for this test are presented below.

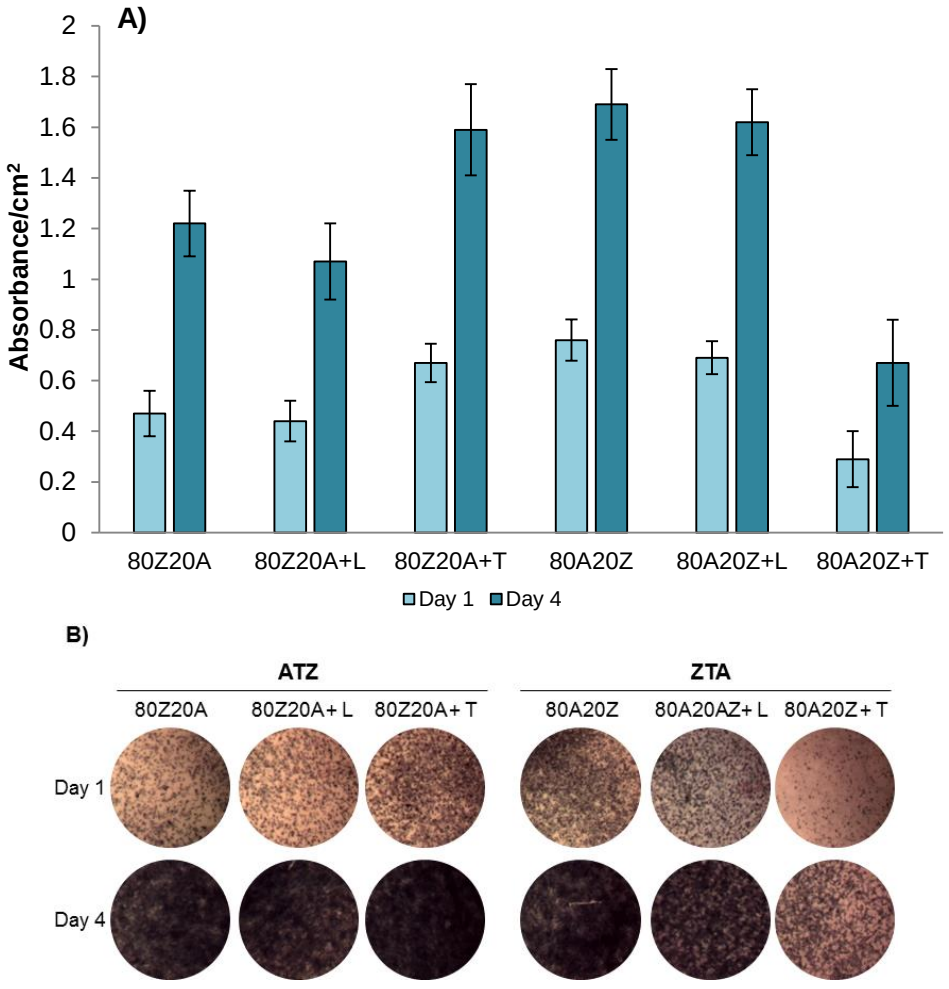


**Figure 4.45 - Cell viability/proliferation of MG63 cells cultured on the doped composite samples for 1 and 4 days, evaluated by the MTT assay. A) Quantitative evaluation; B) Representative images of the colonized composites showing the formation of the insoluble dark blue formazan compound by viable cells.**

From the absorbance measures of the MTT assay it is clearly noticed a decrease in the cell viability presented by the ZTA composite doped with $Ta_2O_5$. However, the ATZ

sample doped with this oxide presents the opposite behavior, reaching the highest value of cell viability/proliferation among the ATZ samples. It was previously reported that $Ta_2O_5$ did not induce toxic effects on MC3T3-E1 cells when added to yttria stabilized zirconia [66].

Both $La_2O_3$ doped composites presented a cell growth similar to that on the corresponding non-doped samples.

ALP activity assays were performed on these samples. Results for ALP activity and staining are shown in Figure 4.46.

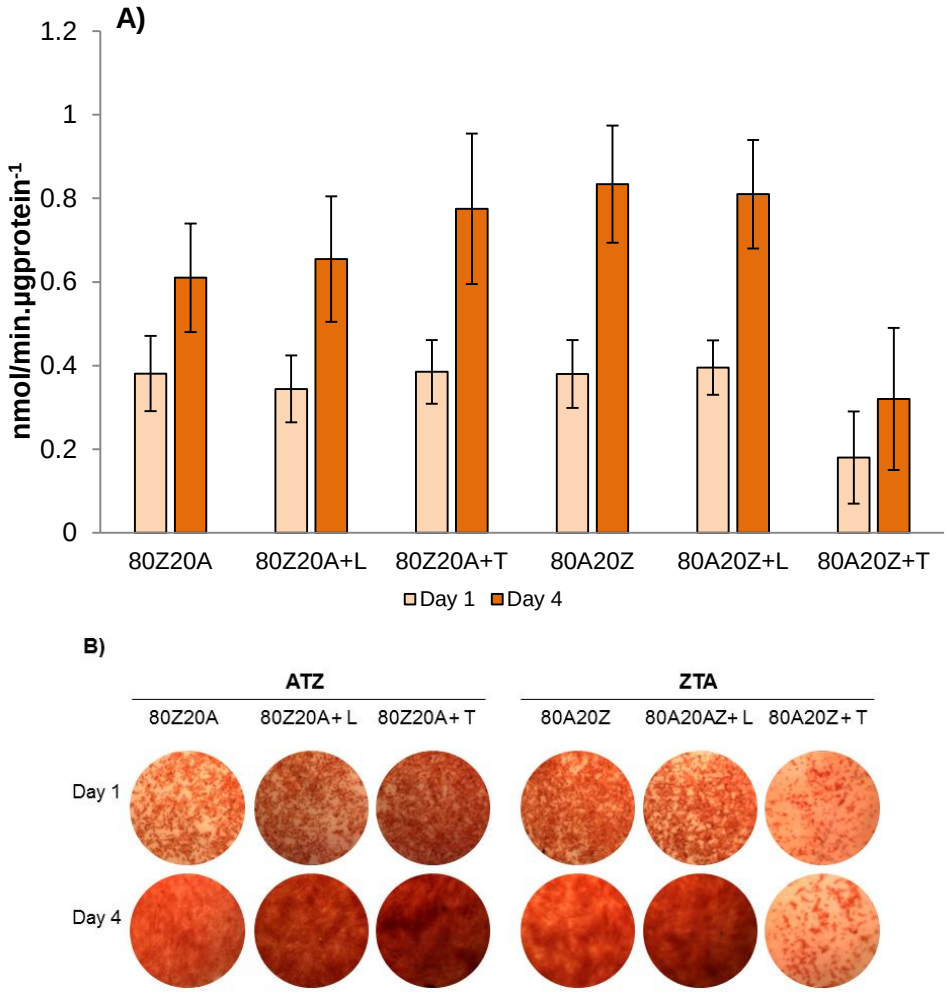


**Figure 4.46 – A) Alkaline phosphatase (ALP) activity of MG63 cells cultured on the doped composite samples for 1 and 4 days. B) Representative images of the colonized composites stained for the presence of ALP.**

In the doped composites, the ALP activity increased from day 1 to day 4. Basically, these results showed a tendency similar to that of the MTT assay. Compared to the respective undoped composites, the obtained values were significantly lower in the ZTA

composites doped with $Ta_2O_5$ but slightly higher in the ATZ composites doped with this oxide.

SEM images of the seeded material were also taken and displayed on Figures 4.47 and 4.48.

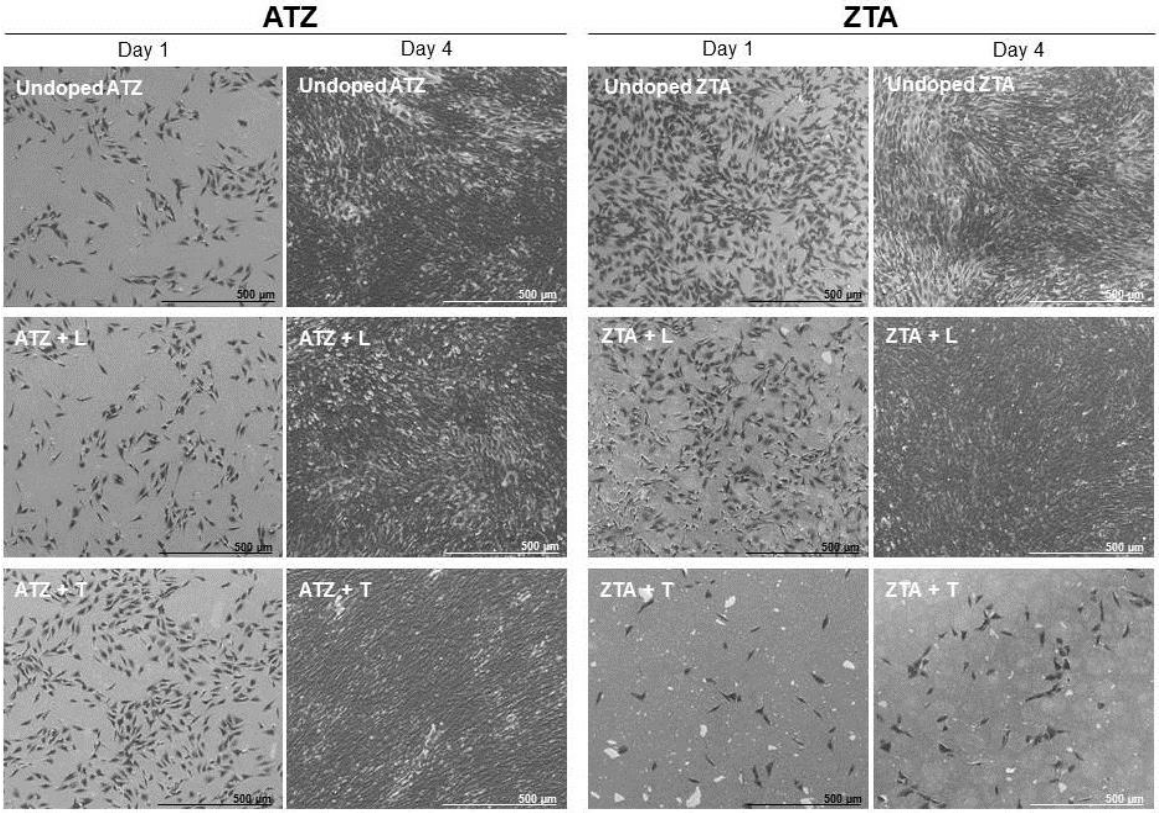


**Figure 4.47 - Representative SEM images of the doped composites material samples cultured with MG63 cells for 1 and 4 days (Bar=500 µm).**

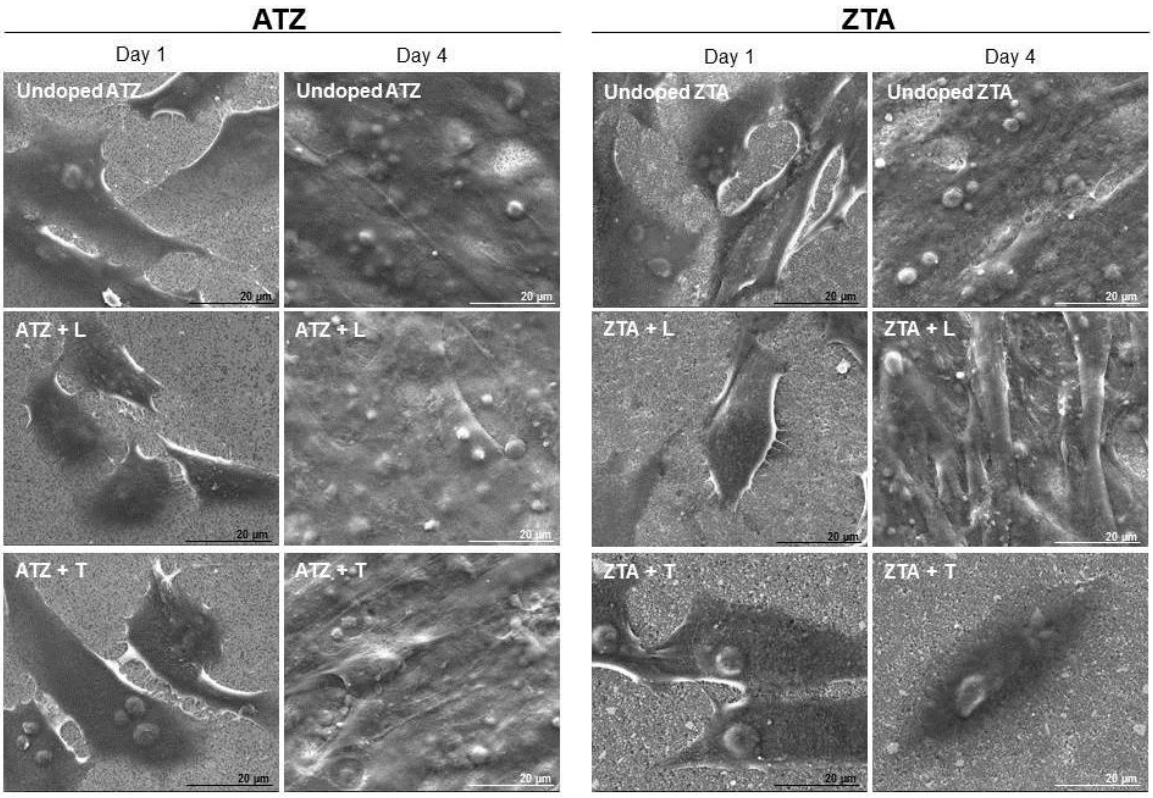


**Figure 4.48 - Representative SEM images of the doped composites material samples cultured with MG63 cells for 1 and 4 days (Bar=500µm and 20µm).**

It is confirmed from the obtained SEM images that the ZTA samples doped with $Ta_2O_5$ presented a poor performance, compared to the other samples. At day 1, only few cells were seen on the surface, which increased little in number at day 4. Additionally, cells showed a more rounded appearance and lower number of cytoplasmic processes interacting with the material surface.

The remaining samples, including the ATZ composite doped with $Ta_2O_5$, presented randomly distributed cells on the material surface with an elongated morphology. The high magnification images obtained (Fig. 4.48) showed that they established numerous cell-to-cell contacts and also a close interaction with the material surface. At day 4, a confluent and well-organized layer of elongated cells was observed on the material surface.

To investigate the obtained difference in the cell viability assay presented by both composites doped with $Ta_2O_5$, the wettability of these samples was investigated and contact angles measurements were performed in the material samples. The obtained images are presented in the next Figure.

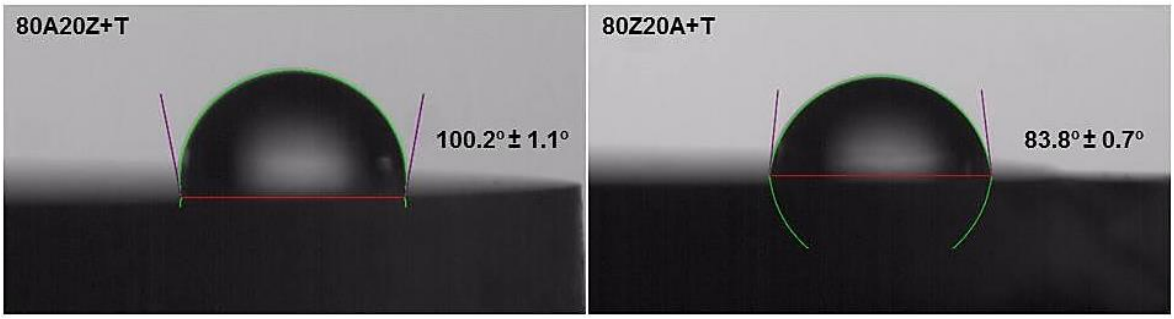


**Figure 4.49 - Images obtained for the contact angles measurements on both composites doped with $Ta_2O_5$.**

The obtained results show that the wettability of the ZTA sample doped with $Ta_2O_5$ has a considerable higher contact angle, which indicates that this sample is hydrophobic. However, the ATZ sample is more hydrophilic, since it presents a smaller contact angle.

These results are in agreement with the ones obtained for cell viability, since the 80A20Z+T sample are hydrophobic, which might contribute to explain the low cell attachment and proliferation in comparison with the 80Z20A+T sample.

The results presented in the section 4.3.4.3 showed that the doped composites present some differences in the microstructure compared with the undoped samples. For the ATZ composites, the mean grain size of the zirconia varied from 353 nm (undoped samples) to 341 nm and 244 nm, respectively in the samples doped with $La_2O_3$ and $Ta_2O_5$. The decreased grain size in the ATZ composites doped with $Ta_2O_5$ would result in changes in the surface properties, apparently favoring cell adhesion.

In the ZTA composites, doping with $La_2O_3$ or $Ta_2O_5$ also introduced some changes in the microstructure, as shown in section 4.3.4.3. Their surface presents a higher irregularity and porosity in comparison with the ATZ ones. This porosity could be an indicator of a good cell adhesion and proliferation since porosity works as anchorage sites for cells. It can be verified that the $La_2O_3$ doped ZTA presents high cell viability/proliferation. However the same is not verified for the $Ta_2O_5$ doped one, so the present porosity was not the key factor in these results.

Regarding previous studies, there is no information on the cell response to ZTA composites doped with $Ta_2O_5$. Thus, a detailed characterization of the surface properties of the $Ta_2O_5$ doped ZTA composite will be helpful in order to explain the poor cell response observed in this specific sample.

# Chapter 5

## Conclusions and future work

# 5. Conclusions and Future Work

In the orthopedics area, the demands for novel devices with higher success rates are on point. A younger, active population, with higher life expectancy requires new products, with reliable materials and designs.

The application of zirconia alumina composites to hip arthroplasty devices might be the answer to these demands, since they eliminate some limitations in the performance of the current used metallic or polyethylene parts. The higher fracture toughness of these composites allows the manufacturing of thinner liners and bigger ball heads that provide a higher range of motion. Also, its inert behavior reduces the adverse reactions that are generated in the implantation of orthopedic devices.

However, these composites require a full control of their characteristics upon the producing stage in order to maximize their mechanical properties, aging resistance and therefore its reliability *in vivo*.

In this work several zirconia alumina composites with different compositions presenting enhanced mechanical properties and aging resistance were successfully obtained. Three compositions of ATZ composites, 80Z20A, 85Z15A and 90Z10A were tested alongside with another three compositions of ZTA composites, 80A20Z, 85A15Z and 90A10Z.

Nanostructured raw powders with a narrow particle size distribution allied with a milling and optimized spray-drying stage allowed the achievement of micrometric dense composite granules. Two stages of pressing (uniaxial and cold isostatic pressing) and a relatively low sintering temperature (1400ºC) were effectively performed to achieve high density pieces (higher than 98%, and 97.5% regarding the theoretical values, for ATZ and ZTA sintered pieces, respectively). Good mechanical properties were achieved with relatively high values of fracture toughness and flexural strength for the ATZ samples, and high values of hardness for the ZTA ones. In addition, an outstanding aging resistance was obtained for both types of composites. Aging tests were performed and the amount of monoclinic zirconia was determined for 5, 12, 24, 48 and 96 hours in an autoclave (at 134ºC, 2 bar). The ZTA composites, with higher amount of alumina did not present any signs of degradation after 96 hours of accelerated aging tests. Even though the ATZ samples showed higher contents of monoclinic zirconia, it was demonstrated that the degradation caused by the aging tests did not progressed into the bulk. The mechanical

properties of the aged samples were tested for all periods of time of the aging tests. It was found that they were not affected, presenting 2% of decay after 5 hours of aging tests, and less than 10% after 96 hours. Even for the 90Z10A sample, which was the ATZ composition presenting a higher content of monoclinic zirconia after 96 hours of aging the mechanical properties were effectively maintained. The cross section of one piece of the aged same composition was observed by SEM, and it was verified that no porosity or grain pull-out was observed on the bulk sample. Therefore, from these evidences it was assumed that the material successfully hindered the degradation and compelled it to the material surface.

Two different types of stabilized zirconia (3 mol% Yttria Stabilized Zirconia, and 2 mol% Yttria Stabilized Zirconia) were also tested in a 80Z20A composition, for its mechanical properties and aging resistance. The same spray-drying, pressing stages and sintering parameters were repeated and similar densities and microstructures were obtained. It was confirmed that a less stable zirconia presents better mechanical properties, especially fracture toughness. A maximum value of 7.94 $MPa.m^{1/2}$ was achieved for the composition with 2 mol% Yttria Stabilized Zirconia, when the composition with 3 mol% Yttria Stabilized Zirconia presented only 4.88 $MPa.m^{1/2}$. However, the aging tests demonstrated that, as expected, this less stable zirconia is also more vulnerable to Low Temperature Degradation, since a higher content of monoclinic zirconia was detected (around 70%). Nonetheless, by the results obtained for the mechanical tests of the aged samples, it was verified that, again, the mechanical properties were maintained in this composite presenting only a decay of 6% for the flexural strength after 96 hours of aging tests. This confirmed that, once again, even in the presence of a less stable material, the material properties stopped the progression of degradation.

Two additives were used in both ATZ and ZTA composition that presented a better set of mechanical properties and aging resistance: 80Z20A and 80A20Z. The additives were selected in order to enhance two crucial properties of these composites: the mechanical properties and the aging resistance. Therefore, $Ta_2O_5$ (0.35 wt%) was chosen to improve the mechanical properties and $La_2O_3$ (0.1 wt%) for its reported enhancement of the aging resistance of zirconia. It was found that no change in the density of the sintered samples was detected with the addition of both dopants. However, some porosity was detected on the surface of the ZTA samples. It was later found that the addition of these additives delays the sintering kinetics and a higher sintering temperature would be required to eliminate the remaining porosity. Despite this, the addition of $Ta_2O_5$ significantly improved all the mechanical properties of both ATZ and ZTA composites. As

previously reported, the addition of $La_2O_3$ did not produce a significant modification in the mechanical properties. Regarding the aging tests, noteworthy results were achieved. In fact, the ATZ composites with both additives presented a lower degradation degree, in comparison with the undoped ones. However, the addition of $Ta_2O_5$ destabilized the 2mol%Yttria Stabilized Zirconia present in the ZTA composites, and around 10% of monoclinic zirconia was detected after 96 hours of aging tests. This destabilization could have been caused by the surface porosity present on these samples. Again, for all aged doped composites, the mechanical properties were tested until 96 hours of aging. The results showed that, similarly to the composites tested previously, the mechanical properties were maintained.

Finally, biocompatibility tests were performed in all produced composites. Cell viability and proliferation assays for 1 and 4 days, showed that all the samples presented a successfully cell adhesion and proliferation. The ZTA samples presented higher cell adhesion and proliferation than the ATZ ones, with a higher amount of zirconia. The amount of yttria also influenced this parameter, since for the ATZ with less yttria (2 mol% Yttria Stabilized Zirconia) it was obtained a faster and higher cell adhesion and proliferation than for the ATZ stabilized with 3 mol% of yttria. The doped samples presented similar results to the undoped ones except for the $Ta_2O_5$ doped ZTA, that oddly presented a poor cell adhesion. It was then verified that this sample had a hydrophobic surface, presenting a higher contact angle than the ATZ doped with the same oxide. Therefore it was assumed that the poor cell viability was caused by some surface reaction rather than the addition of $Ta_2O_5$. Fundamentally, the ZTA composites presented better results than the ATZ ones, and these results might have been influenced by the microstructure presented by each composite type, since it was found that, the ZTA composites had favorable spots for cell attachment in their surface. However the addition of $Ta_2O_5$ induced changes in cell adhesion and proliferation on the ZTA composite, and therefore, a more detailed characterization of this composite would be helpful to determine the cause of these less satisfactory results.

The final conclusion is that, in this work, zirconia alumina composites with enhanced properties were achieved. Several compositions were tested and the maximization of properties was studied. Enhanced mechanical properties were achieved but the major results were obtained for the Low Temperature Degradation resistance, since the produced composites, with good density values and a fine microstructure completely hindered the degradation of the materials, which allowed the maintenance of the mechanical properties after 96 hours of aging tests. With the implementation of the

additives, $La_2O_3$ and $Ta_2O_5$, the monoclinic content on the materials surface was even lower, especially for the ATZ samples. The addition of $Ta_2O_5$ also improved the mechanical properties, even for the ZTA sample, that showed a highly increase in its fracture toughness.

## Future Work

The results obtained in this study have returned a few suggestions for the continuation of this work as well as the unrevealing of certain aspects that would clarify certain results. Therefore, some future work is suggested.

The testing of more ATZ and ZTA compositions, such as 70Z30A or 70A30Z, is suggested in order to fully investigate the ideal zirconia and alumina composition with improvements on both mechanical properties and aging resistance.

An additional stage of hot isostatic pressing is also proposed to optimize the results, by improving the densification (up to 99%) and in particular, to enhance the characteristics of the ZTA composites.

Regarding the doped composites, it is also suggested the production of these compositions with different amounts of these dopants, to find their optimal content.

Since the ATZ produced with 2 mol% Yttria Stabilized Zirconia was the less stable composite, the addition of $La_2O_3$ in order to stabilize the zirconia and simultaneously maintain its mechanical properties, is advised.

Finally, it was found that the ZTA doped samples would require a higher sintering temperature to achieve a better densification. It is then suggested the production of these composites with a higher sintering temperature and also to verify the effect of this parameter on the remaining properties of the materials.

# References


[1] P. Palmero, L. Montanaro, H. Reveron, and J. Chevalier, “Surface Coating of Oxide Powders: A New Synthesis Method to Process Biomedical Grade Nano-Composites,” *Materials (Basel).*, vol. 7, no. 7, pp. 5012–5037, Jul. 2014.

[2] A. De Aza, J. Chevalier, and G. Fantozzi, “Crack growth resistance of alumina, zirconia and zirconia toughened alumina ceramics for joint prostheses,” *Biomaterials*, vol. 23, pp. 937–945, 2002.

[3] P. Boutin, “L’arthroplastie totale de la hanche par prothèse en alumine,” *Int. Orthop.*, vol. 1, no. 2, pp. 87–94, 1977.

[4] I. C. Clarke, M. Manaka, T. Shishido, H. Oonishi, G. A. Gustafson, and M. Boehler, “Tribological and Material Properties for all-Alumina THR -Convergence with Clinical Retrieval Data,” in *Bioceramics in Joint Arthroplasty SE - 1*, H. Zippel and M. Dietrich, Eds. Steinkopff, pp. 3–17, 2003.

[5] G. Pezzotti and K. Yamamoto, “Artificial hip joints: The biomaterials challenge,” *J. Mech. Behav. Biomed. Mater.*, vol. 31, pp. 3–20, 2014.

[6] C. Piconi and G. Maccauro, “Zirconia as a ceramic biomaterial,” *Biomaterials*, vol. 20, 1999.

[7] J. Chevalier, L. Gremillard, A. V. Virkar, and D. R. Clarke, “The Tetragonal-Monoclinic Transformation in Zirconia: Lessons Learned and Future Trends,” *J. Am. Ceram. Soc.*, vol. 92, no. 9, pp. 1901–1920, Sep. 2009.

[8] J. Chevalier, “What future for zirconia as a biomaterial?,” *Biomaterials*, vol. 27, no. 4, pp. 535–43, Feb. 2006.

[9] S. M. Kurtz, S. Kocagöz, C. Arnholt, R. Huet, M. Ueno, and W. L. Walter, “Advances in zirconia toughened alumina biomaterials for total joint replacement.,” *J. Mech. Behav. Biomed. Mater.*, vol. 31, pp. 107–16, Mar. 2014.

[10] M. Hossen, F. Chowdhury, M. Gafur, and A. Abdul, “Effect of Zirconia Substitution on Structural and Mechanical Properties of ZTA Composites,” *iosrjournals.org*, vol. 11, no. 2, pp. 1–7, 2014.

[11] G. Magnani and A. Brillante, “Effect of the composition and sintering process on mechanical properties and residual stresses in zirconia–alumina composites,” *J. Eur. Ceram. Soc.*, vol. 25, no. 15, pp. 3383–3392, Oct. 2005.

[12] V. Naglieri, P. Palmero, L. Montanaro, and J. Chevalier, “Elaboration of Alumina-Zirconia Composites: Role of the Zirconia Content on the Microstructure and Mechanical Properties,” *Materials (Basel).*, vol. 6, no. 5, pp. 2090–2102, May 2013.

[13] S. Lawson, “Environmental Degradation of Zirconia Ceramics .,” vol. 15, pp. 485–502, 1995.

[14] J. L. Masonis, R. B. Bourne, M. D. Ries, R. W. McCalden, A. Salehi, and D. C. Kelman, “Zirconia femoral head fractures,” *J. Arthroplasty*, vol. 19, no. 7, pp. 898–905, Oct. 2004.

[15] I. C. Clarke, “Metastable Nature of Zirconia Femoral Heads From a 20-Year Perspective Of Clinical and Simulator Wear Studies,” *Semin. Arthroplasty*, vol. 17, no. 3–4, pp. 165–178, 2006.

[16] C. Piconi, G. Maccauro, and L. Pilloni, “On the fracture of a zirconia ball head,” *J. Mater. Sci.*, vol. 7, pp. 289–300, 2006.

[17] J. Chevalier, L. Gremillard, and S. Deville, “Low-Temperature Degradation of Zirconia and Implications for Biomedical Implants,” *Annu. Rev. Mater. Res.*, vol. 37, no. 1, pp. 1–32, Aug. 2007.

[18] M. Moraes and C. Elias, “Mechanical properties of alumina-zirconia composites for ceramic abutments,” *Mater. Res.*, vol. 7, no. 4, pp. 643–649, 2004.

[19] F. Kern and P. Palmero, “Microstructure and mechanical properties of alumina 5vol% zirconia nanocomposites prepared by powder coating and powder mixing routes,” *Ceram. Int.*, vol. 39, no. 1, pp. 673–682, Jan. 2013.

[20] W. H. Tuan, R. Z. Chen, T. C. Wang, C. H. Cheng, and P. S. Kuo, “Mechanical properties of $Al_2O_3/ZrO_2$ composites,” vol. 22, pp. 2827–2833, 2002.

[21] F. Cesari, L. Esposito, F. M. Furgiuele, C. Maletta, and a. Tucci, “Fracture toughness of alumina–zirconia composites,” *Ceram. Int.*, vol. 32, no. 3, pp. 249–255, Jan. 2006.

[22] “International Standard Organization No: 13356 - Ceramic materials based on yttria-stabilized tetragonal zirconia (Y-TZP),” vol. 2008, 2008.

[23] S. Saridag, O. Tak, and G. Alniacik, “Basic properties and types of zirconia: An overview,” *World J. Stomatol.*, vol. 2, no. 40, pp. 40–47, 2013.

[24] F. F. Lange, “Transformation toughening,” *J. Mater. Sci.*, vol. 17, no. 1, pp. 240–246, 1982.

[25] Z. K. Wu, N. Li, C. Jian, W. Q. Zhao, and J. Z. Yan, “Low temperature degradation of Al2O3-doped 3Y-TZP sintered at various temperatures,” *Ceram. Int.*, vol. 39, no. 6, pp. 7199–7204, 2013.

[26] C. Pecharroman and J. Bartolomé, “Percolative Mechanism of Aging in Zirconia-Containing Ceramics for Medical Applications,” *Adv. Mater.*, no. 6, pp. 507–511, 2003.

[27] S. Fabris, A. Paxton, and M. Finnis, “A stabilization mechanism of zirconia based on oxygen vacancies only,” *Acta Mater.*, pp. 1–14, 2002.

[28] L. Borchers, M. Stiesch, F. W. Bach, J. C. Buhl, C. Hübsch, T. Kellner, P. Kohorst, and M. Jendras, “Influence of hydrothermal and mechanical conditions on the strength of zirconia,” *Acta Biomater.*, vol. 6, no. 12, pp. 4547–4552, 2010.

[29] S. Deville, J. Chevalier, G. Fantozzi, J. F. Bartolomé, J. Requena, J. S. Moya, R. Torrecillas, and L. A. Díaz, “Low-temperature ageing of zirconia-toughened alumina ceramics and its implication in biomedical implants,” *J. Eur. Ceram. Soc.*, vol. 23, no. 15, pp. 2975–2982, Jan. 2003.

[30] S. Deville, J. Chevalier, and L. Gremillard, “Influence of surface finish and residual stresses on the ageing sensitivity of biomedical grade zirconia.,” *Biomaterials*, vol. 27, no. 10, pp. 2186–92, Apr. 2006.

[31] C. Sanon, J. Chevalier, T. Douillard, M. Cattani-Lorente, S. S. Scherrer, and L. Gremillard, “A new testing protocol for zirconia dental implants,” *Dent. Mater.*, vol. 31, no. 1, pp. 15–25, 2015.

[32] L. Hallmann, P. Ulmer, E. Reusser, M. Louvel, and C. H. F. Hämmerle, “Effect of dopants and sintering temperature on microstructure and low temperature degradation of dental Y-TZP-zirconia,” *J. Eur. Ceram. Soc.*, vol. 32, no. 16, pp. 4091–4104, 2012.

[33] T. Kosmač and A. Kocjan, “Ageing of dental zirconia ceramics,” *J. Eur. Ceram. Soc.*, vol. 32, no. 11, pp. 2613–2622, 2012.

[34] Y. Kawai, M. Uo, Y. Wang, S. Kono, S. Ohnuki, and F. Watari, “Phase transformation of zirconia ceramics by hydrothermal degradation.,” *Dent. Mater. J.*, vol. 30, no. 3, pp. 286–292, 2011.

[35] P. Kohorst, L. Borchers, J. Strempel, M. Stiesch, T. Hassel, F. W. Bach, and C. Hübsch, “Low-temperature degradation of different zirconia ceramics for dental applications,” *Acta Biomater.*, vol. 8, no. 3, pp. 1213–1220, 2012.

[36] J. Chevalier, P. Taddei, L. Gremillard, S. Deville, G. Fantozzi, J. F. Bartolomé, C. Pecharroman, J. S. Moya, L. a Diaz, R. Torrecillas, and S. Affatato, “Reliability assessment in advanced nanocomposite materials for orthopaedic applications.,” *J. Mech. Behav. Biomed. Mater.*, vol. 4, no. 3, pp. 303–14, Apr. 2011.

[37] G. Pezzotti, T. Saito, G. Padeletti, P. Cossari, and K. Yamamoto, “Nano-scale topography of bearing surface in advanced alumina/zirconia hip joint before and after severe exposure in water vapor environment.,” *J. Orthop. Res.*, vol. 28, no. 6, pp. 762–6, Jun. 2010.

[38] P. Fabbri, C. Piconi, E. Burresi, G. Magnani, F. Mazzanti, and C. Mingazzini, “Lifetime estimation of a zirconia-alumina composite for biomedical applications.,” *Dent. Mater.*, vol. 30, no. 2, pp. 138–42, Feb. 2014.

[39] T. Douillard, J. Chevalier, a. Descamps-Mandine, I. Warner, Y. Galais, P. Whitaker, J. J. Wu, and Q. Q. Wang, “Comparative ageing behaviour of commercial, unworn and worn 3Y-TZP and zirconia-toughened alumina hip joint heads,” *J. Eur. Ceram. Soc.*, vol. 32, no. 8, pp. 1529–1540, Jul. 2012.

[40] S. Deville, H. El Attaoui, and J. Chevalier, “Atomic force microscopy of transformation toughening in ceria-stabilized zirconia,” *J. Eur. Ceram. Soc.*, vol. 25, no. 13, pp. 3089–3096, Aug. 2005.

[41] F. Zhang, K. Vanmeensel, M. Inokoshi, M. Batuk, J. Hadermann, B. Van Meerbeek, I. Naert, and J. Vleugels, “Critical influence of alumina content on the low temperature degradation of 2–3mol% yttria-stabilized TZP for dental restorations,” *J. Eur. Ceram. Soc.*, vol. 35, no. 2, pp. 741–750, 2015.

[42] F. Zhang, K. Vanmeensel, M. Inokoshi, M. Batuk, J. Hadermann, B. Van Meerbeek, I. Naert, and J. Vleugels, “3Y-TZP ceramics with improved hydrothermal degradation resistance and fracture toughness,” *J. Eur. Ceram. Soc.*, vol. 34, no. 10, pp. 2453–2463, 2014.

[43] F. Sommer, R. Landfried, F. Kern, and R. Gadow, “Mechanical properties of zirconia toughened alumina with 10–24vol.% 1Y-TZP reinforcement,” *J. Eur. Ceram. Soc.*, vol. 32, no. 16, pp. 4177–4184, Dec. 2012.

[44] R. C. Garvie, R. H. Hannink, and R. T. Pascoe, “Ceramic steel?,” *Nature*, vol. 258, no. 5537, pp. 703–704, Dec. 1975.

[45] D.-J. Kim, H.-J. Jung, J.-W. Jang, and H.-L. Lee, “Fracture Toughness, Ionic Conductivity, and Low-Temperature Phase Stability of Tetragonal Zirconia Codoped with Yttria and Niobium Oxide,” *J Am Ceram. Soc.*, vol. 14, pp. 2309–2314, 1998.

[46] a. M. Hassan, S. M. Naga, and M. Awaad, “Toughening and strengthening of Nb2O5 doped zirconia/alumina (ZTA) composites,” *Int. J. Refract. Met. Hard Mater.*, vol. 48, pp. 338–345, 2015.

[47] J. W. Martin, *Concise encyclopedia of the structure of materials*, 1st ed.. Amsterdam: Amsterdam, 2007.

[48] G. Pezzotti, “Bioceramics for hip joints: The physical chemistry viewpoint,” *Materials (Basel).*, vol. 7, no. 6, pp. 4367–4410, 2014.

[49] P. Li, I.-W. Chen, and J. Penner-Hahn, “Effect of Dopants on Zirconia Stabilization—An X-ray Absorption Study: I, Trivalent Dopants,” *J. Am. Ceram. Soc.*, vol. 77, 1994.

[50] a. a. Nogiwa-Valdez, W. M. Rainforth, P. Zeng, and I. M. Ross, “Deceleration of hydrothermal degradation of 3Y-TZP by alumina and lanthana co-doping,” *Acta Biomater.*, vol. 9, no. 4, pp. 6226–6235, 2013.

[51] J. F. Bartolomé, A. Smirnov, F. Sommer, R. Landfried, and R. Gadow, “Sliding Wear Behavior of ZTA with Different Yttria Stabilizer Content,” *J. Am. Ceram. Soc.*, vol. 7, 2015.

[52] K. Tsukuma and M. Shimada, “Strength, fracture toughness and Vickers hardness of CeO2-stabilized tetragonal ZrO2 polycrystals (Ce-TZP),” *J. Mater. Sci.*, vol. 20, no. 4, pp. 1178–1184, 1985.

[53] H. Schubert and F. Frey, “Stability of Y-TZP during hydrothermal treatment: neutron experiments and stability considerations,” *J. Eur. Ceram. Soc.*, vol. 25, no. 9, pp. 1597–1602, Jun. 2005.

[54] L. Li, O. Van Der Biest, P. L. Wang, J. Vleugels, W. W. Chen, and S. G. Huang, “Estimation of the phase diagram for the ZrO 2 – Y 2 O 3 – CeO 2 system,” *J. Eur. Ceram. Soc.*, vol. 21, pp. 2903–2910, 2001.

[55] W. G. Hamilton, J. P. McAuley, D. a Dennis, J. a Murphy, T. J. Blumenfeld, and J. Politi, “THA with Delta ceramic on ceramic: results of a multicenter investigational device exemption trial.,” *Clin. Orthop. Relat. Res.*, vol. 468, no. 2, pp. 358–66, Feb. 2010.

[56] M. Kuntz, “Live-Time Prediction of BIOLOX® delta,” in *Bioceramics and Alternative Bearings in Joint Arthroplasty SE - 39*, J.-D. Chang and K. Billau, Eds. Steinkopff, 2007, pp. 281–288.

[57] M. Kuntz, “The effect of chromia content on hardness of zirconia platelet toughened alumina composites,” pp. 2–5, 2014.

[58] Ceramtec, “Scientific Information and Performance Data,” *Ceramtec- Biol. Delta*, vol. Brochure.

[59] T. Oungkulsolmongkol, P. Salee-Art, and W. Buggakupta, “Hardness and Fracture Toughness of Alumina-Based Particulate Composites with Zirconia and Strontia Additives,” *J. Met. Mater. Miner.*, vol. 20, no. 2, pp. 71–78, 2010.

[60] G. Pezzotti, M. C. Munisso, A. a Porporati, and K. Lessnau, “On the role of oxygen vacancies and lattice strain in the tetragonal to monoclinic transformation in alumina/zirconia composites and improved environmental stability.,” *Biomaterials*, vol. 31, no. 27, pp. 6901–8, Sep. 2010.

[61] G. Štefanić, S. Popović, and S. Musić, “Influence of Cr2O3 on the stability of low temperature t-ZrO2,” *Mater. Lett.*, vol. 36, no. 5–6, pp. 240–244, 1998.

[62] A. Z. A. Azhar, N. A. Rejab, M. Hasmaliza, M. M. Ratnam, and A. A. Zainal, “The Effects of $Cr_2O_3$ Addition on Fracture Toughness and Phases of ZTA Ceramic Composite,” *Adv. Mater. Res.*, vol. 620, no. 2, pp. 35–39, 2012.

[63] A. Z. A. Azhar, H. Mohamad, M. M. Ratnam, and Z. A. Ahmad, “The effects of MgO addition on microstructure, mechanical properties and wear performance of zirconia-toughened alumina cutting inserts,” *J. Alloys Compd.*, vol. 497, no. 1–2, pp. 316–320, 2010.

[64] D.-H. Riu, Y.-M. Kong, and H.-E. Kim, “Effect of Cr2O3 addition on microstructural evolution and mechanical properties of Al2O3,” *J. Eur. Ceram. Soc.*, vol. 20, no. 10, pp. 1475–1481, 2000.

[65] S. M. Naga, a. M. Hassan, and M. Awaad, “Physical and mechanical properties of Ta2O5 doped zirconia-toughened alumina (ZTA) composites,” *Ceram. Int.*, vol. 41, no. 5, pp. 6248–6255, 2015.

[66] Y. D. Cho, J. C. Shin, H. L. Kim, M. Gerelmaa, H. I. Yoon, H. M. Ryoo, D. J. Kim, and J. S. Han, “Comparison of the osteogenic potential of titanium- and modified zirconia-based bioceramics,” *Int. J. Mol. Sci.*, vol. 15, no. 3, pp. 4442–4452, 2014.

[67] H. Shyh-Lung and I. W. Chen, “Grain size control of tetragonal zirconia polycrystals using the space charge concept,” *J. Am. Ceram. Soc.*, vol. 73, no. 11, pp. 3269–32773277, 1990.

[68] I. M. Ross, W. M. Rainforth, D. W. McComb, a. J. Scott, and R. Brydson, “The role of trace additions of alumina to yttria-tetragonal zirconia polycrystals (Y-TZP),” *Scr. Mater.*, vol. 45, no. 6, pp. 653–660, 2001.

[69] F. Zhang, K. Vanmeensel, M. Batuk, J. Hadermann, M. Inokoshi, B. Van Meerbeek, I. Naert, and J. Vleugels, “Highly-translucent, strong and aging-resistant 3Y-TZP ceramics for dental restoration by grain boundary segregation,” *Acta Biomater.*, vol. 16, pp. 215–222, 2015.

[70] H. Zhou, J. Li, D. Yi, and L. Xiao, “Effect of manganese oxide on the sintered properties of 8YSZ,” *Phys. Procedia*, vol. 22, pp. 14–19, 2011.

[71] S. Ramesh, S. Meenaloshini, C. Y. Tan, W. J. K. Chew, and W. D. Teng, “Effect of manganese oxide on the sintered properties and low temperature degradation of Y-TZP ceramics,” *Ceram. Int.*, vol. 34, no. 7, pp. 1603–1608, 2008.

[72] S. Ramesh, W. J. K. Chew, C. Y. Tan, J. Purbolaksono, A. M. Noor, M. A. Hassan, U. Sutharsini, M. Satgunam, W. D. Teng, M. Oxide, and M. Properties, “Influence of Manganese on the sintering properties of tetragonal zirconia,” *Ceram. - Silikaty*, vol. 57, no. 1, pp. 28–32, 2013.

[73] D. Ragurajan, M. Satgunam, and M. Golieskardi, “The Effect of Cerium Oxide Addition on the Properties and Behavior of Y-TZP,” vol. 2014, 2014.

[74] N. A. Rejab, A. Z. A. Azhar, M. M. Ratnam, and Z. A. Ahmad, “The effects of CeO2 addition on the physical, microstructural and mechanical properties of yttria stabilized zirconia toughened alumina (ZTA),” *Int. J. Refract. Met. Hard Mater.*, vol. 36, pp. 162–166, 2013.

[75] R. V. Mangalaraja, B. K. Chandrasekhar, and P. Manohar, “Effect of ceria on the physical, mechanical and thermal properties of yttria stabilized zirconia toughened alumina,” *Mater. Sci. Eng. A*, vol. 343, no. 1–2, pp. 71–75, 2003.

[76] N. A. Rejab, A. Z. A. Azhar, M. M. Ratnam, and Z. A. Ahmad, “The relationship between microstructure and fracture toughness of zirconia toughened alumina (ZTA) added with MgO and CeO2,” *Int. J. Refract. Met. Hard Mater.*, vol. 41, pp. 522–530, 2013.

[77] J. Wang, S. Y. Lim, S. C. Ng, C. H. Chew, and L. M. Gan, “Dramatic effect of a small amount of MgO addition on the sintering of Al2O3-5 vol% SiC nanocomposite,” *Mater. Lett.*, vol. 33, no. 5–6, pp. 273–277, 1998.

[78] a. Rittidech, L. Portia, and T. Bongkarn, “The relationship between microstructure and mechanical properties of Al2O3-MgO ceramics,” *Mater. Sci. Eng. A*, vol. 438–440, no. SPEC. ISS., pp. 395–398, 2006.

[79] A. Z. A. Azhar, H. Mohamad, M. M. Ratnam, and Z. A. Ahmad, “Effect of MgO particle size on the microstructure, mechanical properties and wear performance of ZTA-MgO ceramic cutting inserts,” *Int. J. Refract. Met. Hard Mater.*, vol. 29, no. 4, pp. 456–461, 2011.

[80] D. Casellas, M. M. Nagl, L. Llanes, and M. Anglada, “Fracture toughness of alumina and ZTA ceramics: Microstructural coarsening effects,” *J. Mater. Process. Technol.*, vol. 143–144, no. 1, pp. 148–152, 2003.

[81] S. N. B. Hodgson and J. Cawley, “The effect of titanium oxide additions on the properties and behaviour of Y-TZP,” *J. Mater. Process. Technol.*, vol. 119, no. 1–3, pp. 112–116, 2001.

[82] M. Zhao, X. Ren, and W. Pan, “Effect of Lattice Distortion and Disordering on the Mechanical Properties of Titania-Doped Yttria-Stabilized Zirconia,” *J. Am. Ceram. Soc.*, vol. 97, no. 5, pp. 1566–1571, 2014.

[83] H. Erkalfa, Z. Misirli, and T. Baykara, “The effect of TiO2 and MnO2 on densification and microstructural development of alumina,” *Ceram. Int.*, vol. 24, no. 2, pp. 81–90, 1998.

[84] H. Manshor, S. M. Aris, A. Z. A. Azhar, E. C. Abullah, and A. A. Zainal, “Effects of TiO2 addition on the phase, mechanical properties, and microstructure of zirconia toughened alumina ceramic composite,” *Ceram. Int.*, vol. 41, pp. 3961–3967, 2015.

[85] C. J. Wang and C. Y. Huang, “Effect of TiO2 addition on the sintering behavior, hardness and fracture toughness of an ultrafine alumina,” *Mater. Sci. Eng. A*, vol. 492, no. 1–2, pp. 306–310, 2008.

[86] Y. Yang, D. Yan, Y. Dong, X. Chen, L. Wang, Z. Chu, J. Zhang, and J. He, “Preparing of nanostructured Al2O3–TiO2–ZrO2 composite powders and plasma spraying nanostructured composite coating,” *Vacuum*, vol. 96, pp. 39–45, 2013.

[87] R. D. Bagley, I. B. Cutler, and D. L. Johnson, “Effect of $TiO_2$ on Initial Sintering of $Al_2O_3$,” *J. Am. Ceram. Soc.*, vol. 53, no. 3, pp. 136–141, 1970.

[88] E. R. Winkler, J. F. Sarver, and I. B. Cutler, “Solid Solution of Titanium Dioxide in Aluminum Oxide,” *J. Am. Ceram. Soc.*, vol. 49, no. 12, pp. 634–637, 1966.

[89] M. Sathiyakumar and F. D. Gnanam, “Influence of MnO and TiO 2 additives on density, microstructure and mechanical properties of Al 2 O 3,” *Ceram. Int.*, vol. 28, no. 2, pp. 195–200, 2002.

[90] K. Kobayashi, “Total electrical conductivity measurements of TiO2 doped YSZ ceramics,” *Ceram. Soc. Japan*, vol. 44, no. 9, pp. P328–P329, 1988.

[91] Y. Zu, G. Chen, X. Fu, K. Luo, C. Wang, S. Song, and W. Zhou, “Effects of liquid phases on densification of TiO2-doped Al2O3–ZrO2 composite ceramics,” *Ceram. Int.*, vol. 40, no. 3, pp. 3989–3993, 2014.

[92] O. Ormanci, I. Akin, F. Sahin, O. Yucel, V. Simon, S. Cavalu, and G. Goller, “Spark plasma sintered Al2O3-YSZ-TiO2 composites: Processing, characterization and in vivo evaluation,” *Mater. Sci. Eng. C*, vol. 40, pp. 16–23, 2014.

[93] T. Nakamura, H. Usami, H. Ohnishi, M. Takeuchi, H. Nishida, T. Sekino, and H. Yatani, “The effect of adding silica to zirconia to counteract zirconia’s tendency to degrade at low temperatures.,” *Dent. Mater. J.*, vol. 30, no. 3, pp. 330–335, 2011.

[94] L. Gremillard, J. Chevalier, T. Epicier, and G. Fantozzi, “Improving the Durability of a Biomedical-Grade Zirconia Ceramic by the Addition of Silica,” *J. Am. Ceram. Soc.*, vol. 85, no. 2, pp. 401–7, 2002.

[95] A. Samodurova, A. Kocjan, M. V. Swain, and T. Kosmač, “The combined effect of alumina and silica co-doping on the ageing resistance of 3Y-TZP bioceramics,” *Acta Biomater.*, vol. 11, pp. 477–487, 2015.

[96] Y.-J. Lin, P. Angelini, and M. L. Mecartney, “Microstructural and Chemical Influences of Silicate Grain-Boundary Phases in Yttria-Stabilized Zirconia,” *J. Am. Ceram. Soc.*, vol. 73, no. 9, pp. 2728–2735, 1990.

[97] L. Gremillard, T. Epicier, J. Chevalier, and G. Fantozzi, “Microstructural study of silica-doped zirconia ceramics,” *Acta Mater.*, vol. 48, no. 18–19, pp. 4647–4652, 2000.

[98] A. M. Hassan, M. Awaad, F. Bondioli, and S. M. Naga, “Densification behavior and mechanical properties of niobium-oxide-doped alumina ceramics,” *J. Ceram. Sci. Technol.*, vol. 5, no. 1, pp. 51–56, 2014.

[99] O. Roualdes, M.-E. Duclos, D. Gutknecht, L. Frappart, J. Chevalier, and D. J. Hartmann, “In vitro and in vivo evaluation of an alumina-zirconia composite for arthroplasty applications.,” *Biomaterials*, vol. 31, no. 8, pp. 2043–54, Mar. 2010.

[100] C. Vermes, K. a Roebuck, R. Chandrasekaran, J. G. Dobai, J. J. Jacobs, and T. T. Glant, “Particulate wear debris activates protein tyrosine kinases and nuclear factor kappaB, which down-regulates type I collagen synthesis in human osteoblasts.,” *J. Bone Miner. Res.*, vol. 15, no. 9, pp. 1756–1765, 2000.

[101] C. Vermes, R. Chandrasekaran, J. J. Jacobs, J. O. Galante, K. A. Roebuck, and T. T. Glant, “The Effects of Particulate Wear Debris, Cytokines, and Growth Factors on the Functions of MG-63 Osteoblasts,” *J. Bone & Jt. Surg.*, vol. 83, no. 2, p. 201, Feb. 2001.

[102] T. J. Webster, C. Ergun, R. H. Doremus, R. W. Siegel, and R. Bizios, “Enhanced functions of osteoblasts on nanophase ceramics,” *Biomaterials*, vol. 21, no. 17, pp. 1803–1810, 2000.

[103] T. J. Webster, R. W. Siegel, and R. Bizios, “Osteoblast adhesion on nanophase ceramics,” *Biomaterials*, vol. 20, no. 13, pp. 1221–1227, 1999.

[104] J. Li, Y. Liu, L. Hermansson, and R. Soremark, “Evaluation o biocompatibility of various ceramic powders with human fibroblasts in vitro,” *Clin. Mater.*, vol. 12, no. 4, pp. 197–201, 1993.

[105] I. Dion, L. Bordenave, and F. Lefebre, “Physico-chemistry and cytotoxicity of ceramics Part II Cytotoxicity of ceramics,” *J Mat Sci Mat Med*, vol. 5, pp. 18–24, 1994.

[106] V. Covacci, N. Bruzzese, G. Maccauro, C. Andreassi, G. A. Ricci, C. Piconi, E. Marmo, W. Burger, and A. Cittadini, “In vitro evaluation of the mutagenic and carcinogenic power of high purity zirconia ceramic,” vol. 20, pp. 371–376, 1999.

[107] M. Welander, I. Abrahamsson, and T. Berglundh, “The mucosal barrier at implant abutments of different materials,” *Clin. Oral Implants Res.*, vol. 19, no. 7, pp. 635–641, 2008.

[108] L. Rimondini, L. Cerroni, A. Carrassi, and P. Torricelli, “Bacterial colonization of zirconia ceramic surfaces: an in vitro and in vivo study.,” *Int. J. Oral Maxillofac. Implants*, vol. 17, no. 6, pp. 793–798, 2002.

[109] G. Maccauro, G. Bianchino, S. Sangiorgi, G. Magnani, D. Marotta, P. F. Manicone, L. Raffaelli, P. R. Iommetti, A. Stewart, A. Cittadini, and A. Sgambato, “Development of a New Zirconia-Toughened Alumina: Promising Mechanical Properties and Absence of In Vitro Carcinogenicity,” *Int. J. Immunopathol. Pharmacol.* , vol. 22 , no. 3 , pp. 773–779, Jul. 2009.

[110] G. Maccauro, A. Cittadinp, G. Magnanf, S. Sangiorgf, F. Muratori, P. E. Maniconp, P. R. Iommettp, D. Marotta, A. Chierichini, L. Raffaellp, and A. Sgambatoi, “In vivo characterization of zirconia toughened alumina material : A comparative animal study,” vol. 23, no. 3, pp. 841–846, 2010.

[111] S. Affatato, R. Torrecillas, P. Taddei, M. Rocchi, C. Fagnano, G. Ciapetti, and A. Toni, “Advanced nanocomposite materials for orthopaedic applications. A long-term in vitro wear study of zirconia-toughened alumina.,” *J Biomed Mater Res B Appl Biomater.*, vol. 78, pp. 76–82, 2006.

[112] X. He, Y. Z. Zhang, J. P. Mansell, and B. Su, “Zirconia toughened alumina ceramic foams for potential bone graft applications: Fabrication, bioactivation, and cellular responses,” *J. Mater. Sci. Mater. Med.*, vol. 19, no. 7, pp. 2743–2749, 2008.

[113] F. F. Lange, “Powder Processing Science and Technology for Increased Reliability,” *J. Am. Ceram. Soc.*, vol. 72, no. 1, pp. 3–15, Jan. 1989.

[114] Malvern Instruments Ltd, “ZETASIZER NANO Series brochure,” 2011.

[115] Buchi Labortechnik AG, “Training Papers - Spray Drying.” [Online]. Available: http://static1.buchi.com/sites/default/files/downloads/Set_3_Training_Papers_Spray_Drying_en_01.pdf.

[116] K. Niihara, “A fracture mechanics analysis of indentation-induced Palmqvist crack in ceramics,” *J. Mater. Sci. Lett.*, vol. 2, no. 5, pp. 221–223, 1983.

[117] Malvern Instruments Ltd, “Sample dispersion and refractive index guide Reference manual,” 2000.

[118] A. . Olivares and C. . Forero, “Goodness-of-Fit Testing,” *Int. Encycl. Educ.*, vol. 7, pp. 190–196, 2010.

[119] S. Brunauer, P. H. Emmett, and E. Teller, “Adsorption of Gases in Multimolecular Layers,” *J. Am. Chem. Soc.*, vol. 60, no. 2, pp. 309–319, Feb. 1938.

[120] E. Y. . Keng, “Air and helium pycnometer,” *Powder Technol.*, vol. 3, no. 3, pp. 179–180, 1969.

[121] J. van Meerloo, G. L. Kaspers, and J. Cloos, “Cell Sensitivity Assays: The MTT Assay,” in *Cancer Cell Culture SE - 20*, vol. 731, I. A. Cree, Ed. Humana Press, 2011, pp. 237–245.

[122] R. Supino, “MTT Assays,” in *In Vitro Toxicity Testing Protocols SE - 16*, vol. 43, S. O’Hare and C. Atterwill, Eds. Humana Press, 1995, pp. 137–149.

[123] F. Braet, R. De Zanger, and E. Wisse, “Drying cells for SEM, AFM and TEM by hexamethyldisilazane: a study on hepatic endothelial cells.,” *J. Microsc.*, vol. 186, no. Pt 1, pp. 84–87, 1997.

[124] E. E. Golub and K. Boesze-Battaglia, “The role of alkaline phosphatase in mineralization,” *Curr. Opin. Orthop.*, vol. 18, no. 5, 2007.

[125] G. Bertrand, P. Roy, C. Filiatre, and C. Coddet, “Spray-dried ceramic powders: A quantitative correlation between slurry characteristics and shapes of the granules,” *Chem. Eng. Sci.*, vol. 60, no. 1, pp. 95–102, 2005.

[126] Tosoh, “Advanced Ceramics | Zirconia Powders.” [Online]. Available: http://www.tosoh.com/our-products/advanced-materials/zirconia-powders.

[127] Saint-Gobain, “CY3Z-P Technical Data Sheet,”, p. 1, 2015.

[128] Zircoa, “A Grain Zirconia,” 2011.

[129] M. Frischbier, R. Gadow, and F. Kern, “Determination of Sintering Kinetics of Zirconia Toughened Alumina Ceramics by Analysis of Dilatometry Data,” *Analysis*, no. July, pp. 1099–1104, 2007.

[130] V. Naglieri, D. Gutknecht, V. Garnier, P. Palmero, J. Chevalier, and L. Montanaro, “Optimized slurries for spray drying: Different approaches to obtain homogeneous and deformable alumina-zirconia granules,” *Materials (Basel).*, vol. 6, no. 11, pp. 5382–5397, 2013.

[131] F. Kern and R. Gadow, “Manufacturing of ZTA composites for biomedical applications,” pp. 10–14, 2012.

[132] A. Arab, Z. A. Ahmad, and R. Ahmad, “Effects of yttria stabilized zirconia (3Y-TZP) percentages on the ZTA dynamic mechanical properties,” *Int. J. Refract. Met. Hard Mater.*, vol. 50, pp. 157–162, 2015.

[133] C. Ortmann, T. Oberbach, H. Richter, and P. Puhlfürß, “Preparation and characterization of ZTA bioceramics with and without gradient in composition,” *J. Eur. Ceram. Soc.*, vol. 32, no. 4, pp. 777–785, Apr. 2012.

[134] G. Liu, Z. Xie, and Y. Wu, “Effectively inhibiting abnormal grain growth of alumina in ZTA with low-content fine-sized ZrO2 inclusions introduced by infiltration and in situ precipitation,” *J. Am. Ceram. Soc.*, vol. 93, no. 12, pp. 4001–4004, 2010.

[135] BCE Special Ceramics, “Z 700 20A - Material Specification sheet,” p. 68229, 2015.

[136] S. Ceramaret, “ATZ 80% ZrO2-20%Al2O3 properties,” 2015. [Online]. Available: http://www.ceramaret.ch/en/technologies/ceramic-materials.

[137] E. S. Elshazly and M. E. Ali, “Alumina Effect on the Phase Transformation of 3Y-TZP Ceramics,” *J. Mater. Sci. Technol.*, vol. 24, no. 6, pp. 873–877, 2008.

[138] J. Chevalier, S. Grandjean, M. Kuntz, and G. Pezzotti, “On the kinetics and impact of tetragonal to monoclinic transformation in an alumina/zirconia composite for arthroplasty applications.,” *Biomaterials*, vol. 30, no. 29, pp. 5279–82, Oct. 2009.

[139] X. Liu, G. Lu, and Z. Yan, “Preliminary synthesis and characterization of mesoporous nanocrystalline zirconia,” *J. Nat. Gas Chem.*, vol. 12, pp. 161–166, 2003.

[140] L. Gremillard, J. Chevalier, T. Epicier, S. Deville, and G. Fantozzi, “Modeling the aging kinetics of zirconia ceramics,” *J. Eur. Ceram. Soc.*, vol. 24, no. 13, pp. 3483–3489, 2004.

[141] Y. Takigawa, T. Shibano, Y. Kanzawa, and K. Higashi, “Effect of Small Amount of Insoluble Dopant on Tetragonal to Monoclinic Phase Transformation in Tetragonal Zirconia Polycrystal,” *Mater. Trans.*, vol. 50, no. 5, pp. 1091–1095, 2009.

[142] M. Arita, Y. Takahashi, G. Pezzotti, T. Shishido, T. Masaoka, K. Sano, and K. Yamamoto, “Environmental Stability and Residual Stresses in Zirconia Femoral Head for Total Hip Arthroplasty: *In Vitro* Aging versus Retrieval Studies,” *Biomed Res. Int.*, vol. 2015, pp. 1–9, 2015.

[143] J. W. Christian, “The Theory of Transformations in Metals and Alloys,” J. W. B. T.-T. T. of T. in M. and A. Christian, Ed. Oxford: Pergamon, pp. 1–22, 1965.

[144] J. Schneider, S. Begand, R. Kriegel, C. Kaps, W. Glien, and T. Oberbach, “Low-Temperature Aging Behavior of Alumina-Toughened Zirconia,” *J. Am. Ceram. Soc.*, vol. 91, no. 11, pp. 3613–3618, 2008.

[145] B. Cales and J. M. Drouin, “Low-Temperature Aging of Y-TZP Ceramics,” vol. 54, pp. 2150–2154, 1999.

[146] H. Tsubakino, “Isothermal Tetragonal-to-Monoclinic Phase Transformation in a Zirconia–Yttria System,” *Mater. Trans.*, vol. 46, no. 7, pp. 1443–1451, 2005.

[147] P. Somasundaran, *Encyclopedia of Surface and Colloid Science*, no. vol. 2. Taylor & Francis, 2006.

[148] L. Bousse, S. Mostarshed, B. Van Der Shoot, N. . de Rooij, P. Gimmel, and W. Göpel, “Zeta potential measurements of Ta2O5 and SiO2 thin films,” *J. Colloid Interface Sci.*, vol. 147, no. 1, pp. 22–32, Nov. 1991.

[149] D.-J. Kim and T.-Y. Tien, “Phase Stability and Physical Properties of Cubic and Tetragonal ZrO2 in the System ZrO2–Y2O3–Ta2O5,” *J. Am. Ceram. Soc.*, vol. 74, no. 12, pp. 3061–3065, Dec. 1991.

[150] A. K. Bhattacharya, V. Shklover, W. Steurer, G. Witz, H. Bossmann, and O. Fabrichnaya, “Ta 2 O 5 – Y 2 O 3 – ZrO 2 system : Experimental study and preliminary thermodynamic description,” *J. Eur. Ceram. Soc.*, vol. 31, no. 3, pp. 249–257, 2011.

[151] J. . Ray, a. . Panda, and P. Pramanik, “Chemical synthesis of nanocrystals of tantalum ion-doped tetragonal zirconia,” *Mater. Lett.*, vol. 53, no. 3, pp. 145–150, 2002.

[152] J. E. Aubin, “Mesenchymal Stem Cells and Osteoblast-Chondroblast Differentiation,” *Eur. Cell. Mater.*, vol. 16, no. page 1, p. 483033, 2008.

[153] S. Bauer, P. Schmuki, K. von der Mark, and J. Park, “Engineering biocompatible implant surfaces,” *Prog. Mater. Sci.*, vol. 58, no. 3, pp. 261–326, Apr. 2013.

[154] A. K. Pandey, F. Pati, D. Mandal, S. Dhara, and K. Biswas, “In vitro evaluation of osteoconductivity and cellular response of zirconia and alumina based ceramics,” *Mater. Sci. Eng. C*, vol. 33, no. 7, pp. 3923–3930, Oct. 2013.

[155] H.-C. Ko, J.-S. Han, M. Bächle, J.-H. Jang, S.-W. Shin, and D.-J. Kim, “Initial osteoblast-like cell response to pure titanium and zirconia/alumina ceramics,” *Dent. Mater.*, vol. 23, no. 11, pp. 1349–1355, Nov. 2015.

[156] R. J. Kohal, M. Baechle, J. S. Han, D. Hueren, U. Huebner, and F. Butz, “In vitro reaction of human osteoblasts on alumina-toughened zirconia,” *Clin. Oral Implants Res.*, vol. 20, no. 11, pp. 1265–1271, Nov. 2009.